An Airborne Laser Scanning Approach to Mapping and Modelling Surface Moisture in an Agricultural Watershed in Nova Scotia

by

Kevin Garroway

Submitted in partial fulfilment of the requirements
for the degree of Master's of Applied Science

at

Dalhousie University
Halifax, Nova Scotia
December 2009

DALHOUSIE UNIVERSITY

Process Engineering and Applied Sciences

The undersigned hereby certify that they have read and recommend to the Faculty of Graduate Studies for acceptance a thesis entitled "An Airborne Laser Scanning Approach to Mapping and Modelling Surface Moisture in an Agricultural Watershed in Nova Scotia" by Kevin Garroway in partial fulfilment of the requirements for the degree of Master of Applied Science.

Dated: December 18, 2009

Co-Supervisor:

_____

Dr. Rob Jamieson

Co-Supervisor:

_____

Dr. Chris Hopkinson

Readers:

_____

Dr. Rob Gordon

_____

James Boxall

Departmental Representative: _____

DALHOUSIE UNIVERSITY

DATE: December 18, 2009

AUTHOR: Kevin Garroway

TITLE: An Airborne Laser Scanning Approach to Mapping and Modelling Surface Moisture in an Agricultural Watershed in Nova Scotia

DEPARTMENT OR SCHOOL: Process Engineering and Applied Science

DEGREE: Master's of Applied Science CONVOCATION: May YEAR: 2010

Permission is herewith granted to Dalhousie University to circulate and to have copied for non-commercial purposes, at its discretion, the above title upon the request of individuals or institutions.

Signature of Author

DEDICATION PAGE

I dedicate this thesis project to my friends, family and especially my fiancée, Shannon. Throughout this process it was the unwavering support of those closest to me that helped me stay focused and get through this project. Shannon, you I owe the most gratitude, you did not hesitate when I told you that I was starting my Master's Thesis instead of getting a job and you stood by me the entire way. Thank you.

Kevin Garroway,
December, 2009

TABLE OF CONTENTS

LIST OF TABLES

LIST OF FIGURES

ABSTRACT

Methods for accurately modeling surface saturation throughout a landscape are still evolving. The overall objective of this research was to develop an efficient approach for mapping areas of surficial wetness in an agricultural landscape. There were three distinct stages to this project, with each using datasets collected via airborne laser scanning (LiDAR), GPS, and a ground sampled time domain reflectometry soil moisture probe. All studies were conducted within the Thomas Brook Watershed, located in the intensively farmed Annapolis Valley region of Nova Scotia. The first stage of the project was to investigate airborne laser scanning intensity data and the relationship to ground reflectance. The second stage involved conducting a GIS analysis of the watershed by mapping topographic layers and comparing them to ground sampled VMC data. In the third stage a multi-scale approach was taken to generating a topographic surface saturation landform classification map. The surficial reflectance mapping technique worked well in areas of little or no vegetation cover; however it was shown that vegetation played a dominant role in surface reflectance. The volumetric moisture content data was consistently spatially organized when measured under wet conditions and it was shown to closely follow topographic drainage patterns, especially under bare earth fields. Other variables, such as soil type distributions, artificial drainage, and vegetation, have key roles in surface saturation distribution and must not be ignored in modeling methods.

LIST OF ABBREVIATIONS USED

AAFC	Agriculture and Agro-Food Canada
ALTM	Airborne Laser Terrain Mapper
ALS	Airborne Laser Scanning
ASL	Above Sea Level
CSRS	Canadian Spatial Referencing System
GHG	Green House Gas
GPS	Global Positioning Satellite
HMC	High Moisture Content
HPN	High Precision Network
HRU	Hydrologic Response Unit
Hz	Hertz
IMU	Inertial Measurement Unit
kHz	Kilohertz
km	Kilometres
LiDAR	Light Detection and Ranging
LMC	Low Moisture Content
MMC	Medium Moisture Content
m	Metres
N	Nitrogen
NAD 83	North American Datum 1983
nm	Nanometres
NO_3	Nitrate
PPK	Post-processed Kinematic
RMSE	Root Mean Square Error
RTK	Real-Time Kinematic
TBW	Thomas Brook Watershed
TDR	Time Domain Reflectometry
TIN	Triangular Irregular Network
TRMI	Topographic Relative Moisture Index
TWI	Topographic Wetness Index
UTM	Universal Transverse Mercator
SSLC	Surface Saturation Landform Classification
SWAT	Soil and Water Assessment Tool
VMC (%)	Volumetric Moisture Content (Percentage)
WGS 84	World Geodetic System 1984

ACKNOWLEDGEMENTS

I would first like to acknowledge Dr. Chris Hopkinson for introducing me to this project in 2006. Dr. Hopkinson taught me how to use LiDAR as a powerful tool and gave me the opportunity to explore its uses in watershed hydrology.

Dr. Rob Jamieson gave me the opportunity to take a small watershed mapping project to the next level and offered me a Master's education to continue the work I began while at AGRG. Dr. Rob Jamieson and Dalhousie have been an excellent advantage to my education.

I would also like to acknowledge the following:

Rob Gordon for providing financial support for my initial AGRG contract and Master's Degree. James Boxall for assisting me with the GIS, helping with the guidance of the thesis and grammatical corrects to this document. Dr. Laura Chasmer for spending countless hours flying LiDAR missions over my study area. Canadian Geophysical Union, Canadian Aeronautics and Space Institute, Atlantic Canadian Association of Geographers, and the Canadian Journal of Remote Sensing for providing excellent forums for me to present my work to my peers across the country. And finally to my fellow students who have assisted me in one way or another throughout the years, Peter Horne, Travis Val, Doug Stiff, John Kwong, Andrew Sinclair, Lee Hynes, and Katie Campbell.

CHAPTER 1 INTRODUCTION

1.1 BACKGROUND AND OBJECTIVES

Topography is widely recognized as a dominant factor on a landscape's hydrologic, geomorphologic, and biologic processes, and therefore the Digital Elevation Model (DEM) has become the most powerful tool for hydrologic modelling (Moore et al, 1991). In recent years the airborne laser scanned DEM has become a popular tool for topographic modeling and analysis. Accurately modeling saturation zones from a DEM throughout a landscape has been a challenge however, and has yet to have a perfected solution.

Agricultural activities can lead to several environmental problems. In particular, Nitrogen (N) can have a negative impact on air and water quality. There are many sources and forms of N in the environment and its losses have the potential to substantially impact atmospheric, terrestrial and aquatic ecosystems (Conrad, 1996; Groffman and Hanson, 1997). The benefit to crop yields and plant growth make N an essential crop additive, however excessive amounts of inorganic N have directly damaging impacts on human health and ecosystem performance. The prediction of N fate requires the simulation of several biological processes which occur in the soil environment (Florinsky *et al*, 2004). The process of denitrification is directly affected by hydrological processes and especially surface moisture. Florinsky *et al.* (2004) determined that in wetter soils denitrification rates were increased directly due to topographic controls, while in drier soils denitrification, while still present, does not depend on the spatial distribution of soil moisture.

There is a need to incorporate the spatial variability of N and denitrification losses into popular watershed-scale modeling efforts such as the Soil and Water Assessment Tool (SWAT). SWAT is one of the most widely used watershed modeling tools with over 250 peer-reviewed published articles (Gassman *et al,* 2007). SWAT is a semi-distributed model which is designed to predict how management practices will affect water resources throughout watersheds. Major modeling components of SWAT include, among others,

hydrology, weather, vegetation, contaminates, and land management. The watersheds are divided into Hydrologic Response Units (HRUs) which consist of similar land use, soil distribution and type, and management practices (Gassman *et al*, 2007). This research project does not employ the SWAT model technique, it examines methods of generating a topographically-based surface wetness zone map which might help improve the nitrogen transformation predictions made in SWAT models, without adding excessive complexity to existing model structures.

Two specific terms for describing surficial wetness are used throughout this project. 'Surface saturation' is water contained in the soil's pore space at the ground surface level, also called surface retention (de Blij, 2005). Further accumulation of precipitation under surface saturation conditions will lead to ponding and overland flow. In the context of this research the term surface saturation refers to the condition of visibly saturated ground surface conditions, where surface ponding is occurring or would occur upon addition of water. 'Soil moisture' is precipitation that has infiltrated into the surface and is contained in the pore spaces of soil. Water will percolate downward through the vadose zone under the force of gravity and be stored in the phreatic zone. The texture and structure of soil will determine its moisture retention characteristics. Field capacity is the amount of water soil can retain in the pore space, before water will drain by gravity forces (Christopherson, 2003). In the context of this research the term 'soil moisture' refers to the volumetric moisture content (VMC) measured at the ground level using a 10 cm ground-penetrating TDR probe. Given that surface wetness and topography are interconnected there is a basis for the theory that zones of saturation can be mapped from digital elevation models.

Remote sensing techniques, such as Light Detection And Ranging (LiDAR) have been used to generate highly accurate DEM's at small scales. This project utilizes LiDAR data in two ways. The first method explores the technology's potential to be used as a direct monitor of surface saturation through the utility of the backscattered energy of the light pulse. The second method is a more traditional approach using the DEM to generate topographic derivatives and map surficial saturation. In this project the approach to map

surficial saturation zones was focused on topographic data in an effort to determine how LiDAR data could be used to adequately map surficial moisture throughout an agricultural watershed.

Throughout the course of this research two underlying themes emerged as key components to studying watersheds and surface moisture. This study took an in-depth look at the topographic component to surface moisture variability, to see how much of the moisture distribution was connected to topography and exclusive from vegetation and soils (i.e. type and distribution). The second emerging theme was the appropriate scale at which surface moisture variability can be captured. Scale influenced both the manner in which ground sampled VMC data is collected and the manner in which GIS-based topographic models are constructed to best capture moisture patterns.

The project was done in three distinct stages; each of the stages was prepared as standalone manuscripts and was compiled as chapters into this document (Chapter 3, 4 and 5). The entire project was conducted in the same study area, the Thomas Brook Watershed (TBW) in Annapolis Valley, Nova Scotia. This introductory chapter outlines the structure of this Thesis, describes the study area for the project, introduces the principals of Light Detection and Ranging (LIDAR) and describes the importance of the DEMs.

In Chapter 2 the data collection and preparation techniques are explored. In Chapter 3 the utility of Airborne Laser Scanning (ALS) for surface saturation mapping is examined. This work was initiated as an exploration of the principles of near infra-red surface scanning using an Optech 3100 ALTM. During LiDAR data collection high-resolution elevation data is collected over a surface via timed light pulses. A measure of the energy returned to the sensor (known as the 'Intensity') for each light pulse is recorded in the process. We explored the interaction of the light pulse with the ground surface and examined the potential of using the intensity data as a mapping technique for surface saturation.

In Chapter 4 we examined topographic attributes that were identified as significant to hydrologic surface modeling. Four topographic attributes (known as 'layers' in a GIS) were examined and included slope angle, catchment area, curvature, and topographic wetness index. The layers were generated using a DEM, constructed from a LiDAR dataset, and the theories of how each layer was affected by moisture movement across the surface were compared with ground sampled volumetric moisture content (VMC) data.

In Chapter 5 the topographic layers examined in Chapter 4 were combined into a landform classification model. A multi-scale approach was developed and an assessment of the technique as a surface saturation classification model was conducted. A landform classification algorithm was augmented to incorporate the topographic layers relevant to hydrologic movement of water and the resultant classification model was compared, at multiple scales, to ground sampled VMC data points.

1.2 STUDY AREA

The study area for this project was the Thomas Brook Watershed (TBW) located north of the town of Berwick in the Annapolis Valley of Nova Scotia (Figure 1.1). The Annapolis Valley is a region of the province that is flanked by two ridges, locally known as 'North Mountain' and 'South Mountain.' Due to this topography the valley drains predominantly to the east and west into two major basins, the Minas Basin (east) and the Annapolis Basin (west), via two rivers, the Annapolis River and the Cornwallis River. The TBW is a small sub watershed of the Cornwallis River consisting of about 1,000 ha (Jamieson et al, 2003) and drains southward originating on the North Mountain and discharges into the Cornwallis River.

The TBW study area was chosen based on the overall size of the watershed, which is small enough to collect a diverse set of ground samples, and accessibility, for both aerial surveys and ground sampling. The site is also part of the Agriculture and Agro-Food Canada (AAFC) Watershed Evaluation for Beneficial Management Practices (WEBs) program.

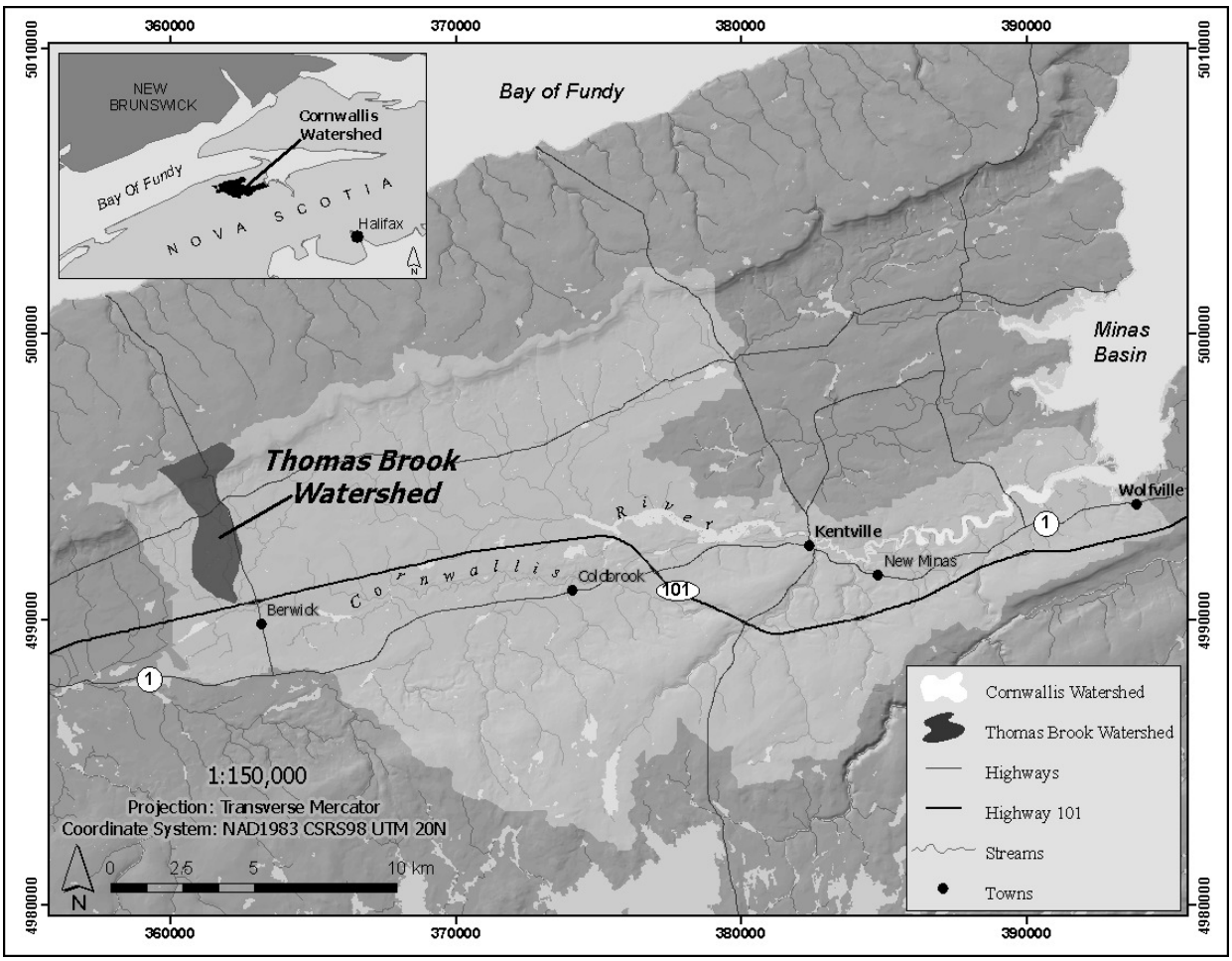

Figure 1.1 The Annapolis Valley, Nova Scotia study area. The Thomas Brook watershed is located in the west-centre of the Valley region and is highlighted in this figure. A shaded relief shows the position of the 'North' and 'South' mountains. The 'North' mountain ridge line is very predominate and well defined, whereas the 'South' mountain ridgeline is subtle and less pronounced.

1.2.1 Soils, Land Use & Climate

The predominant soils in the TBW are glacial till deposits. They range from poorly drained, unsuitable crop land soils, to well drained, good crop land soils (Cann, 1965). The distribution of the soils leads to the valley floor being an agriculturally rich environment. The majority of the landscape features in the watershed are rural anthropogenic. The Thomas Brook passes through many culverts and artificially

straightened sections before reaching the Cornwallis River outflow. The area around the brook is heavily agricultural in the lower reaches with small areas of natural forest and vegetation remaining on the face of the 'North' mountain. Within the TBW agricultural land makes up 60% of the overall land use leaving only 40% for non-agriculture such as housing, roads, and natural vegetation (Table 1.1). The climate of the Annapolis Valley is impacted by the adjacency to the Atlantic Ocean, which keeps the temperature moderate year round. The meteorological records from the nearby town of Kentville indicate that the mean annual precipitation total is 1211mm and the average daily temperature is 6.9^{o}C (Environment Canada, 2006).

Landuse	Field Count	Average Area (km2)	Total Area (km2)	Percentage of Watershed
Longterm Crop	16	0.07	1.20	15.4%
Rotational Crop	26	0.12	3.22	41.6%
Inactive	2	0.01	0.02	0.2%
Support	7	0.01	0.14	1.9%
Agricultural			4.58	59.1%
Non-Agricultural			3.17	40.9%
TOTAL	51		7.75	100.0%

Table 1.1 Landuse summary for TBW (Data provided by AAFC)

1.2.3 Slope

In general the landscape of the watershed slopes an average grade of 7% with the highest elevation of the watershed in the North (213 m ASL). The watershed is characterized by two highly differing slope sections. The upper section of the watershed flows down from the North Mountain and has an average slope of 10.5%, with an elevation range of 192 m and mean elevation of 120 m ASL. The lower section of the watershed flows across the valley floor at a much lower gradient, an average of 3.5% slope with an elevation change of 34 m and mean elevation of 20 m ASL.

1.2.4 Subplots

The landuse of the study area was defined by a data GIS layer provided by AAFC. Sixteen agricultural fields within the TBW were identified as growing long-term crops in

the 2006 growing season and were selected as candidate locations for field study. The crop types varied from corn, pasture, forage and barley. The criteria for selecting subplots for the field research was different land cover types (i.e. crop type for the 2006 growing season), geographic location in the watershed, topographic condition, and accessibility. Of the sixteen fields three were selected for further research. The fields were limited to three because during a typical data collection day it would take the full day to visit the three locations. Each field had a different crop type, corn, barley, forage (e.g. hay). The vegetation in the fields varied from low grass to bare earth in the spring and knee-high barley, hay and 2 m tall corn rows in the late summer (Figure 1.2).

The soil types within each field varied, as well as the soils drainage class (Table 1.2). This information was accessed from the CanSIS soils database, which describes the soils within the province in detail. The soils type and distribution for this study area was not available at the same fine resolution as the topographic information. The soils data was not included in the modeling of surficial moisture.

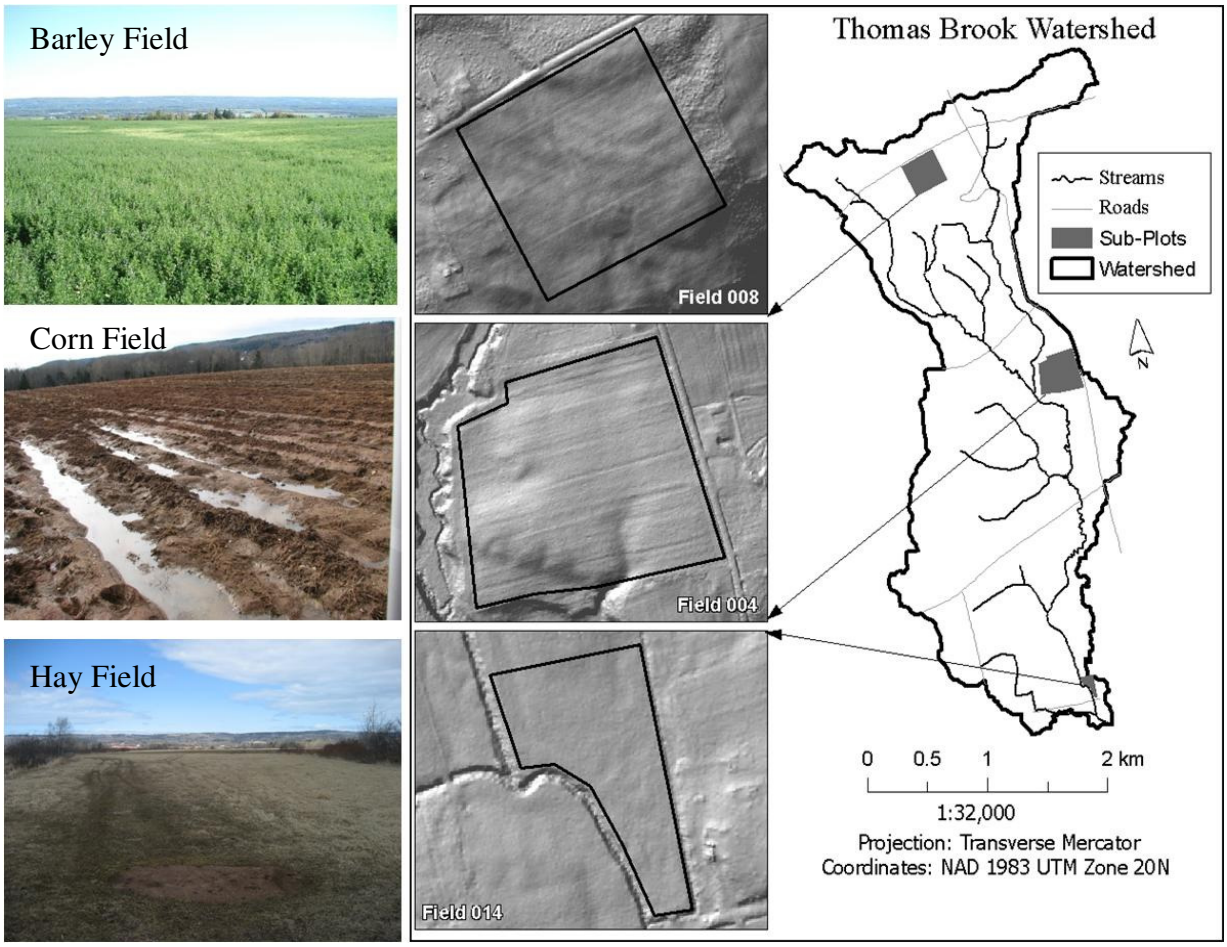

Figure 1.2 TBW Subplots. Field 008 corresponds to the Barley field pictured in the top-left. Field 004 corresponds to the Corn field pictured mid-left. Field 014 corresponds to the Hay field pictured bottom-left.

Field	Soil Series	Surface and Subsoil	Topography	Soil Drainage Class	Soil Capability
Barley Field	Glenmont	Greyish-brown to brown coarse sandy loam over yellowish-brown coarse sandy loam	Gently undulating	Moderately well drained	Good to fair crop land
	Rossway	Dark-brown friable silt loam over dark reddish brown loam or silt loam	Gently to moderately undulating	Well Drained	Poor crop land
	Tiddville	Organic dark greyish brown fine sandy loam over strong-brown fine sandy loam; strongly mottled	Depressional	Poorly drained	Unsuitable crop land
Corn Field	Bridgeville	Dark-brown friable sandy loam to loam over mottled brown sandy loam to loam	Level	Imperfectly drained	Good crop land
	Eroded	Eroding or eroded land, including steep forested slopes, gullies and some shallow areas	Undulating to steep	Variably drained	unsuitable crop land
	Pelton	Dark reddish brown fine sandy loam to loam over yellowish-red loam; friable	Gently undulating to hilly	Well Drained	Good crop land
	Woodville	Dark reddish brown friable sandy loam over yellowish-red sandy loam	Gently to moderately undulating	Well Drained	Good crop land
Hay Field	Stewiacke	Reddish-brown silt loam over reddish-brown loam or silt loam; some mottling	Level	Moderately to well drained	Good crop land

Table 1.2 Soils table for each subplot located within the TBW. The soils data was taken from Cann *et al*, 1965.

1.2.4.1 The Barley field (Field 008)

This area was chosen as a subplot based on its location in the watershed, ease of access and short-height vegetation cover. During the early spring this field's ground cover is low grass, while during the late summer the field is covered with low-growing barley. The field's location made this a desirable study area as it is the only subplot that was not on the valley floor and was located 200 m above the other fields on the North Mountain.

1.2.4.2 The Corn field (Field 004)

This field was chosen as a study area because it was centrally located in the watershed, it was located just off of a main road for easy access, there was other research being

conducted in the field and therefore some of the data points could be cross-referenced. This field was also desirable because it was a tilled field with low level, evenly distributed vegetation cover until late in the growing season at which time the vegetation would grow to approximately 2 m high.

1.2.4.3 The Hay field (Field 014)

Located at the southern most point of the watershed, this field was chosen for its ease of access, location in relation to the other sub plots, and vegetation characteristics. This field is a hay field with low-level vegetation cover in the spring and low hay in the fall. This is the smallest of the three sub plots. Due to the location of the field in relation to the rest of the watershed this field is typically wetter than the others.

1.3 LIGHT DETECTION AND RANGING

Airborne Laser Scanning (ALS) is a widely accepted method for high resolution topographic modelling (Axelsson, 1999; Baltsavias, 1999; and Wehr and Lohr, 1999). The ALS system is mounted in an aircraft and is comprised of five major components, the laser rangefinder, differential GPS, the inertial measurement unit (IMU), the scan mirror and the computer. The laser diode emits a short, near-infrared light pulse which travels from the scanner to a target (i.e. the ground), backscatters, and some of this energy returns to the scanner. Modern ALS systems are capable of acquiring multiple measurements from one laser pulse. As the light pulse travels to the target it may encounter and reflect from multiple targets. The multiple pulse returns are called "echoes" and many systems can record up to four or more echoes per pulse (Hollaus et al, 2005).

The laser scanner is capable of sending and receiving millions of light pulses during a typical survey. The precise time between pulse emission and reception is measured and the range from laser scanner to target is calculated. The differential GPS measures the

precise location of the aircraft at the time of the pulse. The attitude of the aircraft is measured by the IMU to obtain the vector of the emitted pulse. The scan mirror directs the laser pulses side to side, perpendicular to the direction of the aircraft flight path in a "saw-toothed" pattern. When these measurements are combined the result is a very accurate and precise set of points measured from the air of the ground surface.

The body of research on LiDAR's surface measuring application is well established, however, relatively little research has been focused on the utility of the backscattered intensity information of the laser pulse that is also collected in the ALS data collection process. LiDAR intensity data is directly related to the strength of the pulse energy emitted (Hopkinson, 2007) and the received power from the albedo target (Kassalainen *et al*. 2007). The recent body of research into the use of laser pulse intensity data has primarily been focused on vegetation classification algorithms (Brennan and Webster, 2007; Hopkinson and Chasmer, 2007). Kassalainen *et al* (2005) suggested that this deficit of useful applications of the ALS intensity data was due to a lack of calibration methods for intensity and that technique's needed to be developed to correct for directional and atmospheric influences on the laser pulse.

Researchers have begun reporting on the utility of calibration techniques of ALS intensity data. Kassalainen *et al*, (2005) proposed a calibration based on known reflectance of ground targets, although in their study they concluded that other surface characteristics dominated over surface reflectance properties of the targets. Kassalainen *et al.* (2007) added that the angle of incidence (the angle that which the laser interacts with the target) was a crucial factor in intensity measurements.

Coren and Sterzai (2006) proposed a radiometric calibration that accounted for the affect of beam divergence, the effect of angle of incidence with the target and assumed a Lambertian distribution of the backscattered intensity. Coren and Sterzai (2006) went on to suggest that laser backscatter intensity was a function of multiple factors including distance to target, incidence angle, reflectivity of the target and absorption by the "transmission medium" (air).

Mazzarini *et al.* (2007) took a simpler approach to laser intensity normalization and accounted for the terrain-airplane distance (the range) in a study on Mount Etna lidar intensities. Mazzarini *et al.* (2007) found that by accounting for the range in the intensity data the remaining influence on the intensity data was the surface roughness and angle of incidence.

Hopkinson (2007) conducted research on intensity normalization using data collected over a homogenous surface (highway) and presented a first approximation equation to normalize intensity values assuming a lambertian albedo surface and that the scan angle (θ) represented mean angle of incidence:

$$I_{cor} = I_{obs} \left(R^2_{obs} / (R_{ref} * \cos \theta)^2\right)$$

Equation 1.1 Hopkinson (2007) LiDAR intensity calibration method

Where I_{cor} = corrected (normalized) intensity, I_{obs} = observed intensity, R_{obs} = observed range and R_{ref} = reference range. Hopkinson (2007) suggested that intensity values could be relatively calibrated without the need for an atmospheric attenuation coefficient, surface roughness value, and true angle of incidence value. While adding those parameters would improve the calibration, a simpler method, Equation 1.1, provided a first approximation and can be calculated directly from the lidar data.

This case study focuses on the effect of the pulse's interaction with the ground surface and vegetation. A calibration of the laser pulse intensity data was performed which resembled the proposed equation by Hopkinson (2007). The calibration was performed during the post-processing of the LiDAR data in Optech's proprietary software 'REALM'. This calibration was considered a 'range normalization' and was conducted to improve the internal comparability of the intensity data. The range of each dataset was calibrated to 900m.

1.4 TOPOGRAPHY AND SOIL SATURATION

The ability to map zones of surface saturation would be very useful for modeling areas within watersheds where higher levels of denitrification may occur. In turn these models could be useful for monitoring greenhouse gas emission potential from agricultural environments. The spatial distribution of surface saturation has been directly linked to topography through many studies in the past (Beven and Kirkby, 1979; Parker, 1982; O'Loughlin, 1986; Burt and Butcher, 1985; Moore *et al.*, 1993).

Water will enter the ground surface through the pore space of soils. The role of infiltration depends on the physical characteristics of the soil, how much moisture is already available in the soil, the type and extent of vegetation, the slope of the topography, and precipitation. Soil structure and level of compaction are two of the most important characteristics to infiltration potential (de Blij, 2005). Coarse, sandy soils will speed up infiltration as pore space is increased with these soil types, while clay soils will slow infiltration as pore space is limited by compaction. Wet soil will allow less infiltration because wet soil is more compacted by precipitation, particles, water and soil swelling will cause pore space to be limited and lead to saturation conditions (de Blij, 2005). Agriculture is known to have a pronounced influence on soil infiltration rates. In vegetated landscapes soil infiltration will be increased due to precipitation interception on the foiliage prior to striking the soil. The type of vegetation will also affect infiltration rates, grass and barley will act to increase infiltration while tilled corn rows will be less effective at slowing precipitation's impact on the soil surface.

Several methodologies have been proposed for site moisture characterisation. Beven and Kirkby (1979) built on research into the spatial pattern of storm-flow source areas conducted by Hewlett and Troendle (1975) and utilized a contour-based DEM to manually generate a model for the prediction of the flow pathway of water throughout a catchment area (TOPMODEL) (Quinn *et al.*, 1995). The TOPMODEL wetness index is expressed as the natural log of the area draining through a point divided by the tangent of the local slope gradient (Beven, 1997) and has the form:

$$\ln(\alpha/\tan\beta)$$

Equation 1.2 The wetness index equation proposed by Beven and Kirkby (1979).

where α = the upslope contribution area and tan β = the local slope angle of each cell of the DEM (Quinn *et al.*, 1995). This type of formula was ideal for automated application using gridded DEMs (Quinn *et al*, 1991).

Another catchment modeling algorithm was developed by O'Loughlin (1981, 1986) and utilized the observation that local topography is a prime contributor to the high spatial variability of surficial moisture. The concept and subsequent model developed by O'Loughlin was similar to that of Beven and Kirkby (1979) in its attempt to model "… local saturation occur[ing] wherever the drainage flux from upslope exceed[ed] the capacity of a soil profile to conduct that flux." O'loughlin's model was written as

$$Aq/b > TM$$

Equation 1. 3 Wetness index proposed by O'loughlin (1981).

where A = partial upslope catchment, q = areal drainage flux, b = element contour length, T = local soil transmissivity, and M = local surface gradient. While the O'loughlin model's usage may be useful for mapping surface wetness it's usage was not considered in this study because it was developed primarily to be used with contour-based DEM's while this study was using exclusively raster based DEM's.

Parker (1982) developed yet another wetness index tool, called the Topographic Relative Moisture Index (TRMI). His research identified four approaches to modeling topography and moisture: (i) direct monitoring, (ii) water balance climatology, (iii) site index determination, (iv) and inferential techniques based on topographic parameters. Parker's model, an inferential technique, relied on generating multiple slope models from a grid based DEM (relative slope position, slope gradient, slope shape, and slope aspect) (Manis *et al.*, 2001). The model was generated by a summed scalar approach for weighting the

topographic elements and was designed to be flexible for individual study areas. Parker's TRMI was designed for moderate to high relief topography (Manis *et al.,* 2001) and therefore was of little utility to this project.

Burt and Butcher (1985) furthered the discussion on topographic controls of soil moisture by suggesting that hillslope hollows, low gradient slopes and plan/profile concave curvature areas would have higher soil wetness values than other areas. Their research involved testing the $\ln(\alpha/\tan\beta)$ wetness index against soil moisture measurements and found an average correlation of $r = 0.4 – 0.5$. Moore *et al* (1991) discussed the demand for simple techniques to assist with day-to-day land management decisions and presented a number of methods for generating primary topographic derivatives from DEM's to predict moisture patterns, among them was the popular wetness index $\ln(\alpha/\tan\beta)$. Quinn *et al* (1991) revisited TOPMODEL and addressed some of the issues of flow pathway derivation, also suggesting that increasing the DEM resolution may result in increased inaccuracies associated with flow pathways and therefore making a case for researching higher resolution DEM's and topographic saturation modeling. Zhang and Montgomery (1994) further tested the effects of DEM resolution on derived flow pathways and suggested that the most appropriate DEM grid cell size would be finer than the hillslope scale measured in the field. Tarboton (1997) developed new techniques for modelling flow pathways from infinite directions and a plug-in for GIS software (ESRI ArcGIS).

As technology continues to advance better quality and higher resolution topographic grid maps are made available for modelling. Many of the original hydrologic models, such as TOPMODEL and the TRMI, were generated on coarse scale map grids. With the availability of high-resolution map grids new challenges of spatial accuracy, model accuracy and appropriate scale arose. The recent bodies of research have had more focus on these new spatial accuracy challenges associated with hydrologic modelling.

In 2001 Andrew Weiss presented a poster at an ESRI User Conference that outlined a technique for landform classification using a DEM. The research was unique in its approach because it considered DEM resolution and neighbourhood scale as key inputs

into the classification algorithm. The Topographic Position Index (TPI) developed by Weiss (2001) is used extensively in this project (see Chapter 5).

Schmidt and Persson (2003) used RTK-GPS and an ALS DEM to model a TWI. They found that the TWI did not result in a linear spatial relationship with soil moisture measurements collected via gravimetric samples and TDR. They were able to increase the TWI performance by applying a mean filter to the dataset, which reduced the tendency of the TWI to over-concentrate high wetness values in bottoms of valleys and channels. However, they concluded that TWI was only correlated with soil moisture values during a wet season and not during a dry season, and that only fields with high elevation differences had significant correlation.

CHAPTER 2 DATA PROCESSING AND PREPARATION

2.1 DIGITAL ELEVATION MODEL GENERATION

The digital elevation model (DEM) is a critical component of any topographic landscape analysis. DEM's are represented by a variety of data types such as contours, TIN's, GRID rasters (Wise, 1998), and XYZ data points. For this project the grid based DEM was used. The regularly spaced grid contains one elevation value for each grid cell and lends itself well to applying mathematical functions. The DEM is the most critical component of this study. It is the data layer from which all topographic attributes will be derived from for this study. The accuracy of the DEM was therefore critical. A detailed description of DEM generation from LiDAR is presented.

On March 29, 2006 a LiDAR survey was conducted over the Thomas Brook Watershed (TBW). An Optech ALTM 3100 (Optech Incorporated, Toronto, Canada) light detection and ranging (LiDAR) mapping system was used to collect a high density 3d point cloud of the study area environment. The survey consisted of 8 survey flightlines collected with 50% overlap. The Optech ALTM 3100 sensor was set to a pulse repetition rate of 50 kHz, a scan frequency of 30Hz, and a scan angle of +/- 18^{o}. The survey was flown using a Piper Navajo aircraft at an air speed of 120 knots and was collected at an altitude of 1300m above ground level. These apparatus settings, overlap coverage, and seasonal timing of data collection, are excellent conditions to yield high quality data for DEM generation.

During LiDAR data collection the raw data is stored on a hard drive that is part of the system in the aircraft. The data is extracted and processed into a "point cloud," (a series of data points, each of which contain a reference value of XYZ and together form a 3D cloud of points, in this case, representing a landscape) which is then interpolated into grid based DEM. For data collected with the Optech ALTM 3100 a proprietary software package called REALM was used to process the raw data and produced *.las files. Each file contained information about one flightline.

The data were cleaned, processed, and prepared for topographic surface modelling. The advantage of using LiDAR technology to generate a surface model is that it is capable of measuring precise elevations completely throughout a landscape, even under forest and vegetation canopies. The DEM creation process was started by classifying the data, the Bentley Microstation V8 2004 with Terrascan software was used for this classification. This software was used to breakdown the data into smaller, more manageable file sizes, classify out unwanted data and export the data into ASCII "xyz" files.

The *.xyz ASCII files were then gridded and mosaicked together to form a DEM. This process was completed with Golden Software Surfer: Surface Mapping Software (http://www.goldensoftware.com/demo.shtml). The Surfer software was used for viewing LiDAR derived digital elevation models (Figure 2.1).

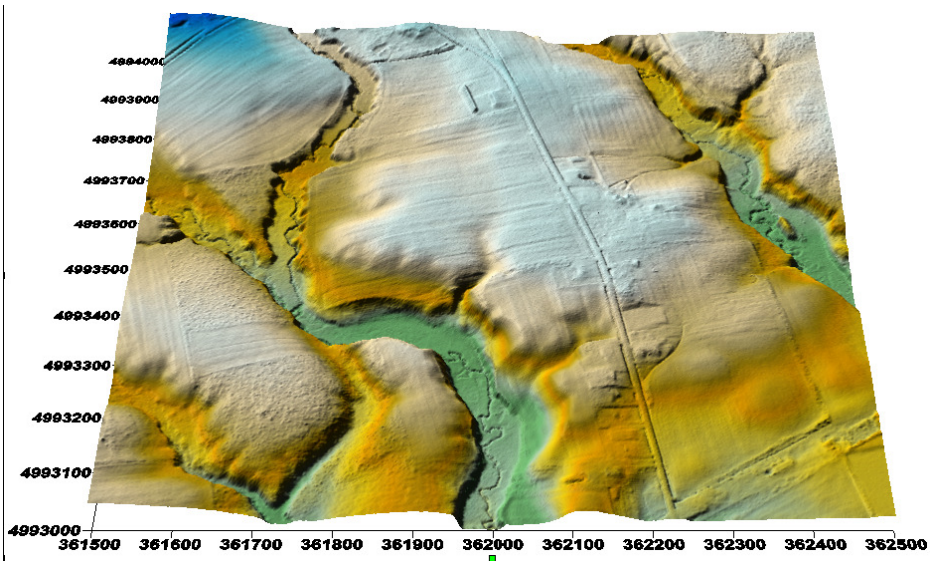

Figure 2. 1 Surfer example image of Tile #20 Ground Classification from the March 29, 2006 data set. This image has a 1:15 cm vertical exaggeration.

The Surfer software utilizes an automation program called Scripter. Using the Scripter program multiple files were gridded and converted into ArcGIS ASCII files at once. A script, "xyztogrd.bas" (APPENDIX A), generated by the Applied Geomatics Research Group (AGRG, Middleton, Nova Scotia) researchers Doug Stiff and Jon Kwong was

used for this process. ArcGIS *.asc files are ESRI 3D ASCII files, which can be used to generate GIS data layers (rasters and feature classes).

Once the data was processed by the Surfer script the ASCII files were imported into ESRI ArcGIS ArcMap so that the gridded points could be converted to rasters. The data was converted from the ASCII format to raster format using a standard inverse distance weighting algorithm, projected, and loaded into a file geodatabase for storage. This process was completed through the use of models built into the ArcGIS software. The rasters were projected to the WGS 84 UTM Zone 20 N projection. Once the raster's were in the geodatabase the files were mosaicked together using the "Mosaic to New Raster" tool setting the cell size to 1, 5, or 10, which generated the DEM for the entire study area. The DEM was prepared at three resolutions for this project, 1 m, 5 m and 10 m. For the research conducted in Chapter 3 and Chapter 4 the 5 m DEM was used exclusively. For the multi-scale topographic classification research conducted in Chapter 5 the 1 m, 5 m and 10 m DEM's were utilized.

2.1.1 Measuring Error within the DEM

The DEM is an attractive method of displaying 3D GIS data and the raster DEM is a valuable method of presenting a DEM due to its grid based data structure. Zhou and Liu (2004) took an in-depth look at slope and aspect calculation accuracy from raster based DEM's. They found that increased DEM resolution did not assure higher slope and aspect accuracy, but rather DEM data accuracy was the only contributing factor to modeling accurate slope and aspect derivatives. They were able to show this by using a series of mathematically calculated surfaces. Wise (2007) added to the discussion on DEM error that the largest error is found at the local scale of the data points used to generate DEM's. This effect is directly related to the strong autocorrelation found in elevation point data.

Wechsler (2007) suggested that the common approach to quantifying DEM accuracy is the Root Mean Square Error (RMSE) statistic. Although a quantitative measurement of DEM accuracy is a valuable quality control statistic, the RMSE is not "an accurate assessment of how well each cell in a DEM represents a true elevation" (Wechsler, 2007,

p. 1483). Nonetheless the RMSE is still the standard method for DEM error assessment and is utilized in this study. The RMSE is calculated by taking the difference between two datasets, squaring the results, averaging the squares and reporting the square root of the average. For this project GPS data was used to calculate the RMSE error for the LiDAR derived DEM. The GPS data was collected with a Leica 500-series dual-phase GPS system operating in Post-Processed Kinematic (PPK) mode. In order to assess the accuracy of the DEM the accuracy of the GPS data must also be accounted for.

The GPS data was processed using Leica's Ski-PRO software. It is proprietary software developed by Leica for processing PPK and RTK (Real-Time Kinematic) GPS data. The software is used to read the raw GPS data files that were collected via the two GPS receivers. One of the receivers collected data at a static point location known as a High Precision Network (HPN) point. This GPS point and receiver are known as the base station. The HPN monuments are known locations that have been surveyed into position by Service Nova Scotia in the early 1990's (Coordinate Referencing System, www.gov.ns.ca/). The base station was located at HPN7153 (44^{o}59'52.880W and 64^{o}56'47.013N) which is located just outside the town of Kingston, Nova Scotia (about 10 km west of the study area). The second receiver, known as the rover, was used to collect data throughout the study area. The rover is a backpack mounted GPS unit with an antenna attached to a 2 m tall pole. In March of 2006 447 points were collected throughout the study area and were used to assess the DEM accuracy (Figure 2.2).

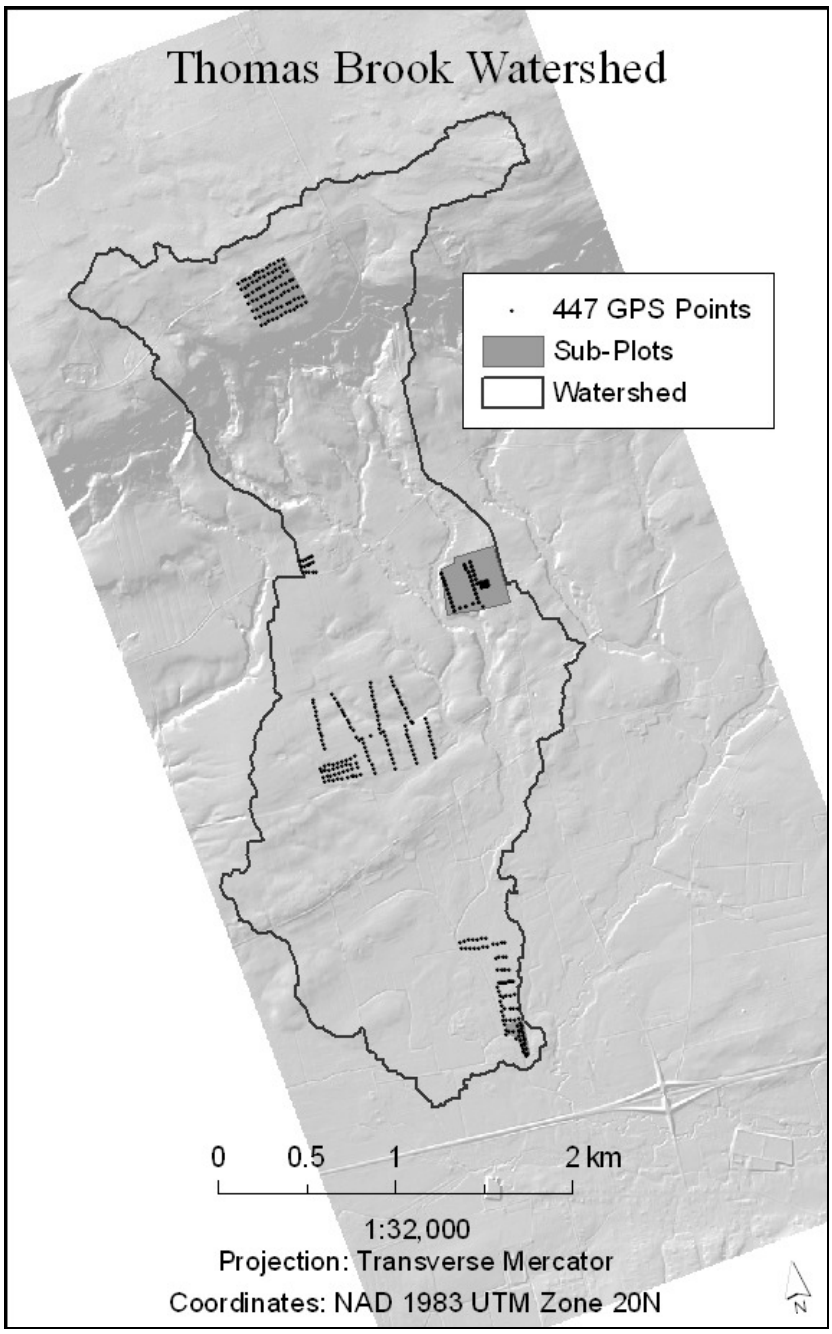

Figure 2.2 Map image of the 447 GPS points collected throughout the TBW which were used to validate the DEM.

The two GPS datasets (the base station and rover) were processed in Ski-PRO. The base station data was used to differentially correct the rover data. The standard deviation between the measured GPS data and the corrected value of each point were then used to calculate the precision of the GPS data. The RMSE of the GPS data was very low, meaning that the GPS data was highly accurate. The GPS was computed to be accurate to

within 1 cm horizontal and to within 2 cm vertical. These findings indicated that the GPS data was of very good quality.

One method for assessing DEM accuracy is to test the modelled elevation to that of data with superior accuracy. The 447 GPS points were used to assess the vertical accuracy of the 5m DEM. The RMSE of the absolute difference between the interpolated DEM and the GPS points was calculated to be 0.18 m, which means that the 5m DEM had a vertical accuracy of less than 20 cm. Therefore it was determined that the DEM was of good quality for this project.

2.2 WATERSHED MODELLING

The DEM provided the core data for the topographic models. One of the most important products created for this project was the watershed delineation. DEM's are an essential tool for delineating watershed boundaries. At higher resolutions watershed boundaries become more precise and accurate. Delineating a watershed with LiDAR data requires some data preparation and a system of cleaning the data.

The first step was to use ArcGIS to fill the 'sinks' in the DEM. A sink, or pit, is a digital phenomenon that is common in DEM's and can be described as an "area of internal drainage" (ArcGIS Desktop Help, 2007). The second step was to calculate the flow direction of the landscape. Flow direction can be described as the direction that water would flow from cell to cell based on the elevation change between grid cells. The third step was to calculate the flow accumulation of each cell. Flow accumulation is the number of cells that flow into each cell; it is a method of describing surface flow patterns based on elevation change between cells. The fourth step was to investigate the flow accumulation model and identify irregularities in the flow patterns.

Using a high-resolution DEM created from a LiDAR dataset has some inherent problems. The data was collected from the air and gaps under bridges and culverts are absent from the data, thus creating barriers to streams. These hydrologic features must be recreated through a process called "Trench Burning" (Figure 2.3) (see Hellweger, 1997; Saunders, 2000; Webster, 2006 for further examples). After "trenches" had been created and burned into the DEM the first four steps were repeated. The entire process was reiterated until the stream network was satisfactory. The accuracy of the watershed was dependant on the amount of time and care taken to create the stream network. For this watershed 5 iterations of the four step process were conducted to get a reliable stream network.

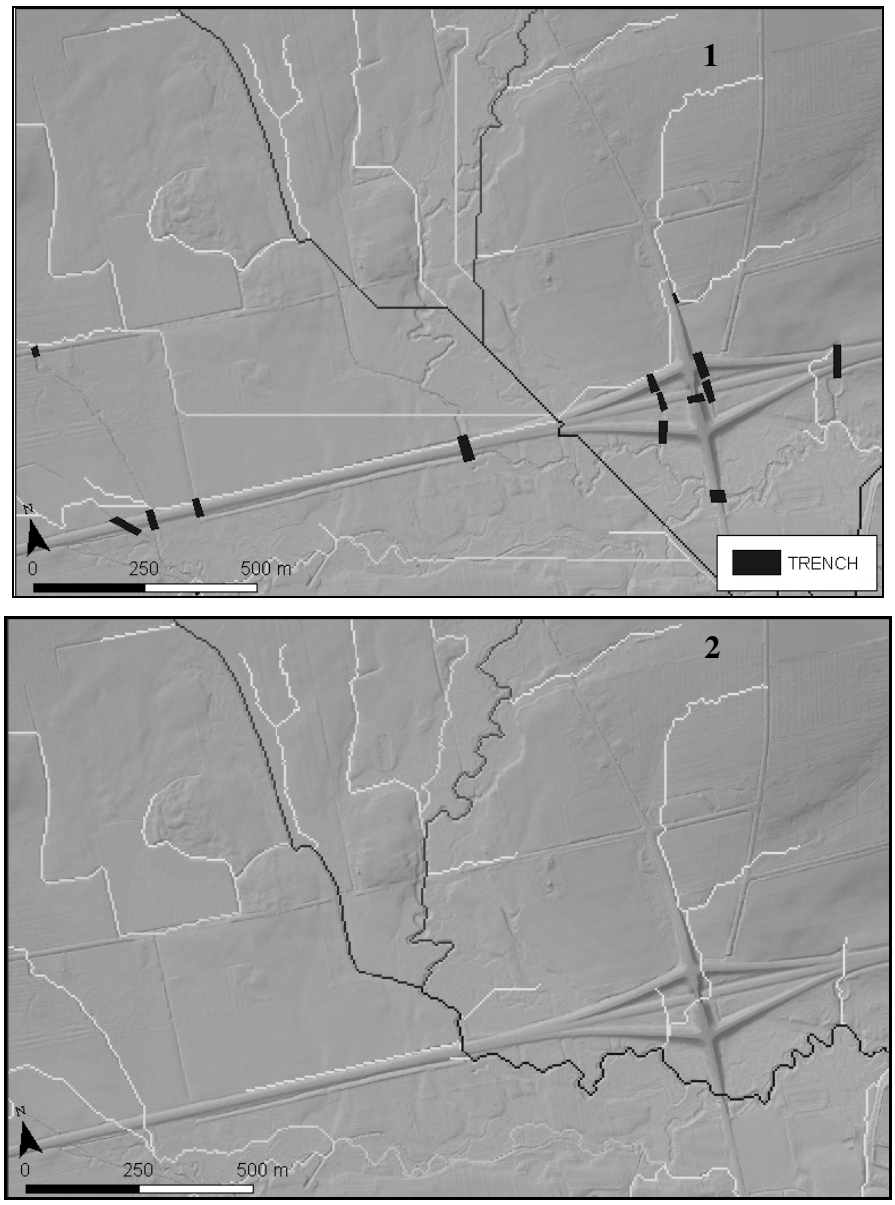

Figure 2.3 DEM Watershed Preparation, "Trench Burning." Image 1 shows the DEM with the stream network before the trench burning process. The polygons were used as the trenches. Image 2 shows the final, cleaned DEM after the trenches had been burned into the surface and the four stage procedure had been repeated.

After the stream network had been created and care was taken to determine that the water course followed the drainage pattern of the landscape the watershed was generated. The watershed was created using a free ArcGIS add-on toolbar, the Hydrologic Modelling Toolbar (available online: http://edndoc.esri.com/arcobjects/9.2/). The Hydrologic Modelling Toolbar allowed the user to do all of the steps mentioned above, and also

create a watershed. For this project only the watershed generation tool was used. On the toolbar there was a watershed delineation button that created a watershed by selecting the desired outflow location, or the lowest reach, of the watershed. The watershed was then automatically delineated, which included all grid cells that contribute flow to the location selected as the outflow location (Figure 2.4). The last step was to convert the watershed from a temporary ArcGIS drawing to a raster and finally a shapefile.

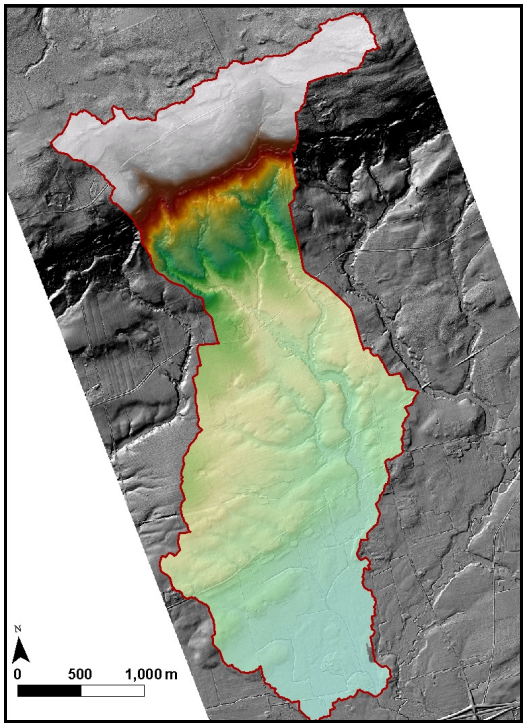

Figure 2.4 Thomas Brook Watershed, 5 m resolution

CHAPTER 3 INVESTIGATING THE INFLUENCE OF SURFACE MOISTURE AND VEGETATION COVER ON AIRBORNE LIDAR INTENSITY DATA

3.1 ABSTRACT

Airborne Laser Scanning (ALS) provides more information about scanned surfaces than just elevation. Backscattered laser pulses are recorded during typical LiDAR scanning and are visually affected by surficial reflectance properties. In this study the impact of soil moisture and vegetation on Optech's ALTM 3100 laser pulse intensity was explored. The study area, an agricultural watershed in the Annapolis Valley of Nova Scotia, was scanned several times over an eighteen month period using comparable survey configuration settings. The intensity data for all data collections were normalized to account for range bias effects and scaled to an 8-bit range. Tests included comparing raw intensity data to range-normalized intensity data, comparing daily data to assess temporal changes in intensity, and correlating intensity data to spatially coincident soil surface volumetric moisture content measurements. The range-normalized intensity data comparison revealed that there are still unresolved issues with the normalization technique, which was highlighted when adjacent flightlines were mosaicked. Temporal intensity variations were observed through change detection methods, however due to vegetation growth on the ground surfaces, it was not always straight forward to isolate the influence of moisture on the intensity signal. Ground sampled volumetric moisture content and intensity were not strongly correlated, however it was shown that the two methods were measuring similar trends over some of the areas studied. This study revealed that while soil moisture conditions can have an influence on the laser intensity signal over bare earth ground cover, the influence of vegetation has a much more pronounced influence on the attenuation and change in signal intensity.

3.2 INTRODUCTION

Airborne Laser Scanning (ALS) is a widely adopted method for producing high-quality, remotely sensed elevation data. ALS has been proven as a powerful tool for many surface centric, landform modeling studies in a variety of geophysical disciplines (Lloyd, 2002; Wack, 2002; Macmillan, 2003; Hollaus et al, 2005; Boyd, 2007). Compared to the amount of research on LiDAR's surface mapping potential relatively little research has been focused on the utility of the backscattered intensity information of the laser pulse that is also collected in the ALS data collection process (Coren and Sterzai, 2005; Kassalainen et al, 2005 & 2007; Hopkinson, 2007; Mazzarini et al, 2007). The recent body of research into the use of laser pulse intensity data has primarily been focused on vegetation classification algorithms (Brennan and Webster, 2007; Hopkinson and Chasmer, 2007). This case study focuses on the effect of the pulse's interaction with the ground surface and vegetation.

Many ALS systems utilize a light pulse emitted in the near infrared wavelength of the light spectrum (e.g. 1.064 um for the Optech ALTM). It is known that due to the absorption properties of water at infrared wavelengths, moisture can affect the reflectance property of soil (Weidong et al, 2002; Whiting et al, 2003; Kaleita et al, 2005). Hopkinson (2007) suggested that intensity values could be relatively normalized without the need for an atmospheric attenuation coefficient, surface roughness value, and true angle of incidence value, as the dominant factor in laser pulse return (LPR) intensity will be the amount of energy emitted. Therefore it is assumed that intensity fluctuations of the LPR (assuming all else being equal) can be attributed to the spectral reflectance properties of the surface that is being scanned. It follows that backscattered near infrared light pulses could possibly be used to identify and map areas of surface saturation and potentially moisture content at the ground surface. For the purpose of this study the term 'surface saturation' is defined as the measureable amount of volumetric moisture at the surface level, as measured by a 10cm ground penetrating TDR probe.

In previous studies gamma radiation (Carroll, 1981), thermal infrared (Price, 1982) and microwave radiation (Jackson et al., 1999) have been used to estimate soil moisture. One of the key benefits of microwave radiation was its ability to penetrate the surface and vegetation at longer wavelengths. This functionality is limited due to resolution; as wavelength increases, penetration through solid objects (i.e. ground and vegetation) increases but footprint size also increases, thus resolution decreases (Kaleita et al, 2005). Remote sensing systems that utilize laser optics and operate in the near-infrared of the spectrum are more spatially accurate than microwave sensors and possess the ability to scan the surface beneath the foliage cover, but cannot penetrate the soil surface.

The question remains, to what extent does surface saturation and landcover alter the intensity properties of ALS data? This case study employs techniques for researching near infrared light pulse technology and provides an assessment of the influence of surface saturation and vegetation on the reflected intensity data.

3.3 OBJECTIVE

In this chapter two primary research questions were addressed; to what extent does soil moisture and landcover alter the intensity properties of ALS data, and does the intensity data reveal a systematic correlation to soil moisture in such a way that zones of surface saturation can be mapped? This case study employed techniques for researching near infrared light pulse technology and provided an assessment of the influence of surface moisture, time, and vegetation on the reflected intensity data.

3.4 METHODOLOGY

3.4.1 LiDAR data collection and system settings

LiDAR missions were flown in 2006 and in 2007 over the Thomas Brook Watershed in the Annapolis Valley, Nova Scotia. The ALTM system settings, flight operation, and the data processing methods were kept constant so that any observed differences in intensity would be due to differences in ground surface level reflectance rather than to hardware or

methodological influences. The first dataset, collected on March 29, 2006 (Julian Day 088), was developed into a Digital Elevation Model (DEM). In a temperate, 4-season climate, collecting LiDAR data in the spring is a good time for producing high-quality DEMs because the leaves on the trees are not yet fully developed which allows more of the surface under the forest canopy to be scanned by the laser. Also, the ground foliage is pressed down from the winter snow-pack, which means that the laser pulses have higher probability of reflecting off of the actual ground surface as opposed to low vegetation (Hopkinson et al, 2005). The survey consisted of 8 survey flightlines collected with 50% overlap. The Optech ALTM 3100 sensor was set to a pulse repetition rate of 50 kHz, a scan frequency of 30Hz, and a scan angle of +/- 18^{o}. The survey was flown using a Piper Navajo aircraft at an air speed of 120 knots and was collected at an altitude of 1300m above ground level. These settings, overlap, and seasonal timing of data collection, were suitable to yield high quality data for DEM generation.

The remaining datasets from 2006 were collected in August (Julian days 221 and 222). Each survey was flown at times of sensor and aircraft availability with the same LiDAR unit and each dataset was collected using the same procedure and apparatus settings. Three flight lines of data were collected for each survey. In 2007 more data was collected over the study area. The first dataset was collected in March (Julian day 090) and two more datasets were collected in September and October (Julian days 273 and 274). The dataset from March was flown with the same ALTM 3100 sensor as the data collected in 2006. The data from September and October were flown using a different ALTM 3100 sensor. All of the system settings and flight configurations remained constant despite the different ALTM sensors. The data was collected with a pulse repetition rate of 70 kHz, scan frequency of 39 Hz and scan angle of +/- 24^{o}. The altitude of these surveys was 900m above ground level with a flight speed around 120 knots.

3.4.2 Intensity data normalization

The LiDAR data was processed twice using Optech's REALM software, once without the range correction (non-normalized) option applied and once with the range correction

(normalized) applied. Raw, uncorrected, intensity data displayed a clear scan angle and range bias which was evident in the form of weaker returns at the outer edge of scans and at lower elevations in the Valley. While flying altitude remained uniform the ground surface elevation varied by almost 210m. The intensity of each return was affected by the dynamic range between the sensor and the target. The range normalization scaled intensity values to an optimal range (typically the average range for the data collection) to account for the influence of range variation due to changing terrain height and scan angle. The normalized datasets demonstrate a uniform range of intensity values throughout the image, whereas the non-normalized data had greater variation in brightness (Figure 3.1). The normalized image showed more detail and definition and consequently a greater amount of information could be extracted from the normalized datasets.

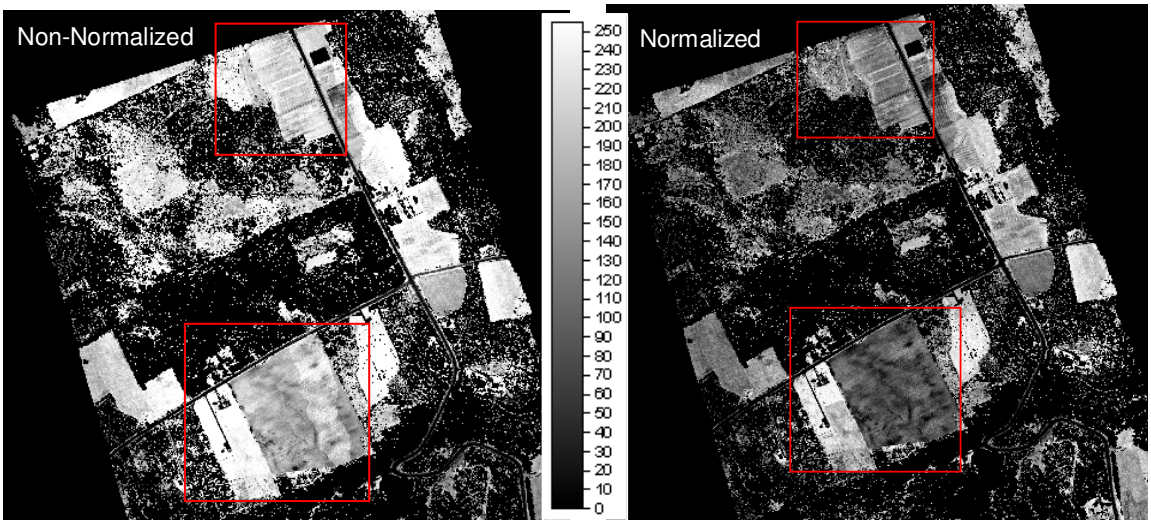

Figure 3.1 The image displays non-normalized intensity data vs. normalized intensity data. The image on the left shows the intensity of the raw data collected on day 148 (2006). The image on the right shows the same data after the normalization has been applied. The boxed areas display areas of good data coverage where the normalization effect can be observed in great detail.

Once the data was normalized in REALM, the intensity values were scaled to a standardized 1 – 255 digital number scale. The scaling was performed to ensure that each dataset was comparable for a change detection analysis. The method for scaling the intensity to 8-bit was a 95th percentile upper and lower bound cutoff. Applied Imagery

QT Modeler software was used to automate this process. By removing the upper and lower extremes of the histograms of each dataset the means are effectively shifted. While there is the potential to cause some of the subtle intensity variations to be masked out during this scaling procedure the method also removed outlying data that could have been caused by multi-path returns or specular reflection off water bodies.

3.4.3 Data filtering

Modern ALS sensors, such as the ALTM 3100, can record multiple returns. Each time the pulse is broken by a surface object a portion of the energy is reflected back to the sensor and is recorded as an echo. The system will record up to four echoes per pulse, first, last and two in-between. This functionality of LiDAR makes the data unique to other remote sensing technologies. Where multiple echoes were returned the outgoing pulse had been split by encountering more than one object in its path and, consequently, the associated ground level data point could not be considered to represent true surficial reflectance conditions. The data was filtered so that all of the data points with multiple echoes were removed.

To ensure that only ground reflected, single echo data points were considered for analysis filtering for data points that were within 1m vertical of the DEM data collected in March 2006 was performed. Single echo returns will occur in fields, on roads, buildings, canopies, etc, which means that all of the "non-ground" single returns had to be filtered out. The results of the filtering are shown in Figure 3. 1. The boxed areas in the figure represent fields where good coverage of single echo data points was retained. The areas adjacent to the boxed areas have sparse data coverage indicating that the area contained large amounts of multiple returned echoes, or the area contained a large amount of non-ground data points (forest or vegetation) and was therefore filtered out of the dataset.

Data collected off-nadir was subjected to longer travel time to the target and back to the sensor, which lead to a greater expense of energy and therefore a lower intensity return. Off-nadir data was also subjected to higher angle of incidence with the target and a

greater chance of foliage aberrations causing signal attenuation, which could cause systematic dampening of the returned intensity. We used multiple flightline data mosaicked into a single dataset and compared the change in intensity from two days of data collection. We then tested single flightline data to mitigate issues with angle of incidence, scan angle signal decay, and footprint size.

3.4.4 Temporal change detection analysis

A temporal analysis, in which a change detection procedure was implemented, was conducted. The intensity data was prepared for analysis with two tests performed on the data, one using multiple flightlines of data for a particular dataset and the other using only one flightline collected at nadir to the study area. The change in intensity was calculated by using the first day of data collection as a base grid, with each subsequent day of data subtracted from it (Figure 3.2). This procedure created a time series that allowed the change in data to be viewed day by day. All else being equal the change in the intensity between collection dates would reveal patterns of reflectance change on the surface.

Figure 3.2 Change detection example image. Figure 3.2-A and Figure 3.2-B are intensity images. Darker colours represent lower intensity returns whereas lighter colours represent higher intensity returns. Figure 3.2-B is subtracted from Figure 3.2-A to generate the change detection image, Figure 3.2-C, "A – B = C". Figure 3.2-C has been coloured so that positive change in the data is white (i.e. higher intensity in 2-B than 2-A) and negative change in the data is black (i.e. lower intensity in 2-B than 2-A). The grey sections are areas of "no data".

3.4.5 Ground reflectance

To identify whether wet surface conditions directly affected laser pulse intensity the following hypothesis was tested: the reflectance variation of soils would be correlated to high and low surface wetness values such that a negative correlation existed between simultaneously collected normalized intensity data and volumetric moisture content percentage (VMC%), whereby high values of VMC% related to low values of LiDAR intensity.

During the collection of two of the datasets from 2007, collected in the spring and fall (March 31, 2007 [090], September 30, 2007 [273]), soil surface moisture was measured simultaneously. These datasets were separated into individual flightlines for each collection day. Only one flightline, collected at nadir to the study area (to mitigate the angle of incidence and footprint size issues), was examined from each collection day. The LiDAR data was prepared for analysis using the techniques outlined above. The VMC soil saturation datasets were collected using a Campbell Scientific Hydrosense 10cm TDR probe and tracked via GPS (RTK Leica 500 series) on March 28-30, 2007 [087, 088, 089] and September 30, 2007 [273]. The coincident LIDAR data within a 1m radius of each GPS point were then isolated. The VMC data was collected throughout three fields within the study area (see 1.2.4 Subplots). The fields were selected based on minimal ground cover (i.e. short height or no vegetation) and accessibility.

To test the hypothesis we did two tests, a regression analysis and a classification comparison, to evaluate the strength of the moisture influence on the laser pulse. The rational of using two tests was that if the relationship was strong we might see the results in the regression test, however if the relationship was weak it might come out in the classification test. If both tests failed than the conclusion would be that there was no influence of surface saturation on laser pulse intensity.

3.4.6 Data classification technique

The VMC datasets were stratified into three categories, low moisture content (LMC) contained all intensity values that corresponded to VMC% values less than 20%, moderate moisture content (MMC) contained all intensity values that corresponded to VMC% values between 20% and 30%, and high moisture content (HMC) contained all intensity values that corresponded to VMC% values greater than 30%. The mean values of the intensity data were calculated for each category. The category break-values were based on stratifying the data across the saturation spectrum capabilities of the Hydrosense TDR sensor. Campbell Scientific reported that typical saturation level is VMC = 50% (Hydrosense Manual, 2001). By assuming that the upper boundary of wetness was saturation level (i.e. VMC 50%) then creating break values of <20% for LMC and >30% for HMC effectively created upper and lower boundaries masking out the mid-range moisture levels.

T-tests were used to identify the significant differences between mean LiDAR intensity values of the LMC versus mean intensity values of the HMC. For this experiment only the mean intensity value of low moisture (LMC) readings and high moisture (HMC) readings were compared. The MMC values were excluded because the intention of the test was to determine the difference between the reflectivity of a wetter soil versus a dryer soil. The theory was that the difference between the means of the LMC and the HMC would show decreasing intensity with increasing VMC%. If the mean intensity of the HMC were consistently lower than the mean intensity of the LMC this would indicate that the data was behaving in agreement with the hypothesis.

The t-tests were calculated on the three subplot datasets for each collection day. Two of the sub-plot fields were vegetated (Barley and Hay fields) while the third was bare soil (Corn field).

3.5 RESULTS

3.5.1 Temporal Change Detection Analysis

In Figure 3.3 the change detection results are displayed from the multiple flightline dataset. The climate data indicated a period of surface drying between the two collection days. The change detection image (Figure 3.3-C) revealed that there was an increase in intensity between the two data collection periods. The trend was that the intensity increased between data collections. All else being equal that would suggest that the surface reflectance had increased between day 221 and 222 which would indicate that the surface was drying out and would be consistent with the weather data that showed a storm event on day 219 followed by warm, dry weather(the precipitation that occurred on day 222 was post-data collection).

In Figure 3.3-A there was a distinct contrast in intensity values from one flightline to the next that split the study area to the right-centre of the field. In the flightline overlap zone the intensity values varied significantly. This data variance displayed prominently in the change detection image, Figure 3.3-C, where the sharp intensity contrast was clearly visible. Despite the control enforced during the data collection and data processing the intensity data remained variable which highlighted that the range normalization function of the REALM software did not account for variables such as angle of incidence or beam divergence.

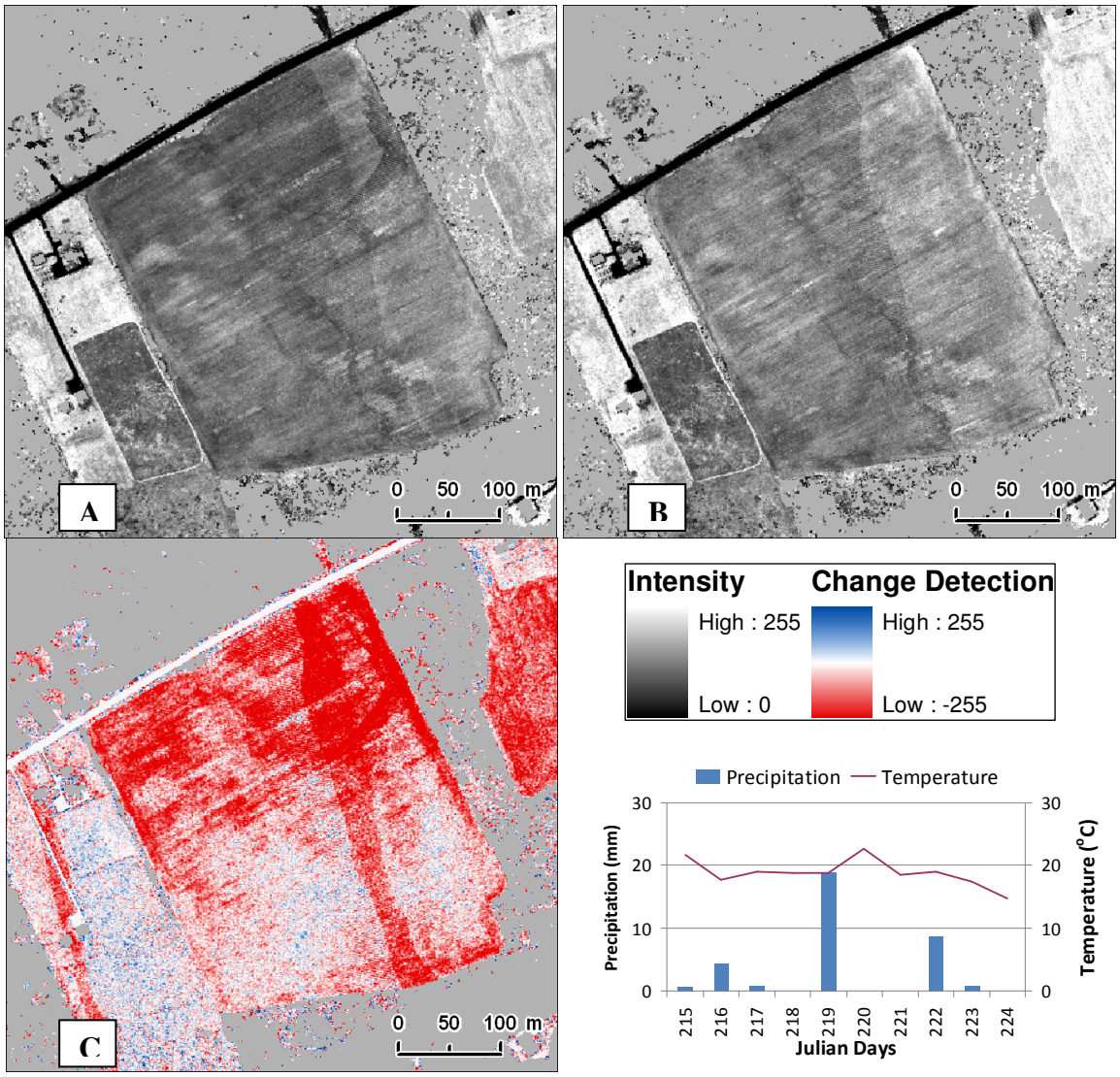

Figure 3.3 Change detection imagery from August 2006 data (Julian days 221 and 222). Figure 3.3-A shows the normalized and scaled intensity data collected on day 221, 2006. Figure 3.3-B shows the normalized and scaled intensity data collected on day 222, 2006. Figure 3.3-C is the Change Detection result. Figure 3.3-C displayed the inconsistent change in intensity data from the combined flightlines, the data collected at the edge of the flightline was affected to a higher degree of vegetation attenuation than that of the data collected directly nadir to the aircraft. The result was an artifact in the change analysis in the area of flightline overlap.

Processing the intensity data from all flightlines of a single dataset revealed a data issue whereby adjacent flightline intensity data may vary significantly. To account for this the intensity data was then re-sampled and processed flightline by flightline (Figure 3.4) rather than as one dataset, to examine how the data responded to the change detection. By isolating flightlines and looking at the data collected closer to nadir the attenuation issue

was mitigated and the change in the intensity of the data between collection days was more likely the result of change in reflectance of the surface rather than change in intensity as an artifact of data collection.

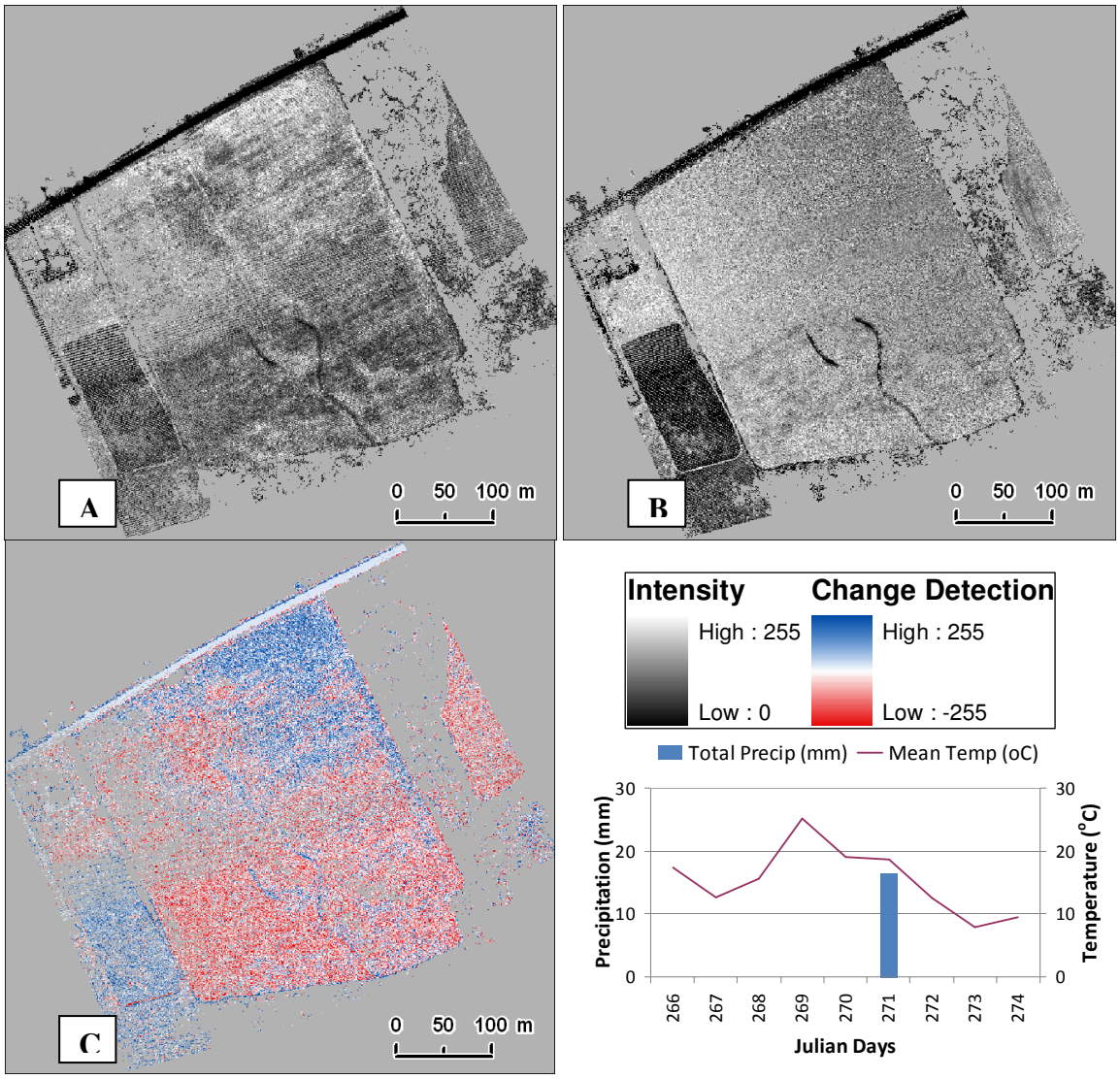

Figure 3. 4 Figure 3.4-A is an image of one flightline of data collected on day 273, 2007. Figure 3.4-B is an image of one flightline of data collected on data 274, 2007. Figure 3.4-C is the change detection image. The harsh intensity artifact was no longer an issue when only one flightline of data was considered for analysis.

In the imagery of Figure 3.4 the sharp contrast in intensity values that was clear in Figure 3.3 were eliminated. By isolating the data into single flightlines one more source of interference was eliminated and the change in intensity between the two collection

days was more likely due to changing surface reflectance than intensity artifacts. There are branches of drainage clearly visible in both images. In Figure 3.4-C the intensity change between Figure 3.4-A and Figure 3.4-B indicated that the reflected intensity had decreased in the northern areas of the field while increased in the southern portion of the field between the two data collection days.

An increase in intensity between the two days was expected as the weather conditions for the two days of data collection indicated a drying out period on the ground. The increase in intensity in the lower (southern) part of the field was also explainable. The laser pulse was being affected by other factors than just surficial saturation. This study area was vegetated and the intensity of the pulse was affected by the vegetation. Another explanation is supported by the increasing slope angle of the field (sloping north to south), which would cause the surface moisture to drain more rapidly in the lower portion of the field than the northern portion (Figure 3.5).

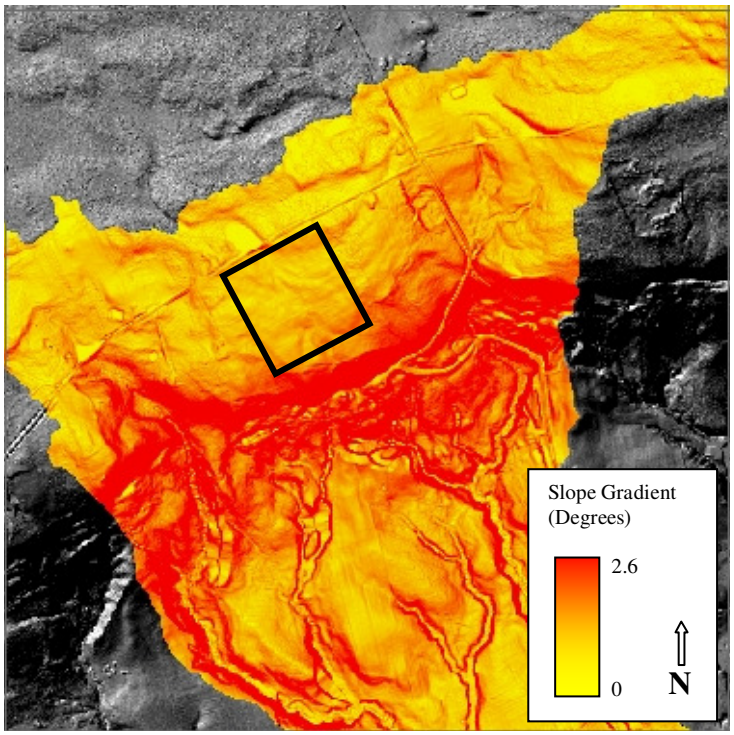

Figure 3.5 Slope gradient map of the TBW. The barley field study area is highlighted. As indicated by the slope model the gradient of slope in this field ranges from nearly level in the northern portion of the field to between 1° and 2.6° in the southern portion of the field.

3.5.2 Ground reflectance

The results of the surface reflection regression test are summarized in Table 3.1. The results showed that there was little direct correlation between the normalized intensity data and the ground sampled VMC% data suggesting that soil wetness was not a strong influence on reflectance in the near-infrared light spectrum. Despite low direct correlation between normalized intensity and VMC%, the regression models did reveal some indication that the data was performing in accordance with the theory (i.e. low intensity values where VMC% values were high).

Field Landcover	Collection Day	Flightline ID	R^2
Barley	090	4	0.000
Barley	273	3	0.007
Corn	090	5	0.110
Corn	273	4	0.161
Hay	090	4	0.157
Hay	273	3	0.005

Table 3.1 Regression analysis summary table for two data collection days (090, 273) and three subplots

Using the T-tests a relationship between surface reflectance and surface saturation was identified. The results from the corn field revealed that the data did agree with the hypothesis for both collection days (Table 3.2), the relationship was negatively correlated and the means were significantly different. A box-plot showed that the mean of the LMC was higher than the mean of the HMC. This indicated that where VMC% was low mean intensity was high and vice versa.

Field Landcover	Collection Day	Low Moisture Content			High Moisture Content			P-Value
		Mean	St. Dev.	N	Mean	St. Dev.	N	
Barley	090	20.68	1.60	6	20.96	2.51	382	0.696
Corn	090	**9.34**	1.79	33	**7.93**	1.90	185	**0.000**
Corn	273	**8.71**	1.50	35	**7.18**	0.98	11	**0.001**
Hay	090	**15.48**	1.23	122	**14.91**	1.53	33	**0.055**

Table 3.2 T-test summary table for significant difference of mean intensity values. The mean intensity data was higher where low moisture content was measured on both data collection days for the corn field and on the first collection day for the hay field. The mean intensity data in the barley field revealed negligible difference between the high and low moisture content.

The barley field and the hay field results showed that the mean intensity values for the HMC and LMC were not significantly different (Table 3.2). These results were not unexpected for these two subplots when the ground cover was taken into consideration. Both fields had low vegetation cover, too low for the data to be discerned and separated during the processing control procedures. The low vegetation caused a layer of separation between the laser pulse data and the ground sampled TDR moisture probe data, which lead to the signal attenuation that caused the discrepancy between the airborne data and the ground data.

3.6 DISCUSSION

Throughout this investigation we have demonstrated several methods of viewing laser pulse intensity data for analysis of change in reflectance caused by surface conditions. This case study has explored some of the influences on intensity and we now have a better understanding of the surface/laser pulse interaction.

The range normalization technique used to adjust the intensity values to account for the range bias effect worked to some degree. The change detection test demonstrated that despite the normalization process some ground surface reflectance effects could not be accounted for; this led to observations of intensity artifacts in the overlapping areas of multi-flightline datasets. The variability of intensity values between flightlines of data

was not accounted for in the normalization technique, which should be a consideration when utilizing this type of data for classification and mapping purposes.

In Figure 3.4 the climate data between the two days of data collection indicated a period of surficial drying, yet the change in intensity between the two collection days (Figure 3.4-C) revealed a large portion of the field where the intensity values decreased. There were two potential explanations for this occurrence, one based on the physical ground conditions and the other caused by systematic influence. The systematic cause would be the scaling of the intensity data to the 8-bit range, which could have artificially amplified low intensity returns in one dataset and not the other. The other explanation could be that the climate conditions between the two days may have revealed a drying out trend, however the low-level vegetation in the field (~60cm tall barley) could have acted to increase the signal return. The spectral influence of low-level vegetation will cause the intensity signal to increase. This effect that low vegetation has on near infrared light pulses could have acted to increase the signal return values in one area of the field and not the other area of the field due to the angle of incidence with the surface. More energy will be associated with a high angle of incidence (Kaasalainen, 2005) and in turn the signal will be further amplified by the vegetations reflectance properties. This would cause the intensity signal to be affected and increase in one portion of the field and not the other. This effect could mask the climatic conditions which indicated a drying out period and thus an increase in surface reflectance.

In the corn field sub plot the ground cover was bare earth, no vegetation, during the first data collection period and corn stalks (~2m height) during the second data collection period. The processing control procedures were used to remove data that reflected off of the corn and left only data that reflected off of the ground surface. Even though strict processing controls were employed to extract LiDAR data points that returned off the ground surface the discrete pulse return ALTM sensor cannot distinguish split pulse returns spaced less than approximately 1.5m apart. This means that some of the data points collected in the corn field will likely be influenced by the corn stalks, which could

lead to an elongated and attenuated signal (Figure 3.6). A pulse encountering tall crop vegetation would most likely display a reduced amplitude return compared to a pulse reflecting off the ground. In Figure 3.6-C the theoretical bare ground and vegetated returns are compared. The vegetated signal's peak intensity value is dampened compared to the unaffected signal due to the structural reflectance interference of the corn stalk. This phenomenon could lead to systematic intensity signal dampening over surfaces with tall vegetation cover. This will only occur in areas of tall ground level vegetation (such as corn crops) because short vegetation (such as lawn grass) will not structurally attenuate the signal but the spectral characteristics of the short vegetation target will increase the amplitude of the return; case in point the Barley field study (Figure 3.4).

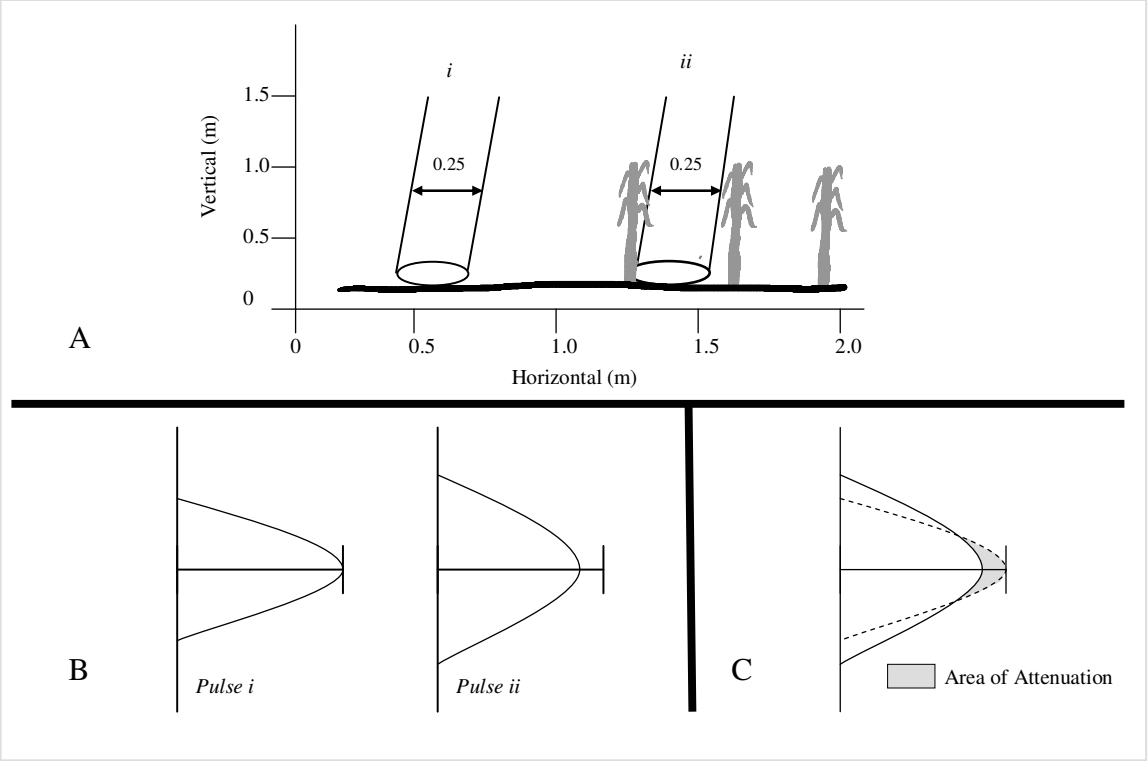

Figure 3.6 Signal return attenuation from vegetated surfaces. Figure 3.6-A is a diagram of two laser pulses reaching the ground surface. *Pulse i* is not affected by vegetation whereas *Pulse ii* is affected by low surface vegetation under 1m in height. Figure 3.6-B displays the same two pulse's signal as read by the sensor. *Pulse i* signal peaks at maximum return potential whereas *Pulse ii* signal amplitude is reduced due to the influence of ground foliage. Figure 3.6-C is a direct comparison of the two pulse signals. The area of attenuation denotes the signals affected portion of energy.

Despite this vegetation issue, laser pulse returns would have still reached the surface unaffected by foliage. Many of the airborne laser pulse data, especially collected over the corn field, were measuring the same surface phenomenon as the ground sampled VMC% data. This was shown in the data comparison between the ground sampled VMC data and the extracted intensity data. In the corn field the mean of the LMC data were higher than the mean of the HMC data, indicating a negative relationship. That would suggest that when the VMC% data was high (i.e. wetter surface condition) the laser pulse intensity data was low, and vice versa. For the data collected on day 090 this observation indicated that the laser pulse intensity data was capturing the surface reflectance change caused by the surface moisture as there was no vegetation on in the field at time of collection. However, on day 273 the corn had grown to about 1.5m and the correlation between HMC and low intensity signal cannot 100% be attributed to the ground moisture as the vegetation would have attenuated the pulse signal and caused a dampening of the intensity. The vegetation clearly plays the dominant role in influencing the intensity signal in the two other study area fields. Neither field's intensity data correlated with the ground sampled VMC data.

These observations of vegetation's ability to attenuate near infrared signals has lead to research on the intensity signal for vegetation classification (Brennan and Webster, 2006; Antonarakis *et al,* 2008; Wu *et al*, 2009). Clearly we have demonstrated that not only vegetation affects the signal intensity, but also surficial moisture conditions. Intensity can potentially be used for classification but such methods cannot be universally applied because of the systematic controlling factors on intensity, such as the spectral and structural affects of vegetation. Many authors incorrectly implicitly assume that the surface reflectance characteristics play the dominant role in the intensity signal (e.g. in tree classification) but we have shown that pulse splitting and attenuation actually reduces the intensity signal even though the surface spectral reflectance of vegetation might be higher. Tall ground vegetation affects the structural properties of the pulse

return by elongating the reflecting surface along the travel path, whereas increased moisture conditions affect the spectral response by absorbing the near infrared energy.

3.7 CONCLUSION

A series of tests were conducted on the intensity signal measuring surface reflectance change. The ground reflectance tests revealed that intensity was affected by surface reflectance change on bare soil caused by surface saturation. Statistical tests showed that the mean intensity value of the LMC was higher than that of the mean intensity value of the HMC. The difference in the means was shown to be significantly different which indicated that the surface reflectance had changed due to the change in moisture content.

However, on a short-height vegetated surface the tests were not able to show the same results. The mean intensity of the LMC points was not significantly different from the mean intensity of the HMC points. This result meant that the surface reflectance was being affected by some other factor that moisture. The vegetation most likely caused aberrations in the intensity signal. Vegetation caused the signal to be affected two ways; the signal can be spectrally amplified by short level vegetation or structurally dampened by taller vegetation (under 1.5m).

The temporal analysis revealed that intensity data was best studied on a flightline by flightline basis, rather than a full mosiacked dataset, as systematic intensity artifacts from adjacent flightlines can lead to problems when attempting to identify ground reflectance change. While the data normalization was utilized to mitigate the range bias effect, the technique was not as successful at mitigating the scan angle effect. The evidence was clear in Figure 3 where there was an artifact that affected the change detection. The change detection analysis also showed that subtle changes in intensity can be masked by the spectral and structural reflectance of vegetation.

This study has shown that factors such as survey configuration, vegetation cover, and soil moisture need to be considered if intensity based change detection or land surface

classification is to be carried out. These revelations about ALS signal intensity have shown that the ability to map zones of surface moisture directly was not universal and not applicable to the watershed that was monitored. Vegetation played a dominant role in influencing the backscattered intensity of the pulse signal, which therefore affected the signals ability to monitor the direct influence of surface saturation. In areas where there was no vegetation cover or tall vegetation cover that could be filtered, the intensity signal was shown to be affected by the surface reflectance influenced by surface moisture.

CHAPTER 4 MODELLING TOPOGRAPHIC DERIVATIVES FOR SURFACE SATURATION MAPPING

4.1 ABSTRACT

The production of accurate maps of soil saturation zones within an agricultural watershed would be very useful for many applications. Agricultural watersheds are generally highly modified environments. Accurately modelling topographic features in these environments can be difficult due to surface modifications inherent to agricultural practice. This study examines whether a 5m DEM was an appropriate scale for mapping surficial saturation zones. In March of 2006 a LiDAR dataset was collected in the Thomas Brook Watershed located in Annapolis Valley, Nova Scotia. This data was collected over the watershed for DEM production and modelling. Multiple topographic indices including topographic wetness index, slope gradient, curvature, and catchment area were modelled at 5 m resolutions. The models were then compared to ground sampled volumetric moisture content data that were collected and surveyed (via GPS) during the 2006 and 2007 field seasons. The modeled topographic indices were shown to have poor linear relationships with the VMC data. Student's T-test's revealed that the models were mapping the surficial saturation distribution; however it was unclear whether the 5m DEM was the appropriate modeling resolution for this topographic data. Data collected throughout a tilled field revealed the strongest relationship to the ground sampled data.

4.2 INTRODUCTION

4.2.1 Soil Surface Saturation and Topography

Topography plays an important role in surface moisture movement and distribution throughout a watershed. There are many influencing factors that contribute to topography's control on moisture movement. Modelling a surface's moisture distribution potential would require identifying the influencing topographic factors to moisture movement. A model built using topographic derivatives may be able to successfully map a surface's potential for saturation. The challenge is to identify the most dominant topographic controls on moisture movement and generate a topographic model that is accurate and captures the movement potential of water throughout the landscape.

Many topographic models can be generated from a DEM. Topographic models represent different aspects of the surface and can be used to obtain information about landforms and characterize the landscape. Florinsky *et al* (2004) identified that slope gradient, curvature, and catchment area were three features that could be closely correlated to soil moisture. Topographic wetness index has been long used for hydrological modelling, rarely however, has its use been documented in high-resolution DEM studies (Quinn *et al*, 1991). Four topographic models were identified as key components to hydrologic landscape classification; "slope," "curvature," "catchment area," and "topographic wetness index".

The scale of a DEM is important. In section 2.1.1 it was demonstrated that the vertical resolution of the 5 m DEM was on the order of 20 cm. This LiDAR dataset was capable of generating a DEM at 1 m or better horizontal resolution DEM. The question remained, however, if a 5 m resolution DEM was an appropriate size for modeling topography and capturing surface moisture variability. The rationale for this was that 1 m DEM's are not widely available, while coarser, 5 m and 10 m DEMs are more common. Therefore if this study could show that these topographic models could capture the spatial variability of surface moisture at the coarser resolution the applicability of this study would be much wider.

In this Chapter the four topographic parameters, slope, catchment area, curvature, and topographic wetness, were each modelled from the same DEM. The 5 m resolution was upheld for the study. Ground sampled soil moisture and GPS data was then used to assess how well each layer was modeling surface moisture.

4.2.2 Objectives

The objective of this study was to generate a topographic model to be used for identifying zones of surface moisture in a small agricultural watershed in the Annapolis Valley, Nova Scotia. This objective was completed in two stages, which are described in this Chapter and Chapter 5. The first stage, described in this chapter, utilized the LiDAR data for the terrain modelling, delineating the watershed boundary from the DEM, and generating the four topographic models for comparison to ground sampled soil moisture data. In the second stage, as described in the next chapter, the topographic models were used to augment a landform classification algorithm to generate a surface saturation classification map.

4.3 MATERIALS AND METHODS

4.3.1 Soil Moisture Data Collection

During the 2006 and 2007 field seasons the TBW was surveyed for soil surface moisture using a handheld 12 cm ground penetrating Campbell Scientific Hydrosense soil moisture probe. The Hydrosense probe comes fully calibrated and collects data using the Volumetric Moisture Content Percentage (VMC %) data type. Campbell Scientific reported that saturated soils would typically possess a VMC percentage of 50%.

On August 11, 2006, 101 soil surface moisture readings were collected in the Corn field in TBW. Throughout the 2007 season 11 more datasets were collected in the Corn Field plus two other fields throughout the TBW (the Barley Field and Hay Field). Up to 161

data points were collected per day in the three subplots in random patterns to ensure capture of the overall moisture conditions (Figure 4.1). Each soil moisture data point was surveyed into position with a Leica 500-series dual-phase GPS system operating in Post-Processed Kinematic (PPK) mode. This GPS apparatus setup is capable of yielding high accuracy GPS measurements to the sub-decimetre (<10 cm) level.

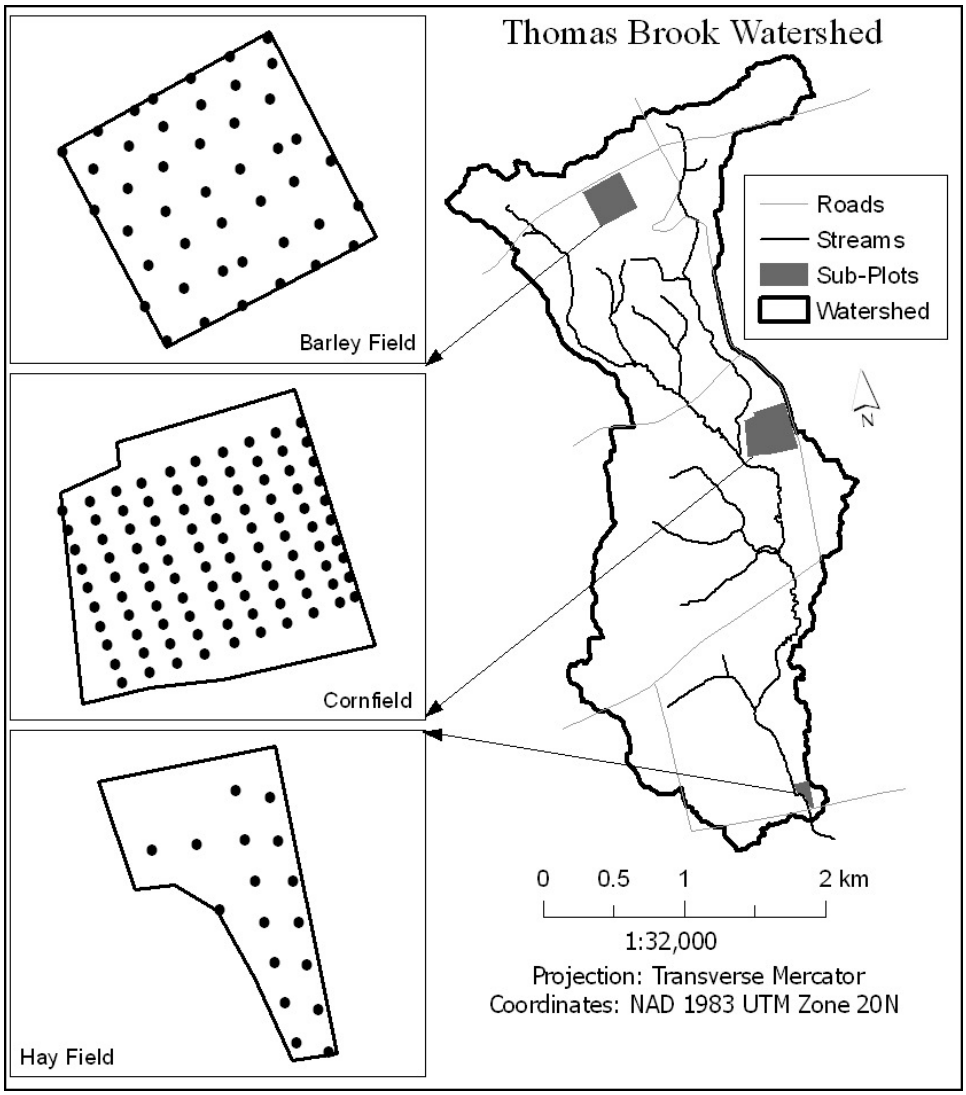

Figure 4.1 Map of VMC sample locations throughout the TBW.

4.3.2 Topographic Models

Using the LiDAR derived DEM the topographic parameters were modeled. All of the GIS layers were created using ESRI's ArcGIS 9.2 software. For this study the DEM was

generated as per the methodology in section 2.1 Digital Elevation Model Generation, and the resolution was set to 5 m.

Each model was generated using two different directional flow methods. The traditional D-8 method modeled the directional flow of water into one of eight cardinal directions from a central cell in a grid-based DEM. The direction will be the steepest downward descent to the adjacent cell. The second method, the D-Infinity method, allows the flow direction to be assigned to multiple cells based on a triangulation faucet technique (Tarboton, 1997). Both the D-8 and D-Infinity methods were tested to determine if one method yielded superior results to the other.

4.3.3 Slope

In raster GIS a slope model is defined as the maximum rate of change between a cell and its neighbour cells (ArcGIS Desktop help, 2007). Slope is an important factor in hydrology as it determines the natural direction that water will flow across a landscape (Figure 4.2).

The theory of the slope gradient attribute is that when the slope gradient is a low value the surface is relatively flat. When the slope gradient value is higher the surface is steeper. Generally water will tend to be stored on flatter surfaces longer than on steep surfaces. Therefore the theory is that when the slope gradient is low the VMC% value will be high and when the slope gradient is high the VMC% value will be low.

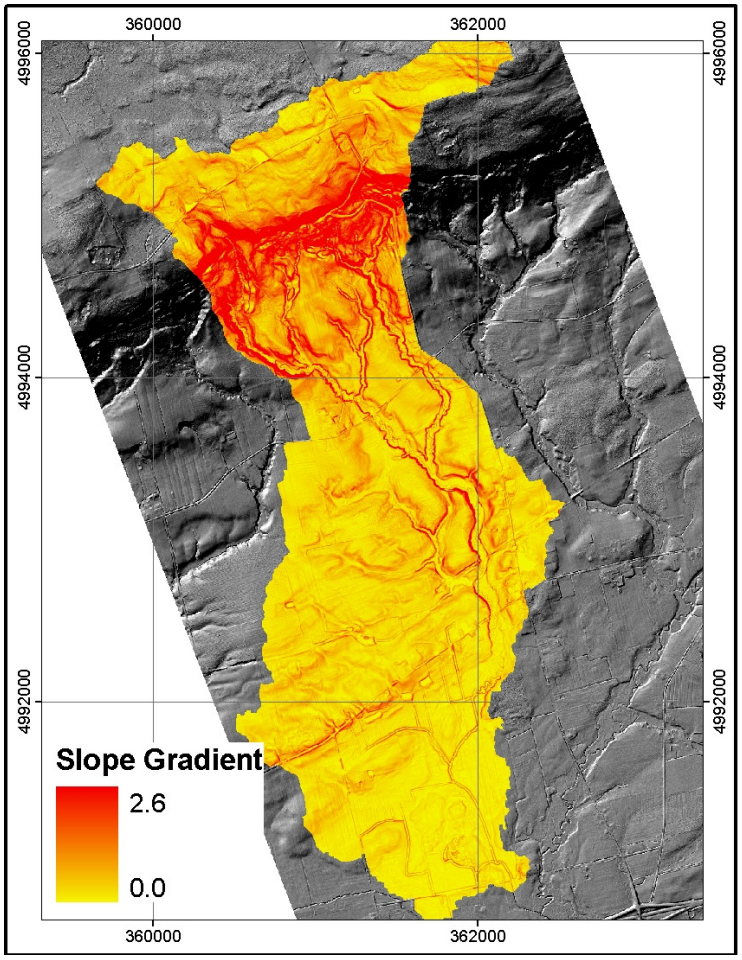

Figure 4.2 Slope Gradient Layer

4.3.4 Catchment Area

The calculated catchment area of a raster is the number of upslope cells that flow into a cell. The catchment area of a specific cell gives an indication of the surface area contributing flow upslope from that cell. A cell with a large catchment area value has many cells "flowing" into that cell, thus indicating that the cell may be a part of a stream network or drainage channel (Figure 4.3). A cell with a small catchment area value has only a small upslope contributing area and cells are mostly flowing away from that cell, indicating that the cell is probably not part of a stream network. This topographic layer was modelled using both the D-8 and D-Infinity methods.

Catchment area is an indication of watercourse and moisture movement potential in a watershed. The theory for this attribute is that when catchment area values are high (many cells flowing into one cell) then the corresponding wetness value for that cells location should also be high.

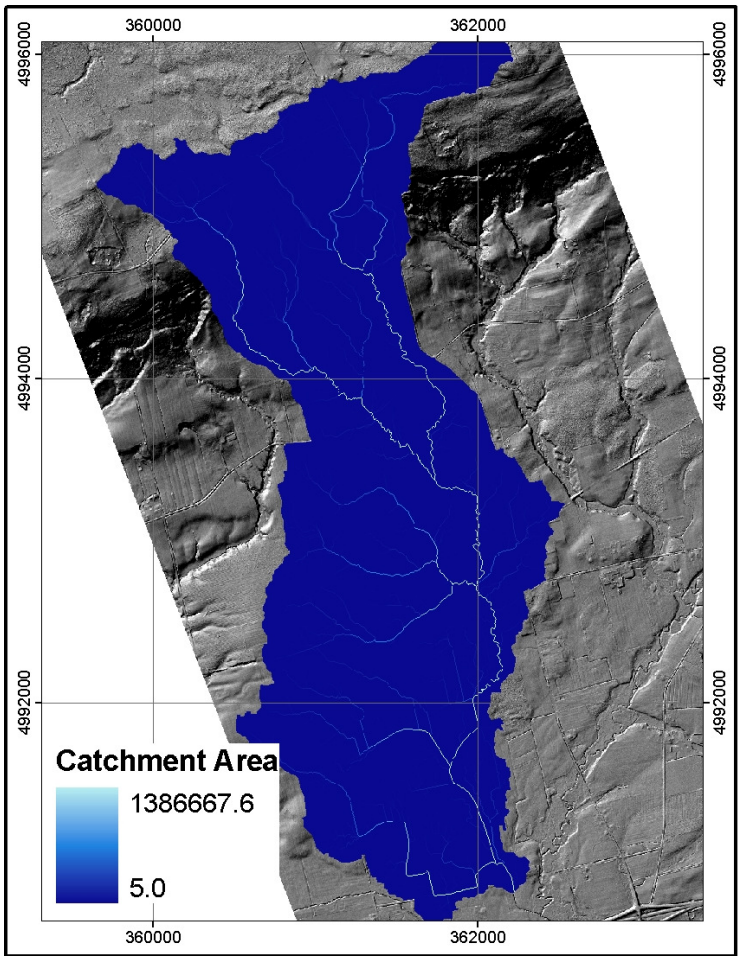

Figure 4.3 Catchment Area Layer

4.3.5 Topographic Wetness Index

The Topographic Wetness Index (TWI) is a surface modelling technique that combines the slope gradient model and the catchment area model. The TWI uses the two aforementioned grids to predict drainage channels throughout a landscape (Figure 4.4). The TWI method used was adopted from Beven and Kirkby's 1979 TOPMODEL method. The TOPMODEL wetness index is expressed as the natural log of the area

draining through a point divided by the tangent of the local slope gradient (Beven, 1997) (Equation 4.1). The TWI model has been used with varying degrees of success at coarser grid resolutions (Zhang and Montgomery, 1994; Quinn et al, 1995; Franchini et al, 1996; Beven, 1997; Ibbit and Woods, 2004). For this test the TWI was modelled using the two directional methods, D-8 and D-Infinity.

The TWI is a combination of the catchment area grid and slope grid. The grid cells correspond to predicted flow patterns whereby grid cells with high values of TWI indicate areas of high probability to be flow channels and cells with low values indicate areas of low probability of flow. Therefore the theory of the TWI test was that when the TWI values were higher the soil moisture values at the same location should also be high, and when the TWI values were lower the soil moisture values should also be low.

$$TWI = \ln(\alpha/\tan\beta)$$

Where:

TWI = Topographic Wetness Index
α = Slope gradient in degrees
β = Upslope contributing area

Equation 4.1 The TOPMODEL Equation (Beven and Kirkby, 1979)

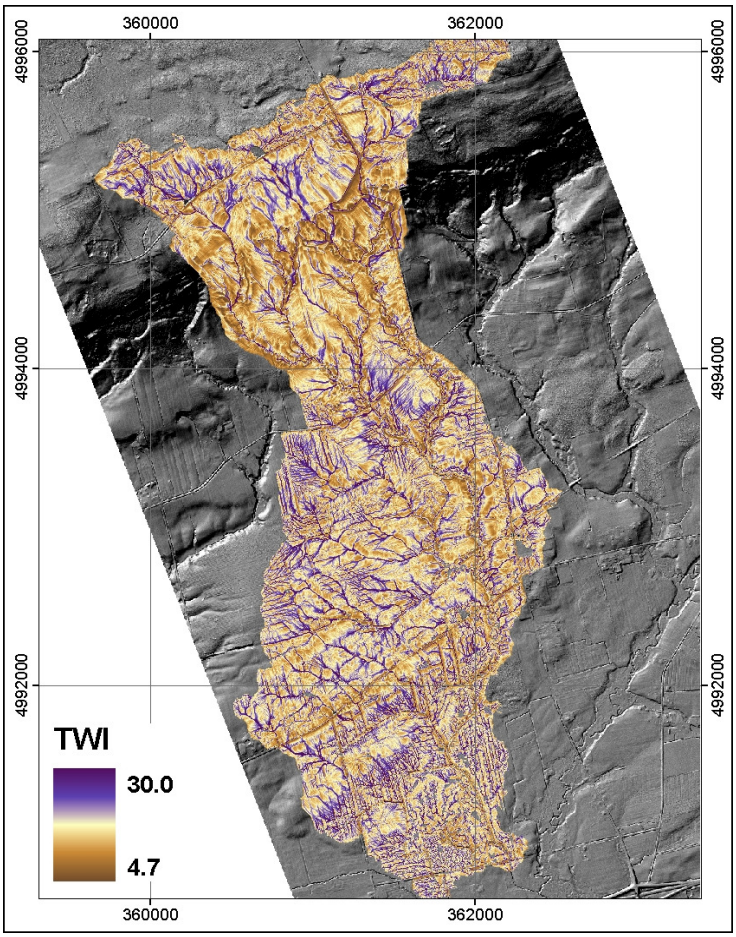

Figure 4.4 Topographic Wetness Index Layer

4.3.6 Curvature

The curvature of a surface is an indication of the shape of that surface. It is a topographic attribute that describes the slope of a landscape as being concave, convex or linear (Figure 4.5). The shape of a slope will affect the way water interacts with it. Water will tend to accumulate in areas of concave curvature and will disperse from areas with convex curvature. In ArcGIS the curvature tool is used to create a second derivative of the DEM surface or "the slope of the slope" (ArcGIS Desktop Help, 2007). The tool outputs two rasters. One raster which describes the slope parallel to the maximum slope, the "profile slope", the other raster describes the slope of the surface perpendicular to the maximum slope, the "planar slope". Combining these two rasters will create a surface that describes each cell's shape in two directions as being a combination of convex,

concave, or linear (Figure 4.6). Once the two rasters are combined the grid values represent the shapes displayed in Figure 4.6.

The theory is that the corresponding VMC% value would be high in areas of concave slope and low in areas of convex slope. To test this theory each of the curvature values were ranked in moisture holding potential (from best to worst = 51, 11, 55, 15). The curvature values were then used to classify the VMC% values into the four shape classes (Concave - concave, Convex - concave, Concave - convex, Convex - convex).

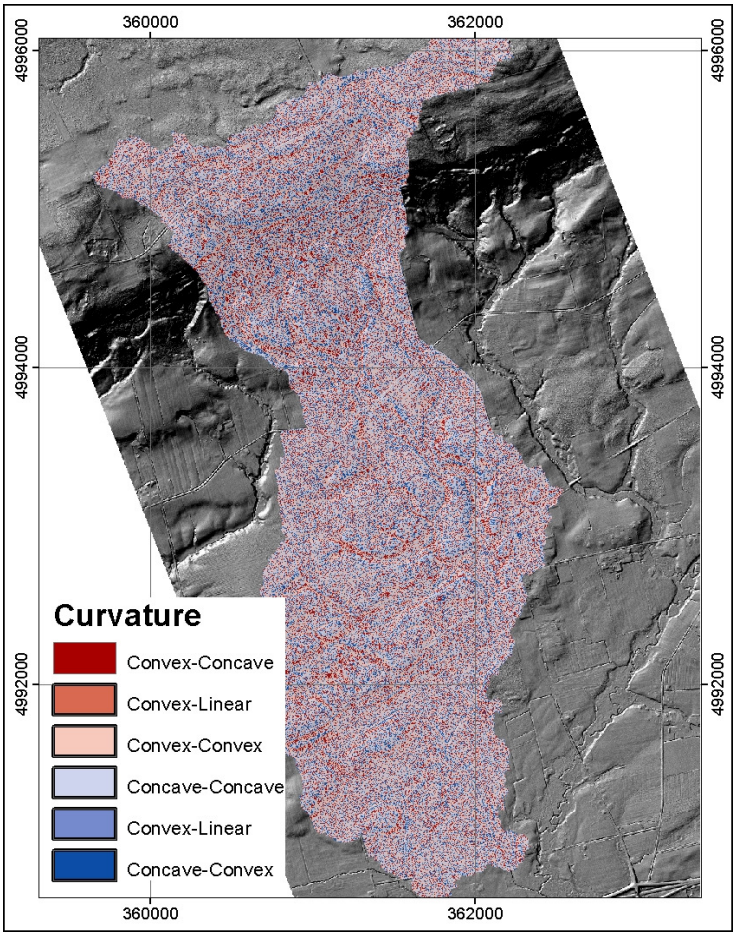

Figure 4.5 Curvature Layer

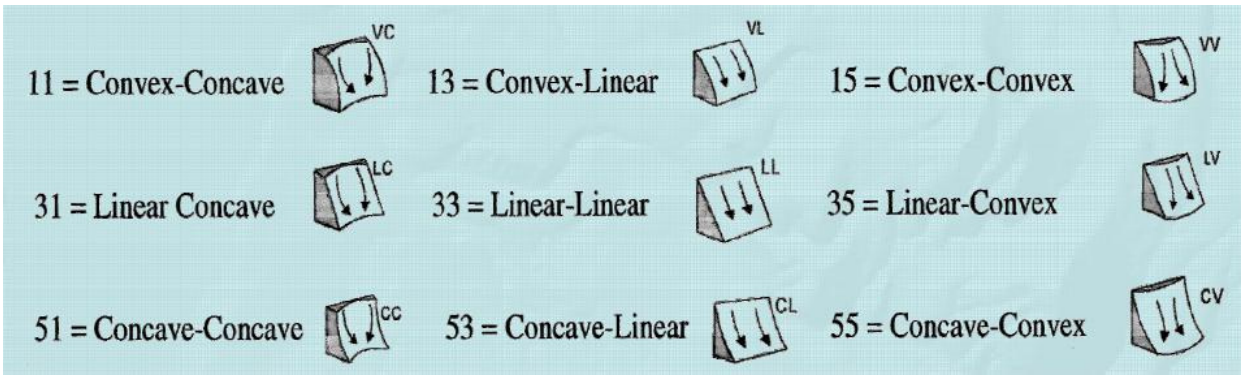

Image: USDA, 2007

	Convex	Linear	Concave
Profile Grid	1	3	5
Planar Grid	5	3	1

Figure 4.6 Slope curvature classification technique developed by the USDA, 2007.

4.3.7 Statistical Methods

Each of the topographic model layers was compared to the ground sampled soil moisture data using an independent 2-sample t-test. This was performed to test the hypotheses of each model theory of surface wetness. The first step for this test was to determine a threshold wetness value for each dataset (W). This threshold value was generated by averaging all VMC% data for each field per day (Table 4.1). The data was then classed as 'low-wetness', 'medium-wetness', or 'high-wetness' depending on whether each VMC% value per field was less than, equal to or greater than W +/- 2.5. The second step was to compute the average and standard deviation of the topographic model values that corresponded to the low-wetness and high-wetness values. Statistically significant differences were tested at the 95% level using Minitab 15 Statistical Software.

Date	Hay Field	Corn Field	Barley Field
11-Aug-06		37.4	
28-Mar-07	54.9	31.9	
29-Mar-07		26.8	34.3
30-Mar-07	45.8	26.2	
15-Apr-07	57.1	33.0	
20-Apr-07	54.8	29.7	
31-May-07		20.2	
29-Jun-07	28.7	22.9	15.6
10-Jul-07		17.4	
15-Jul-07		20.9	
30-Sep-07	33.9	25.0	21.4
26-Nov-07	46.2	34.3	34.3

Table 4.1 Volumetric Moisture Content mean values (per field per day)

The test for how curvature related to soil moisture was done using a different approach. This test was conducted by averaging all of the VMC% values that corresponded to the 4 curvature types. The types were ranked from highest potential to store water to lowest. To agree with the theory the highest average VMC% value should correspond to the highest ranked curvature type (i.e. the Concave – concave type).

4.4 RESULTS

4.4.1 Slope Gradient Summary

The results are presented in the tables below. The dates where the results matched the theory are shaded grey. The P-values significant at the $\alpha = 0.05$ level are in bold. The slope gradient attribute test yielded results that were consistent with the theory. In Table 4.2 the data is displayed for all the ground data collection days in the corn field. On every collection day the average low wetness conditions corresponded to higher average slopes. This observation was true for both the D-infinity and the D-8 directional methods. The strength of the observations was not strong. Only 6 of 12 tests had significantly different means, as shown by the p-values.

	D-Infinity Method			D-8 Method		
Date	Low Wetness	High Wetness	P-Value	Low Wetness	High Wetness	P-Value
11-Aug-06	0.05	0.02	**0.00**	0.04	0.02	**0.00**
28-Mar-07	0.06	0.03	0.08	0.05	0.03	0.08
29-Mar-07	0.06	0.03	0.08	0.06	0.03	0.08
30-Mar-07	0.06	0.03	**0.03**	0.06	0.02	**0.03**
15-Apr-07	0.06	0.03	0.11	0.06	0.03	0.10
20-Apr-07	0.06	0.03	0.11	0.06	0.03	0.10
31-May-07	0.04	0.03	0.08	0.04	0.03	0.09
29-Jun-07	0.04	0.02	**0.01**	0.04	0.02	**0.01**
10-Jul-07	0.04	0.03	0.16	0.04	0.03	0.15
15-Jul-07	0.04	0.03	**0.03**	0.04	0.03	**0.03**
30-Sep-07	0.04	0.02	**0.01**	0.04	0.02	**0.01**
26-Nov-07	0.05	0.02	**0.01**	0.05	0.02	**0.01**

Table 4.2 Corn Field Table, Slope Gradient

Table 4.3 displays the results for the Barley field. Of the 4 collection days 3 had observations that were consistent with the theory, using both the D-Infinity and D-8 methods. However, the p-values revealed that only 2 of the 4 dates had significantly different means.

	D-Infinity Method			D-8 Method		
Date	Low Wetness	High Wetness	P-Value	Low Wetness	High Wetness	P-Value
29-Mar-07	0.06	0.08	0.18	0.06	0.07	0.19
29-Jun-07	0.08	0.05	**0.01**	0.08	0.05	**0.01**
30-Sep-07	0.08	0.05	**0.02**	0.08	0.05	**0.02**
26-Nov-07	0.07	0.07	0.93	0.07	0.07	0.91

Table 4.3 Barley Field Table, Slope Gradient

Table 4.4 shows the slope gradient data for the Hay field. There were 7 days of collection in the Hay field. All 7 days showed that the low wetness corresponded to higher slope values and that the higher wetness corresponded to lower slope values. This observation was consistent with the theory. However, once again the p-values showed that none of the means were significantly different.

	D-Infinity Method			D-8 Method		
Date	Low Wetness	High Wetness	P-Value	Low Wetness	High Wetness	P-Value
28-Mar-07	0.04	0.02	0.45	0.04	0.02	0.45
30-Mar-07	0.02	0.01	0.46	0.02	0.01	0.46
15-Apr-07	0.04	0.01	0.20	0.04	0.01	0.20
20-Apr-07	0.05	0.01	0.19	0.05	0.01	0.19
29-Jun-07	0.03	0.03	0.84	0.03	0.03	0.83
30-Sep-07	0.03	0.01	0.50	0.03	0.01	0.50
26-Nov-07	0.04	0.02	0.48	0.04	0.02	0.48

Table 4.4 Hay Field Table, Slope Gradient

4.4.2 Catchment Area Summary

The results for the Catchment Area test were varied. Table 4.5 shows the results from the Corn Field for 12 dates of field collection separated into the two topographic methods (D-Infinity and D-8). Results generated from the D-8 method were more consistent with the theory. However neither of the two methods shown strong results, as shown by the weak p-values.

	D-Infinity Method			D-8 Method		
Date	Low Wetness	High Wetness	P-Value	Low Wetness	High Wetness	P-Value
11-Aug-06	106.0	305.0	0.18	21.9	60.0	0.21
28-Mar-07	39.7	88.0	0.35	6.3	12.8	0.54
29-Mar-07	58.8	62.0	0.94	10.4	12.9	0.83
30-Mar-07	57.1	57.0	0.10	10.9	11.9	0.93
15-Apr-07	56.3	20.1	0.17	12.1	2.0	0.10
20-Apr-07	32.1	94.0	0.23	6.1	12.8	0.53
31-May-07	41.0	275.0	0.13	8.3	51.0	0.16
29-Jun-07	115.0	112.0	0.98	23.0	24.3	0.95
10-Jul-07	93.0	130.0	0.73	20.7	23.9	0.87
15-Jul-07	105.0	285.0	0.27	23.8	58.0	0.32
30-Sep-07	106.0	32.3	0.19	22.8	5.8	0.15
26-Nov-07	24.1	323.0	**0.04**	4.3	66.0	**0.04**

Table 4.5 Corn Field Table, Catchment Area

Table 4.6 shows the results from the Barley Field. The two methods, D-Infinity and D-8, yielded results that disagreed with the theory 75% of the time. Only 1 in 4 tests had low mean moisture values when the mean of the catchment area values were low. The p-values show that none of the means were significantly different.

	D-Infinity Method			D-8 Method		
Date	Low Wetness	High Wetness	P-Value	Low Wetness	High Wetness	P-Value
29-Mar-07	1480.0	152.0	0.29	306.0	50.0	0.40
29-Jun-07	100.0	307.0	0.19	11.1	42.2	0.20
30-Sep-07	112.0	73.7	0.69	11.6	4.8	0.28
26-Nov-07	234.0	186.0	0.69	68.0	49.0	0.70

Table 4.6 Barley Field Table, Catchment Area

Table 4.7 shows the results from the Hay Field, with 4 out of the 7 dates yielding mean moisture values that corresponded to the mean catchment area values in accordance with the theory. Again, none of the results showed significantly different means, as indicated by the p-values.

	D-Infinity Method			D-8 Method		
Date	Low Wetness	High Wetness	P-Value	Low Wetness	High Wetness	P-Value
28-Mar-07	26.8	4277.0	0.35	6.8	859.0	0.35
30-Mar-07	5.5	27.4	0.40	1.2	5.5	0.41
15-Apr-07	5.6	49.1	0.21	1.2	13.7	0.25
20-Apr-07	5.7	17.8	0.38	1.3	3.6	0.40
29-Jun-07	3710.0	58.9	0.36	742.0	16.4	0.36
30-Sep-07	5953.0	57.9	0.38	1192.0	16.2	0.38
26-Nov-07	5933.0	38.7	0.38	1187.0	10.6	0.38

Table 4.7 Hay Field Table, Catchment Area

4.4.3 Topographic Wetness Index Summary

Overall the TWI test yielded results that were in agreement with the theory. The Corn field results showed that the D-8 method performed slightly better than the D-Infinity method (Table 4.8). For the D-Infinity method 10 out of 12 times low TWI means correlated with low VMC% means, whereas with the D-8 method 11 out of 12 times the observations agreed with the theory. The p-values, however, showed that the means were not significantly different in most cases.

	D-Infinity Method			D-8 Method		
Date	Low Wetness	High Wetness	P-Value	Low Wetness	High Wetness	P-Value
11-Aug-06	10.5	11.7	**0.01**	8.8	9.6	0.10
28-Mar-07	29.3	33.9	0.66	10.6	11.1	0.52
29-Mar-07	10.8	10.8	0.93	8.7	9.0	0.66
30-Mar-07	10.8	10.8	0.98	8.8	9.0	0.77
15-Apr-07	10.9	10.2	0.24	9.1	8.2	0.12
20-Apr-07	10.4	11.0	0.29	8.6	8.8	0.69
31-May-07	10.6	11.5	0.11	8.9	9.7	0.11
29-Jun-07	10.6	11.2	0.17	8.8	9.3	0.35
10-Jul-07	11.1	11.1	0.92	9.2	9.5	0.60
15-Jul-07	10.8	11.5	0.12	8.9	9.8	**0.05**
30-Sep-07	10.7	10.8	0.83	9.0	9.0	0.96
26-Nov-07	10.2	11.5	**0.01**	8.5	9.6	**0.03**

Table 4.8 Corn Field Table, Topographic Wetness Index

The Barley field revealed the weakest results for the TWI (Table 4.9). Only 2 out of 4 dates had results that agreed with the theory for the D-Infinity test and only 1 date for the D-8 tests was in agreement. All of the p-values for both tests showed that none of the means were significantly different.

	D-Infinity Method			D-8 Method		
Date	Low Wetness	High Wetness	P-Value	Low Wetness	High Wetness	P-Value
29-Mar-07	11.7	11.1	0.39	9.4	9.3	0.86
29-Jun-07	10.8	11.7	0.14	8.5	9.4	0.14
30-Sep-07	10.4	10.8	0.58	8.7	8.4	0.56
26-Nov-07	11.8	11.0	0.17	9.9	9.0	0.28

Table 4.9 Barley Field Table, Topographic Wetness Index

The results for the Hay field were similar to the Corn field in that there was overall agreement with the theory for both the D-infinity and D-8 methods (Table 4.10). On all sample dates for both the D-infinity and D-8 methods, low TWI values corresponded to low VMC% values. However, once again, all of the p-values showed that the means of each date for both methods were not significantly different.

	D-Infinity Method			D-8 Method		
Date	Low Wetness	High Wetness	P-Value	Low Wetness	High Wetness	P-Value
28-Mar-07	9.3	11.8	0.07	7.8	10.3	0.08
30-Mar-07	10.5	10.8	0.81	8.9	9.2	0.82
15-Apr-07	9.4	11.3	0.08	7.8	9.8	0.09
20-Apr-07	9.2	11.2	0.06	7.6	9.6	0.06
29-Jun-07	9.6	11.4	0.17	8.0	9.9	0.17
30-Sep-07	9.3	11.4	0.14	7.7	10.0	0.14
26-Nov-07	9.3	11.3	0.08	7.8	9.7	0.09

Table 4.10 Hay Field Table, Topographic Wetness Index

4.4.4 Curvature Summary

The curvature test had varied results. The theory was that when the slope was concave shaped the VMC wetness values would be high and when the slope was convex shaped the VMC wetness values would be low. The results of the test for the Corn field are displayed in Table 4.11. Of the 12 collection dates the results showed that 50% of the time the highest VMC% value corresponded with the Concave – Concave curvature type and 50% of the time the highest VMC% value corresponded with the Convex – Convex curvature type.

Corn Field

Date	Concave - Concave	Convex - Concave	Concave - Convex	Convex - Convex
11-Aug-06	37.5	34.4	33.8	42.5
28-Mar-07	34.3	27.3	24.0	35.2
29-Mar-07	29.2	25.8	27.0	24.0
30-Mar-07	28.0	26.8	27.7	22.0
15-Apr-07	38.1	31.4	35.0	26.1
20-Apr-07	33.1	25.6	32.7	27.9
31-May-07	19.4	19.9	20.6	20.9
29-Jun-07	19.4	19.9	20.6	20.9
10-Jul-07	24.3	20.1	22.8	23.4
15-Jul-07	18.1	17.1	16.5	23.0
30-Sep-07	28.6	20.3	23.9	26.2
26-Nov-07	35.3	33.1	32.8	35.4
Summary	50.0%	0.0%	0.0%	50.0%

Table 4.11 Corn field Table, Curvature Summary

The results for the test in the Barley field showed that none of the dates had data that agreed with the theory (Table 4.12). The highest soil moisture VMC% data was not

associated with the Concave – Concave classification, but was split between the other three curvature classes.

Barley Field

Date	Concave - Concave	Convex - Concave	Concave - Convex	Convex - Convex
29-Mar-07	34.3	32.7	37.3	33.5
29-Jun-07	16.1	14.7	16.9	15.1
30-Sep-07	20.8	19.0	21.5	23.5
26-Nov-07	32.8	35.7	35.3	34.7
Summary	0.0%	25.0%	50.0%	25.0%

Table 4.12 Barley Field Table, Curvature Summary

The results from the hay field showed that on 5 out of 7 dates the highest VMC% data was associated with the low-wetness potential classification (Convex – Convex) (Table 4.13). Only 2 of 7 dates had data that agreed with the theory of highest wetness being associated with the Concave – Concave class.

Hay Field

Date	Concave - Concave	Convex - Concave	Concave - Convex	Convex - Convex
28-Mar-07	57.7	55.7	48.3	55.0
30-Mar-07	48.5	42.3	38.7	52.7
15-Apr-07	56.4	55.3	52.3	64.7
20-Apr-07	54.6	53.0	52.3	59.3
10-Jul-07	25.5	31.7	24.0	33.6
30-Sep-07	34.7	33.0	30.7	35.6
26-Nov-07	46.8	49.0	38.0	48.8
Summary	14.3%	14.3%	0.0%	71.4%

Table 4.13 Hay Field Table, Curvature Summary

4.5 DISCUSSION

4.5.1 Overall Data Summary

By summarizing the results an overall assessment of the strength of the relationship between the soil moisture data and the topographic models was revealed (Table 4.14). There were a total of 23 datasets spread out throughout the three subplot fields. Of those 23 datasets the catchment area topographic model agreed with the theory (low catchment area = low soil moisture) 56% - 65% of the time. The difference between the D-8 method and the D-infinity method were only minor. Of the 23 dates of data the slope gradient

topographic model performed very well with the modelled data and soil moisture data agreeing with the theory 96% of the time (i.e. where slope gradient was low (flatter areas) soil moisture values were high (wetter)). The TWI also performed well, agreeing with the theory 83% of the time (Table 4.14).

	Count	Corn Field 12	Barley Field 4	Hay Field 7	Total 23
Catchment Area	Dinf Lo < Hi	66.7%	25.0%	57.1%	56.5%
	D8 Lo < Hi	83.3%	25.0%	57.1%	65.2%
Slope Gradient	Dinf Lo > Hi	100.0%	75.0%	100.0%	95.7%
	D8 Lo > Hi	100.0%	75.0%	100.0%	95.7%
Topographic Wetness	Dinf Lo < Hi	83.3%	50.0%	100.0%	82.6%
	D8 Lo < Hi	83.3%	50.0%	100.0%	82.6%

Table 4.14 Topographic Model Summary Table

All of the test results showed that the models were measuring surface moisture patterns in agreement with the theories of surface moisture and topography, however when the p-values of those results were analyzed the strength of those relationships were revealed to be weak. Table 4.15 shows the summarized results of the p-values. The table shows that overall only 15% of the tests had significantly different mean values. That meant that even though the tests results favoured the theories of topography and wetness, the statistical strength of those results at 95% confidence was not assured. There were no significant improvements in the results when 90% confidence was assumed or when equal variances were assumed.

	Count	Corn Field 12	Barley Field 4	Hay Field 7	Total 23
Catchment Area	D-Infinity	8.3%	0.0%	0.0%	4.3%
	D-8	8.3%	0.0%	0.0%	4.3%
Slope Gradient	D-Infinity	41.7%	50.0%	0.0%	30.4%
	D-8	50.0%	50.0%	0.0%	34.8%
Topographic Wetness	D-Infinity	16.7%	0.0%	0.0%	8.7%
	D-8	16.7%	0.0%	0.0%	8.7%
	Total (Both)	17	4	0	15.2%

Table 4.15 P-values Summary Table

The curvature test had some unexpected results. The theory was that on a sloped surface that was concave shaped the surface would be wetter on average than a sloped surface

that was convex shaped. The data, however, showed that overall 52% of the time the soil moisture data was higher in areas of convex slopes and only 30% of the time was the data higher on concave slopes (Table 4.16). This was opposite of the theory.

Date	Concave - Concave	Convex - Concave	Concave - Convex	Convex - Convex
Corn Field	50.0%	0.0%	0.0%	50.0%
Hay Field	14.3%	14.3%	0.0%	71.4%
Barley Field	0.0%	25.0%	50.0%	25.0%
Overall	30.4%	8.7%	8.7%	52.2%

Table 4.16 Curvature Summary Table

In each of the topographic models it was shown that the unvegetated cornfield performed better than the vegetated fields. Two possible reasons for this observation are that the spatial variability of soil moisture was better represented by the grid pattern of VMC data collection. It is possible that the spacing of the measurements was more appropriate in the cornfield and better represented the surficial wetness conditions that were being modeled from the DEM. A second explanation was that soil moisture patterns are better organized and follow the topography closer under unvegetated surfaces. Soils under vegetation are less susceptible to compaction from precipitation and the vegetation acts to increase pore space within the soil, these factors lead to increased infiltration rates in vegetated landscapes (de Blij, 2005) and a decreased reliance on subsurface lateral flow (Western *et al,* 1999). In the vegetated fields it is possible that we are seeing the result of deeper infiltration of surface wetness that leads to less moisture at the surface and more potential for disorganized patterns of moisture distribution.

The 5 m resolution curvature model may not have been capturing the shape of the slope at a scale that was hydrologically significant. This was seen in the results that reveal that the convex shaped slope areas were modeling higher wetness values in more instances than the concave shaped slope. The question remained as to whether a higher or lower resolution DEM may increase the curvature model's potential to capture the landform shape relevant to the surficial moisture and reveal results that are closer to the theory.

4.5.2 D-8 vs. D-Infinity

Three of the topographic models, slope, TWI, and catchment area, were each modelled two different ways, by using a D-8 algorithm and a D-Infinity algorithm. The tests revealed that both methods for all three topographic models had near identical results. This meant that neither method performed any better than the other. The D-Infinity algorithm, with its dispersive flow dynamics, would be more useful on DEM's with larger slope range and coarser resolution. This watershed had relatively low slope gradient and the difference between the D-8 and D-Infinity models was not captured in this high-resolution DEM. Similar results were discussed in Murphy *et al* (2009) where the suggested reason for the similarities in the results between the convergent and dispersive flow was that LiDAR data was able to significantly capture the topography controlling flow such that the multiple direction flow model was irrelevant. Given that the D-8 method is built into ArcGIS without having to be generated using any add-on tools, and that the D-Infinity method required Tarboton's TauDEM toolset, the D-8 method was retained for modelling and the D-Infinity method was no longer used in this project.

4.6 CONCLUSION

Florinsky *et al* (2004) stated that among others, three topographic attributes, slope gradient, surface curvature, and catchment area, were directly related to surface moisture. Using a 5 m DEM these three topographic derivatives, along with a forth (TWI), were modelled. The four topographic models were compared to soil moisture measurements collected throughout 2006 and 2007. The analysis revealed which attributes were most related to the surface soil moisture. The topographic models performed as expected when compared to ground sampled soil moisture data. The hypothesis that these primary topographic layers could be used to map patterns of surface saturation at 5 m resolution was upheld. The analysis revealed a number of weak relationships between the ground-

sampled data and the topographic models, suggesting that the repeatability of the tests may not reveal consistent results.

All of the topographic parameters were modelled at 5 m resolution from a DEM which was shown to be highly precise. It was shown that the DEM was able to model the soil moisture distribution, however it remained unclear as to whether the 5 m resolution was accurately capturing the surface dynamics for all the hydrologic topographic models. In studies of hydrological modeling and grid cell resolution it is generally accepted that the higher resolution grid cell will improve a hydrological model's accuracy with predicting flow pathways and surface moisture distribution (Quinn *et al*, 1991; Moore, 1991; Western *et al*, 1999). The curvature model revealed that at 5 m resolution there was some confusion with the modelled slope shape and surface moisture. Identifying the correct scale potentially would improve the relationship between the modelled topographic parameters and soil moisture data. Landforms will be represented in the data as more dominant features when presented at different scale resolutions.

This chapter's analysis revealed that it is imperative to take a multi-scale approach to topographic modelling. It was not the focus of this chapter to address this revelation; the issue is addressed in the next chapter. In Chapter 5 the topographic models are re-created at three scales (1 m, 5 m, and 10 m) to identify the optimum resolution to capture the dominant landform process that relates to soil moisture. Scaling the topographic models provided another chance to assess the strength of the relationships between surface moisture distribution and topography. Chapter 5 presents the second stage of this analysis where a multi-scale approach was applied to the topographic modeling.

CHAPTER 5 A DESKTOP GIS APPROACH TO TOPOGRAPHIC MAPPING OF SURFACE SATURATION

5.1 ABSTRACT

Multiple topographic indices, including topographic position index, slope gradient, curvature, and catchment area were modeled using a LiDAR DEM. The models were then used to generate a Surface Saturation Landform Classification (SSLC). The SSLC algorithm incorporated the topographic models based on the theories of surface wetness prediction and was generated at multiple resolutions (1 m, 5 m, and 10 m). Ground moisture data was mapped via GPS and used to extract coincident SSLC data. The data was then grouped by the SSLC units. The results of the test in areas of no vegetation revealed that the SSLC was successful. However, the SSLC did not adequately predict surface wetness potential throughout the entire watershed. This indicated that other factors, such as soil type and distribution, artificial drainage, and vegetation, played larger roles in influencing soil surface moisture than topography alone.

5.2 INTRODUCTION

The potential for saturation throughout a landscape is a position dependant attribute. Local saturation will occur wherever the flow from the upslope contributing area exceeds the landscape's capacity to handle the drainage (O'Loughlin, 1986). Accurately mapping flow paths of water and saturation zones throughout a landscape has been a challenge and has yet to have a perfected solution. This study utilized an inferential method (i.e. a model) and was developed to characterize surficial moisture patterns using a compound derivative approach (multiple layers combined into one layer). Burt and Butcher (1985) found that combined topographic layers into one layer was a more appropriate technique to modeling surficial moisture that using only one topographic layer alone. By producing one layer that successfully models surface moisture distribution the results could be

easily incorporated into other modeling programs (e.g. SWAT). Techniques, such as the one presented here, the TRMI, and TOPMODEL, are simplified methods of modelling surficial moisture that are designed to assist with land management decisions without having to invest manpower into long-term field measurements.

Topography is widely recognized as a dominant factor on a landscape's hydrologic, geomorphologic, and biologic processes, and therefore the Digital Elevation Model (DEM) has become the most powerful tool for hydrologic modelling of landscapes (Moore et al, 1991). During the latter part of the 20th century advances in computer technology enabled much advancement in applying mathematical models to topographic grid maps to generate predictive flow pathways. Beven and Kirkby (1979) and O'Loughlin (1986) applied the principle that saturation is a position dependant attribute of a landscape and developed topographic models to predict flow paths and saturation zones. More recently Murphy *et al* (2009) produced a 'Depth-to-water' (DTW) index which utilizes only a slope model and a stream network model to generate a map of water table depth. The technique uses the distance of a cell to surface water and a measure of slope as its primary inputs. Murphy *et al* reported that DTW performed better than the more traditional wetness index ($\ln(\alpha/\text{Tan}\beta)$), especially at smaller grid resolutions.

After precipitation occurs over natural, unmodified landforms, surface water will drain from the landscape from topographic high points to topographic low points. Water on highly sloped surfaces will drain faster than water on low sloped, or flat, surfaces. In areas of low slope, and areas of surficial depression, water has a longer residence time and will take more time to move to drainage channels. Under the assumption of these well known hydrologic processes a model was generated to capture the spatial extent of wetness storage.

In Chapter 4 four topographic models (slope, catchment area, TWI, and curvature) were compared to VMC to see which models best represented surface moisture distribution. The results revealed that slope was highly correlated with volumetric moisture content; catchment area, TWI, and curvature were not as directly related to VMC. Still there was

enough potential to justify using the parameters as inputs into a surface saturation classification. Each layer related to surface moisture properties differently. For instance, higher moisture values are associated with lower slope values, higher catchment area values, and higher TWI values. A 5th topographic layer is introduced in this chapter, the topographic position index (TPI), and a multi-scale approach is taken to modeling the original topographic parameters. An algorithm is presented that utilizes four input variables to generate a landscape classification for modeling the surface saturation.

TPI is a DEM classification scheme that reclassifies the cells of a DEM into positive or negative values based on topographic position (Figure 5. 1). Weiss (2001) presented an influential poster that introduced methods for modelling topographic position, slope position, landform classification and watershed metrics. A hilltop, valley bottom, exposed ridge, flood plain, field, or slope are each topographic position classes and each landform would react differently to environmental processes. For instance, processes such as soil erosion, hydrologic response, and weather exposure would affect a landscape differently based on topographic position (Weiss, 2001).

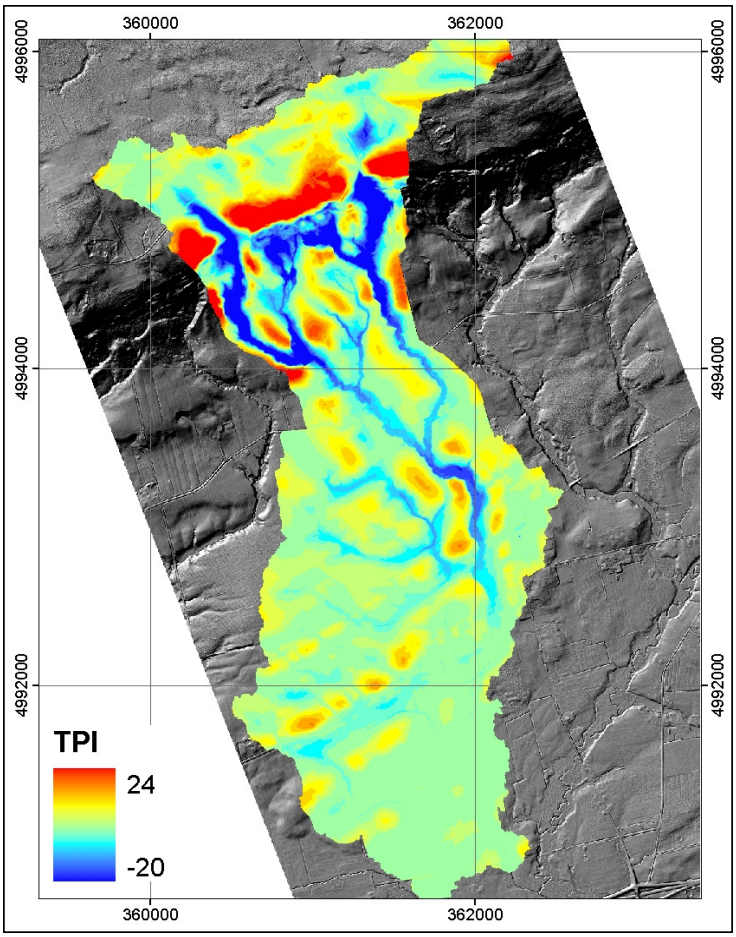

Figure 5. 1 Topographic Position Index Layer, 200 cell neighbourhood

In this chapter the Surface Saturation Landform Classification technique is explained and an assessment of its performance is presented. Using the classification algorithm each layer was spatially overlaid to determine the most likely areas throughout the watershed where the surface would be moist. The input layers used were primary topographic layers, as identified by Moore (1991), which are slope, catchment area, curvature, and topographic position index (TPI). TWI was not used in the enhanced landform classification. TWI is essentially a combination of slope and catchment area, therefore including it would have been redundant.

5.3 OBJECTIVE

The objective of this research was to generate a topographic model for predicting zones of surface saturation within an agricultural watershed. This was undertaken by enhancing

the Weiss (2001) Landform Classification by incorporating four topographic models into the algorithm. The enhanced Landform Classification model (identified as the Surface Saturation Landform Classification model, or SSLC) was then tested for accuracy by comparing the modeled surficial wetness zones to ground sampled VMC data.

5.4 METHODOLOGY

LiDAR data was collected in March of 2006 for production of the DEM that was used in this study. The DEM was generated at 1 m, 5 m and 10 m resolution to assess the effect of scale on the SSLC model. The ground surface throughout the watershed was sampled twelve times during 2006 and 2007. The soil saturation was measured using a 12 cm Time Domain Reflectometry (TDR) probe (Campbell Scientific Hydrosense), collecting volumetric moisture content as percentage (VMC%). Three subplots were selected as sampling sites (1.2 STUDY AREA). An RTK GPS apparatus was set up and the points were collected in grid patterns throughout the sub plot study areas. In the Corn field a 100 point grid was sampled, was oriented to magnetic north and surveyed into position using traditional grid and compass bearing methods. The Barley field was sampled at 44 points in a rough grid pattern. The Hay field was sampled at 17 points (see Figure 4.1). The GPS points were entered into a GIS and each point was assigned a moisture value corresponding to each day of data collection.

Three DEM's were generated from the LiDAR point cloud at 1 m, 5 m, and 10 m resolutions (refer to 2.1 Digital Elevation Model Generation for methodology). Scale was identified in Chapter 4 as an important factor in surface modelling. The scale was tested to identify how changing the resolution of the DEM would affect the topographic models, the TPI, and the overall landform classification. The goal was to determine the optimum spatial resolution of the surface saturation landform classification.

The LiDAR data used for this analysis was collected with point spacing of 1 m (1 point every 1 m). Therefore the data was capable of a maximum DEM resolution of 1 m. However, the best resolution for modelling surface processes was not known. By

comparing the results of the modelling over 3 different scales an assessment of the classification's scale dependency was made. This was done by generating three DEMs (1 m, 5 m and 10 m), generating each of the topographic layers (scale, curvature, catchment area, and TPI), calculating the classification algorithm and comparing the classification results to the ground sampled surface moisture values for each DEM resolution.

5.4.1 Topographic Position Index

TPI is an integral parameter for the Landform Classification, which required a small and a large scale TPI layer as inputs. To calculate TPI from a DEM the spatial analyst extension was required for ArcGIS. The algorithm utilized a single output map algebra function in which the focal mean tool was used. The algorithm worked so that the value of the focal mean calculation was subtracted from the selected DEM cell, then a constant 0.5 was added to the result (Equation 5. 1). The result was either positive or negative indicating the elevation of the cell was either higher (positive) or lower (negative) to the neighbourhood of cells surrounding it.

$$\text{Int}((\ [\text{DEM}] - \text{focalmean}([\text{DEM}], [\text{neighbourhood}], x, y)) + 0.5)$$

Where:

Int	= convert to integer
DEM	= the DEM to be modelled
Neighbourhood	= one of either rectangle, annulus or circular
*x	= number of cell to include in the neighbourhood in the x-direction of the selected cell
*y	= number of cell to include in the neighbourhood in the y-direction of the selected cell

*x and y were changed to the number of inner radius cells and outer radius cells of the Annulus when Annulus was the selected neighbourhood.

Equation 5. 1 Andrew Weiss's TPI algorithm used to generate TPI grids at scales of 2 to 500.

Each of the DEMs was used to generate TPI layers using two methods, annulus and rectangular neighbourhoods. The two methods differed in the way the average elevation

value was calculated from the neighbourhood of cells surrounding a central cell. The annulus grid was created by averaging the elevation values in an annulus shaped neighbourhood around the central cell; whereas the rectangular grid was created by averaging a conventional rectangular shaped neighbourhood around a central cell (Figure 5.2). For example, the annulus TPI50 generated from the 5 m DEM was made up of 5 cells to the inner ring and 10 cells to the outer ring of the annulus. The annulus TPI200 generated from the 1 m DEM was up was made up of 100 cells to the inner ring and 200 cells to the outer ring. The rectangle grid was created by averaging the elevation values in a rectangular shaped neighbourhood around the central cell. The TPI50 was made up of a rectangle with 10 cells horizontal and 10 cells vertical in the neighbourhood. The TPI 200 was made up of 40 cells horizontal and 40 cells vertical in the neighbourhood.

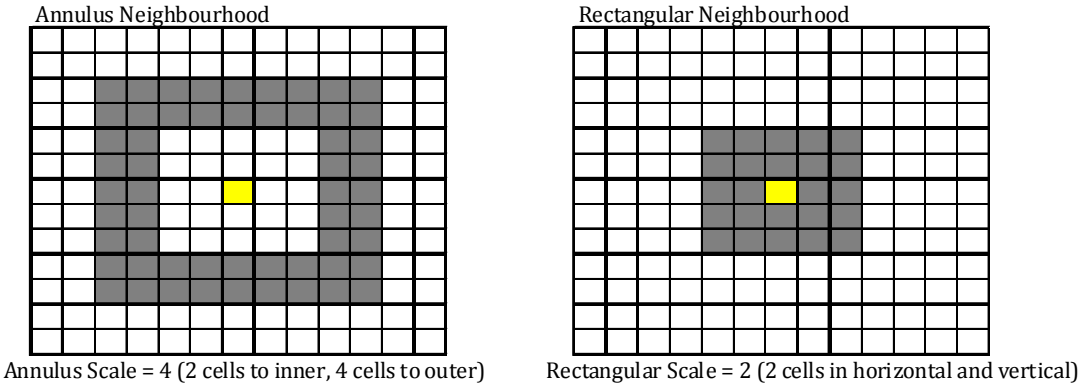

Figure 5.2 Annulus and rectangle shaped neighbourhoods

TPI layers were generated using each neighbourhood method at a variety of scales ranging from 2 cell neighbourhoods to 500 cell neighbourhoods (Table 5.1). For each DEM resolution the largest scaled TPI neighbourhood was generated that computer resources would allow. The larger the neighbourhood size the longer it took to generate. For example, when modelling the 50 m neighbourhood using the 1 m DEM it took over 2 ½ hours of computer processing time to generate the layer compared to 25 minutes for the 20 m neighbourhood using the 1 m DEM. The 500 m neighbourhood modelled from the 10 m DEM did not take as long to generate, however increasing the neighbourhood beyond 500 m was not appropriate for a study area that is only ~10km^2, therefore 500 m

was chosen as an upper-limit to the TPI models. Five neighbourhood scales were used for each DEM resolution and each neighbourhood type for a total of 30 TPI layers.

DEM Resolution (m)	Neighbourhood Scale (m)	Annulus		Rectangle	
		Inner Edge	Outer Edge	Horizontal	Vertical
1	2	1	2	2	2
	5	2	5	5	5
	10	5	10	10	10
	20	10	20	20	20
	50	25	50	50	50
5	10	1	2	2	2
	20	2	4	4	4
	50	5	10	10	10
	100	10	20	20	20
	200	20	40	40	40
10	20	1	2	2	2
	50	2	5	5	5
	100	5	10	10	10
	200	10	20	20	20
	500	25	50	50	50

Table 5.1 Three DEMs of the same area generated at three different resolutions are used to model TPI using five different neighbourhood sizes for each DEM.

Once each of the layers were generated (30 layers total) test areas were extracted to identify an appropriate small scale and large scale for the TPI. The criteria was that there must be a range of TPI values (i.e. not uniform) throughout the test area. A variety of TPI values would indicate that multiple topographic positions were identified throughout the test area, which would lead to more classes for the Landform Classification. The test areas corresponded to the study area fields outlined in section 1.2.4 Subplots (i.e. Hay field, Barley field and Corn field). The comparison also was used to identify which method, rectangle or annulus, yielded a larger variety of TPI values throughout the study area.

The TPI layers were standardized to 0 so that they were compatible with the classification algorithm. The following formula was used to standardise the TPI grids (Equation 5.2) using a single output map algebra function in ArcGIS (Weiss, 2001).

$$Int((((tpi<sf> - mean) / stdv) * 100) + 0.5)$$

Where:

Int	= Converts results to Integer
<sf>	= Scale factor of TPI grid
mean	= Mean of the TPI grid
stdv	= Standard Deviation of the TPI grid

Equation 5.2 TPI Grid standardization equation (Weiss, 2001)

5.4.2 Landform Classification

Weiss (2001) introduced a landform classification algorithm that uses two TPI layers (one small scale and one large scale) to classify landscapes into landform features (Table 5.2). The landform classification was based on Weiss's "general rule" that, "because elevation tends to be spatially autocorrelated, the range of TPI values increases with scale" (Weiss, 2001). Therefore a small-neighbourhood TPI combined with a large-neighbourhood TPI would reveal nested landforms. Nested landforms are scale dependant. For example, at a small scale subtle changes in local lowlands would be identified, whereas at a large scale more dominant ridges and valleys would be identified.

A simplified approach was adopted for determining appropriate small and large scales for the TPI. A More in-depth technique to analyzing the TPI scale dependencies would be to apply variogram analysis and determine the most appropriate kernel size for the scale-breaks. The simplified approach was chosen because this study was a first approximation of the technique at multiple scales and the emphasis was placed on determining the best DEM resolution as opposed to optimizing the TPI filter size. It is recognized that applying the variogram analysis may improve the results of this study and it is an approach that should be given consideration in future studies.

Description	Algorithm
Streams	([TPI50] <= -100 & [TPI200] <= -100)
Mid-slope Drainage	([TPI50] <= -100 & [TPI200] > -100 & [TPI200] < 100)
Upland Drainage	([TPI50] <= -100 & [TPI200] >= 100)
U-Shape valleys	([TPI50] > -100 & [TPI200] < 100 & [TPI200] <= -100)
Plains	([TPI50] > -100 & [TPI50] < 100 & [TPI200] > -100 & [TPI200] < 100 & [Slope] <= 0.5)
Open Slope	([TPI50] > -100 & [TPI50] < 100 & [TPI200] > -100 & [TPI200] < 100 & [Slope] > 0.5)
Upper Slope	([TPI50] > -100 & [TPI50] < 100 & [TPI200] >= 100)
Local Ridge	([TPI50] >= 100 & [TPI200] <= -100)
Mid-slope Ridge	([TPI50] >= 100 & [TPI200] > -100 & [TPI200] < 100)
High Ridge	([TPI50] >= 100 & [TPI200] >= 100)

Table 5.2 Original Weiss Landform Classification Algorithm

5.4.3 Surface Saturation Landform Classification

Using high-resolution DEMs allowed the Landform Classification algorithm to be adjusted to exploit the "Field" class and extract more detail from the landscape. The basic algorithm that Weiss generated for the Landform Classification was adjusted and incorporated the topographic layers into the classification. The "Field" classification was exploited to identify areas of low slope, depressed curvature, and high catchment area. Table 5.3 displays the adjusted Weiss classification algorithm which includes slope, curvature, and catchment area layers. The Surface Saturation Landform Classification (SSLC) algorithm exploits the "Field" classification so that instead of classifying all low-lying, low-sloped areas as Fields, the curvature and catchment area was also accounted for to identify potential surface saturation zones.

Description	Algorithm
Streams	((TPI50 <= -100) or [CatchArea] > 1000)
Mid-slope Drainage	(TPI50 <= -100 & TPI200 > -100 & TPI200 <100)
Upslope Drainage	(TPI50 <= -100 & TPI200 >= 100)
Flood Plain	(TPI50 > -100 & TPI50 < 100 & TPI200 <= -100)
Field Concave Wet	(TPI50 > -100 & TPI50 < 100 & TPI200 > -100 & TPI200 < 100 & [Slope] <= 0.5 & [Concave] > 0 & [CatchArea] > 100 & [CatchArea] <1000)
Field Convex Wet	(TPI50 > -100 & TPI50 < 100 & TPI200 > -100 & TPI200 < 100 & [Slope] <= 0.5 & [Convex] > 0 & [CatchArea] > 100 & [CatchArea] <1000)
Field Concave Dry	(TPI50 > -100 & TPI50 < 100 & TPI200 > -100 & TPI200 < 100 & [Slope] <= 0.5 & [Concave] > 0 & [CatchArea] <100)
Field Convex Dry	(TPI50 > -100 & TPI50 < 100 & TPI200 > -100 & TPI200 < 100 & [Slope] <= 0.5 & [Convex] > 0 & [CatchArea] > 100)
Open Slope	(TPI50 > -100 & TPI50 < 100 & TPI200 > -100 & TPI200 < 100 & [Slope] > 0.5)
Upper Slope	(TPI50 > -100 & TPI50 < 100 & TPI200 >= 100)
Local Ridge	(TPI50 >= 100 & TPI200 <= -100)
Mid-slope Ridge	(TPI50 >= 100 & TPI200 > -100 & TPI 200 <100)
High Ridge	(TPI50 >= 100 & TPI200 >= 100)

Table 5.3 Surface Saturation Landform Classification Algorithm

The landform classification algorithm was implemented by creating an ARC GIS model (APPENDIX B: ArcGIS Model Diagrams). The first step involved deciding which small and large scale TPI models would be used, and standardising the TPI grids to 0 (Equation 5.2). Step two involved calculating each class by running a separate ArcGIS Map Algebra expression. The TPI was used to separate each cell into classes. The slope was then used to separate the TPI classes into steep gradient and low gradient. The curvature was used to distinguish the low sloped areas into positive (mound) and negative (dip) shaped slopes. The catchment area layer was used to determine which cells were streams and drainage channels. Step Three involved creating the final landform classification raster by mosaicking all the rasters together.

Four SSLC layers were generated to cover multiple scales. The TPI neighbourhood's were chosen based on the results of the testing of how scale affected the TPI ranges (see 5.5.1 Neighbourhood modelling technique and size). This was a simplified approach to determining an appropriate filter size for the TPI. One SSLC layer was generated from the 5m DEM with a 50 cell neighbourhood TPI and a 200 cell neighbourhood TPI layer as the small and large scale indices (Figure 5.3). The second SSLC layer was generated from the 10m DEM with 50 cell and 200 cell neighbourhoods TPI (Figure 5.4). The third

SSLC layer was generated from a combination of the 50 cell TPI from the 1 m DEM and the 200 cell TPI from the 5 m DEM (Figure 5.5). The forth SSLC layer was generated from the 10m DEM with a 200 cell TPI and 500 cell TPI (Figure 5.6).

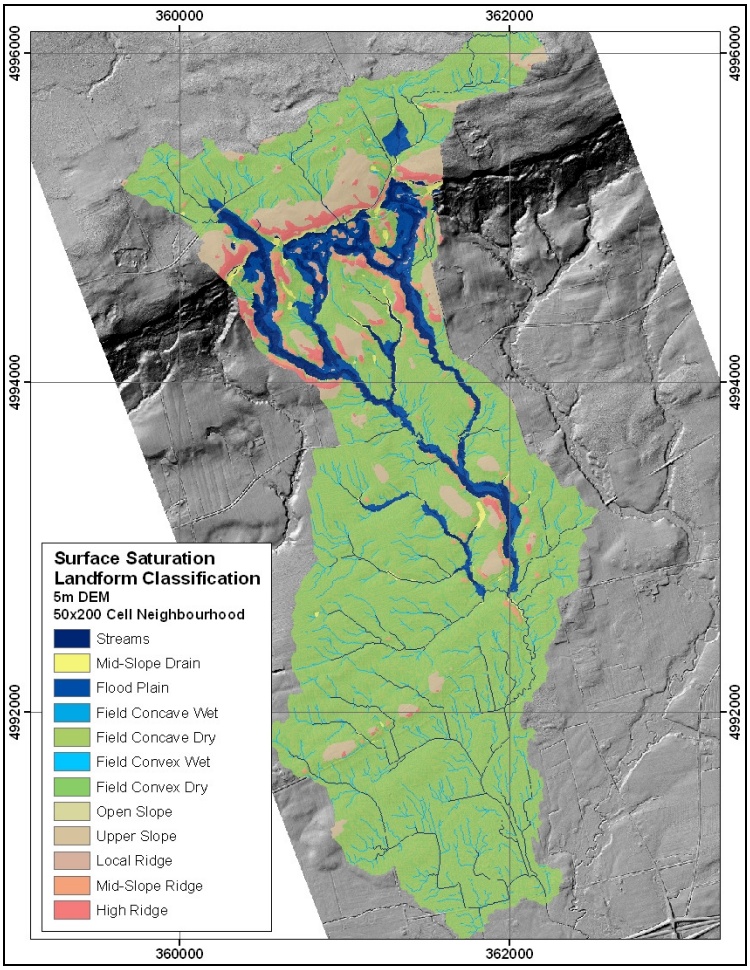

Figure 5.3 This image shows the 5 m SSLC layer modelled using the 50 cell neighbourhood TPI and the 200 cell neighbourhood TPI. Low-lying areas in the watershed are identified as streams and flood plains, steep slopes are ridges. The four field classes represent areas of low slope, either positive or negative curvature (convex or concave, respectively), and catchment area (Wet for high CA value and Dry for low CA value).

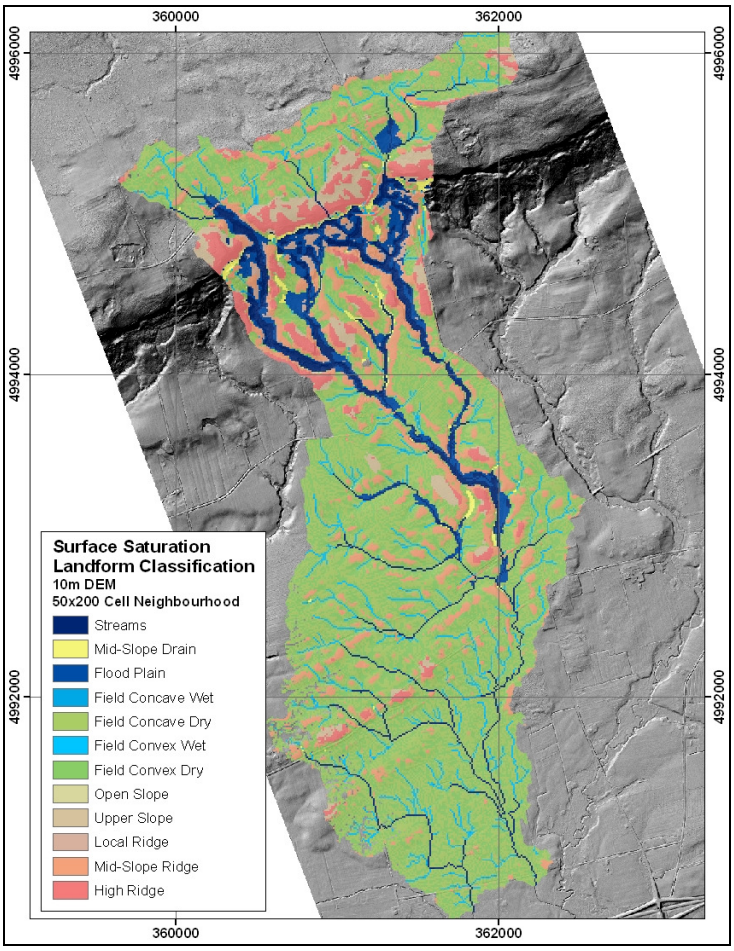

Figure 5.4 This image shows the 10m SSLC layer modelled using the 50 cell neighbourhood TPI and the 200 cell neighbourhood TPI.

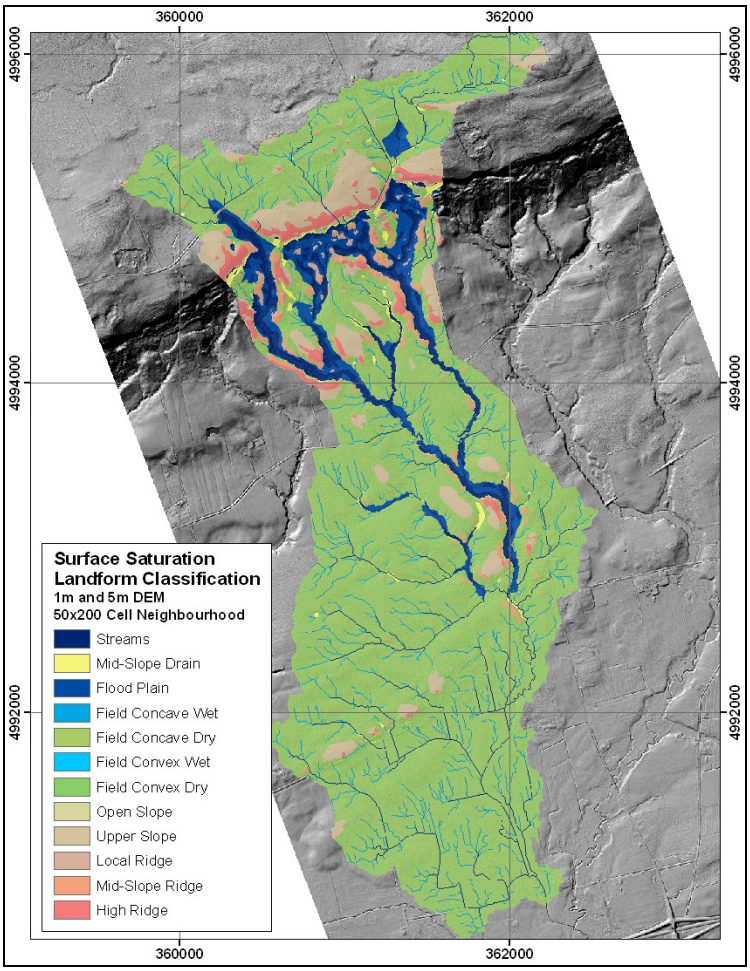

Figure 5.5 This image shows the 1 m and 5 m SSLC layer. This layer was modelled using the 50 cell neighbourhood TPI from the 1m DEM and the 200 cell neighbourhood TPI from the 5m DEM.

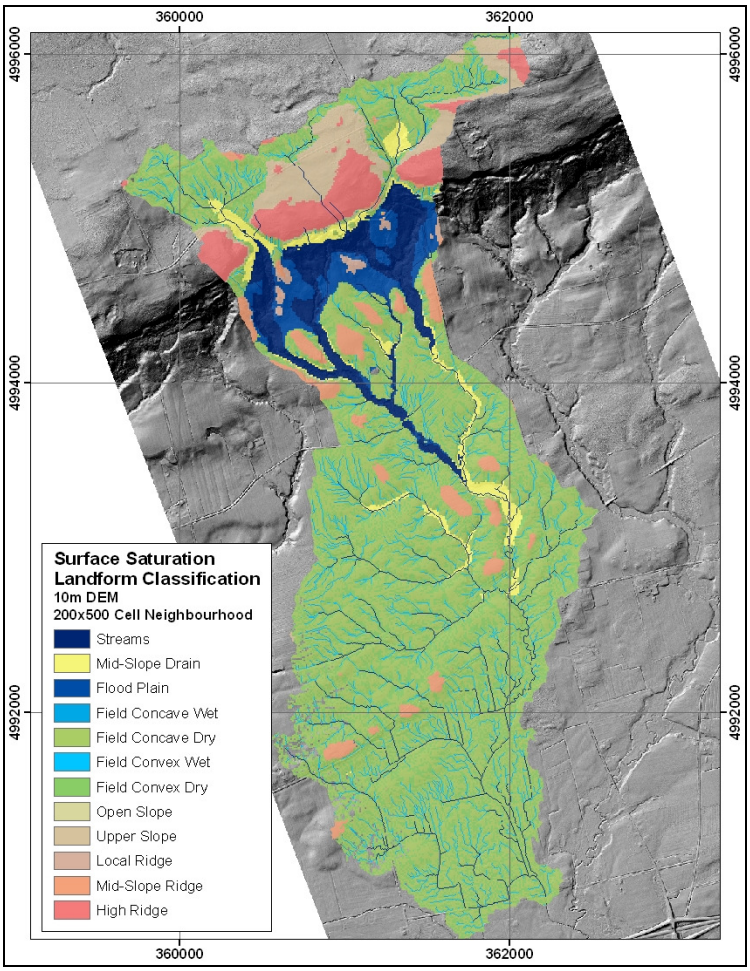

Figure 5.6 This image shows the 10 m SSLC layer modelled using the 200 cell neighbourhood TPI and the 500 cell neighbourhood TPI from the 10 m DEM.

The GPS point data was used to extract the value of the SSLC that spatially coincided with the VMC% data. This was done for each day of ground sampling. In the Surface Saturation Landform Classification layer each cell contained an integer value that represented a landform type. Throughout the watershed twelve landform types were identified (Table 5.4). Of the twelve landform types found throughout the watershed only eight types were represented in the three study area fields. These eight landform types were ranked based on the wetness potential of each type, with slope being the most important variable in the ranking scheme (Burt and Butcher, 1985). Lower ranks represented the highest potential to be wet and the higher ranks represented highest potential to be dry.

Description	Rank
Streams	1
Mid-slope Drainage	-
Flood Plain	-
Field Concave Wet	2
Field Convex Wet	3
Field Concave Dry	4
Field Convex Dry	5
Open Slope	6
Upper Slope	-
Local Ridge	-
Mid-slope Ridge	7
High Ridge	8

Table 5.4 Table of ranked landform classes as identified in the SSLC.

Once extracted the VMC% data was grouped and averaged based on the extracted SSLC rank using Microsoft Excel. Bar charts were generated to visualise the trends in the data An ANOVA table was created to assess the statistical strength of the trends. A significant difference in the means of the low VMC% values and high ranked SSLC values indicated that where the surface was drier the SSLC was modelling low wetness. A significant difference in the means of the high VMC% values and the low ranked SSLC values indicated that where the surface was wetter the SSLC was modelling high wetness.

5.5 RESULTS AND DISCUSSION

5.5.1 Neighbourhood modelling technique and size

For each neighbourhood type and DEM resolution the range of TPI values consistently increased as the TPI scale increased. This was expected because spatial autocorrelation of elevation values decreases with distance, which in turn means that the range of TPI values will always increase with increasing scales (Weiss, 2001). Increasing the neighbourhood size yielded larger ranged TPI layers. The goal of this test was to determine which model method (annulus or rectangle) generated the greater range of TPI values at the smallest scale. The comparison of the TPI neighbourhood sizes revealed that the annulus neighbourhood consistently generated a larger range of TPI values in both the barley field and the corn field than the rectangle neighbourhood. The same was true for each DEM resolution. The hay field, which was relatively smaller and more level, had

only 1 TPI value for both the annulus and rectangle methods for each DEM scale. The test results are summarized in Figure 5.7 and Figure 5.8.

For the Corn field the range of TPI values modelled with the rectangular neighbourhood was less than 2 until TPI scale was increased to 100 m, at which point the range increased to 4. The annulus neighbourhood TPI, however, increased to 4 at 50 m (Figure 5.7). For the Barley field there were similar observations made (the annulus neighbourhood consistently had a greater range of values than the rectangular neighbourhood). It was therefore decided that when using an annulus neighbourhood method to generate the TPI a neighbourhood of at least 50 m was required for the small scale TPI layer. A neighbourhood size of 100 m would be required for using the rectangular neighbourhood for the Landform Classification (Figure 5.8). Three lower limit TPI layers were selected from the annulus neighbourhood method, the 1 m DEM 50 m neighbourhood, 5 m DEM 50 m neighbourhood, and the 10 m DEM 50 m neighbourhood.

The criterion for selecting the upper limit of the TPI scale was to determine the largest possible neighbourhood size (within reason). For this study the largest TPI scale modeled was 500 m using the 10 m DEM. This was the upper limit based on the spatial extent of the study area. For example, with 500 cells modeled on a 10 m resolution DEM the spatial extent expanded to 5000 square metres. In the context of this watershed (approximately 10 km^2) it did not seem appropriate to increase the scale any larger. The upper limit for the 5 m DEM was 200 m; this was chosen because the computation time to generate a larger TPI scale was great and the 200 m neighbourhood had a reasonable range of TPI values. Therefore three upper limit TPI scales were selected: (i) the 5 m DEM 200 m neighbourhood, (ii) the 10 m DEM 200 m neighbourhood, and (iii) the 10 m DEM 500 m neighbourhood.

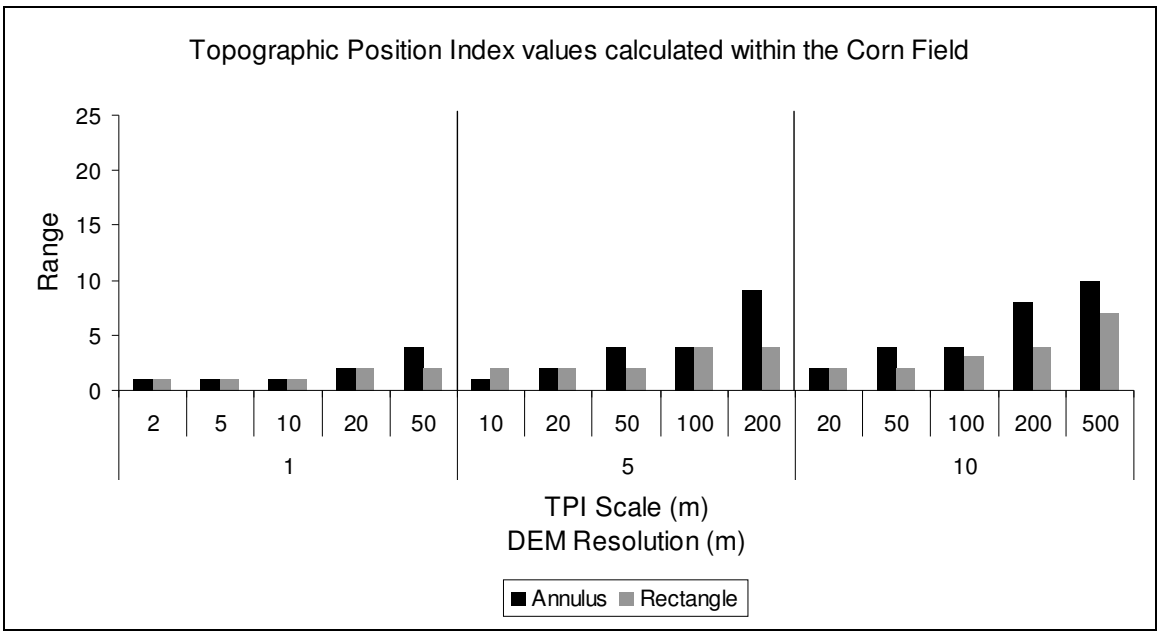

Figure 5.7 A bar chart of the TPI values extracted from the Corn Field.

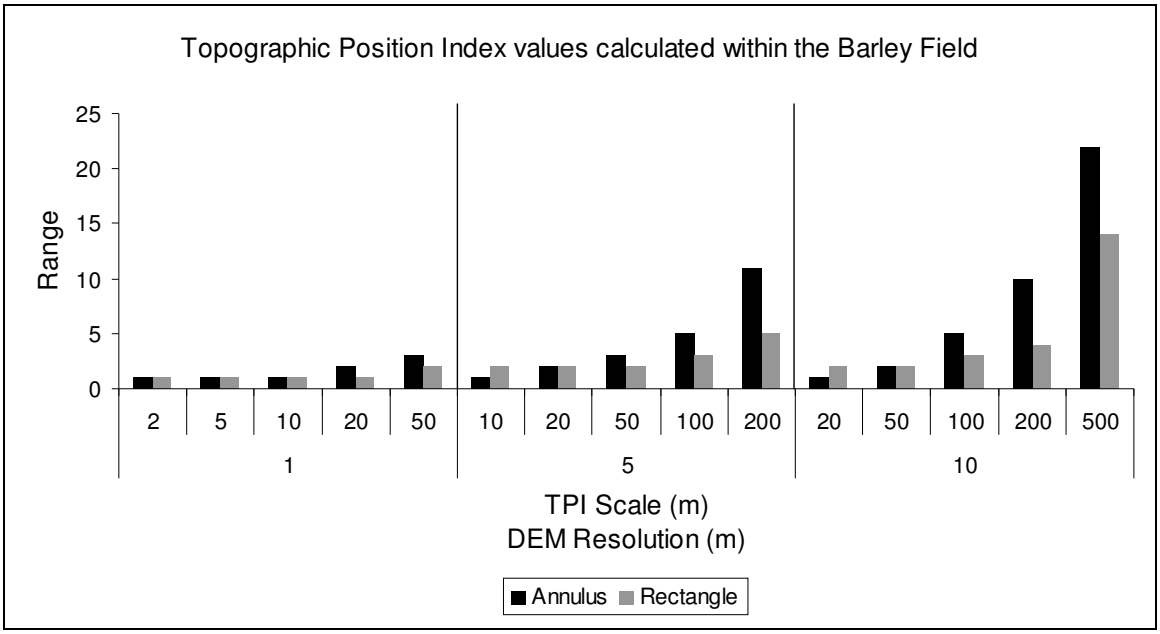

Figure 5.8 A bar chart of the TPI values extracted from the Barley field.

5.5.2 TPI Standardization

Six TPI layers were selected for analysis from the set of 30 layers based on the findings of appropriate scale from the previous tests. All six were annulus layers as the rectangle layers consistently had smaller ranges of values throughout the study areas. Elevation values throughout a natural landscape contain a high degree of spatial autocorrelation. The range of TPI values was greater with the annulus neighbourhood because the shape of the neighbourhood diminished the effect autocorrelation had on the elevation values. The six selected layers had to be standardized so that they could be used in the landform classification algorithm. One of the standardization criteria was that the layers had mean values close to zero (Table 5.5).

DEM Resolution (m)	TPI Scale (m)	Mean	Standard Deviation
1	50	0.16	0.91
5	50	0.16	0.9
5	200	0.4	3.35
10	50	0.15	0.84
10	200	0.4	3.32
10	500	0.58	7.37

Table 5.5 Summary of means and standard deviation of selected TPI layers for Landform Classification

5.5.3 Corn Field Data Summary

Throughout the Corn Field there were seven dates of data collection. For the 1 m and 5 m DEM dataset the results of the SSLC were mixed. Of the 7 days of data collection only 3 revealed results that were consistent with the theory that the higher ranked SSLC value had the higher wetness potential compared to the lower ranked SSLC value. The data collected on August 11, 2006 followed the theory and showed a declining trend of average VMC data corresponding with higher to lower ranked SSLC values (Figure 5.9). The ANOVA test confirmed that the means for the August 11, 2006 data were significantly different. The May 31, 2007 data revealed a similar trend consistent with the theory. However, the ANOVA revealed that the means were not significantly different

(Figure 5.9). The November 26, 2007 dataset was also consistent with the theory, with the ANOVA test confirming the significant difference of the means.

For at least two of the three days that were in agreement with the theory (May 31, 2007 and November 26, 2007) the vegetation conditions during the survey would have been somewhat similar with there being only minimal crop growth during May and post-harvest during November. However the vegetation conditions during August would have been full crop growth with ~2 m tall corn stalks.

The other four dates of data collection did not follow the theory and the ANOVA tests demonstrated that the means were not significantly different. The four instances where the data was not in agreement with the theory would have had somewhat similar vegetation conditions during data collection. Each of the four instances were data collection during the summer months (June, July and September), which were during the growing season. Vegetation could be a reason for why the data collected on these days did not conform to the theory.

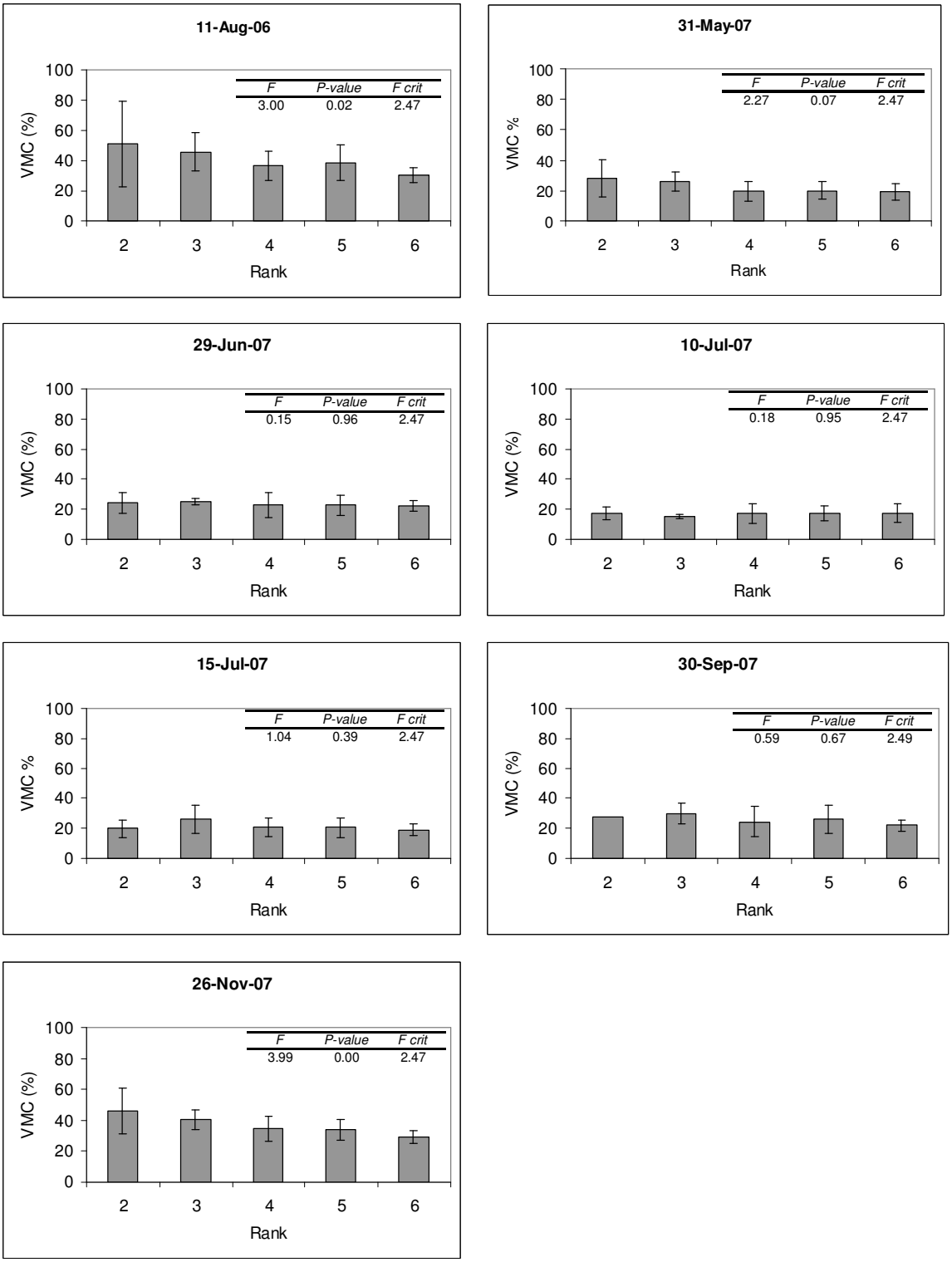

Figure 5.9 Bar charts for the Corn field, 1 m and 5 m DEM (50x200 Cell Neighbourhood)

The 5 m SSLC was also moderately successful with respect to predicting moisture characteristics. Of the 7 dates of soil moisture collection 2 of the datasets were consistent with the modeled surface saturation (Figure 5.10). The data collected on August 11, 2006 and on November 26, 2007 revealed a trend of decreasing mean moisture with increasing SSLC ranks; however the ANOVA revealed that the means of both those datasets were not significantly different. This indicated that the trend in the data was in agreement with the theory however the significance of that trend was weak.

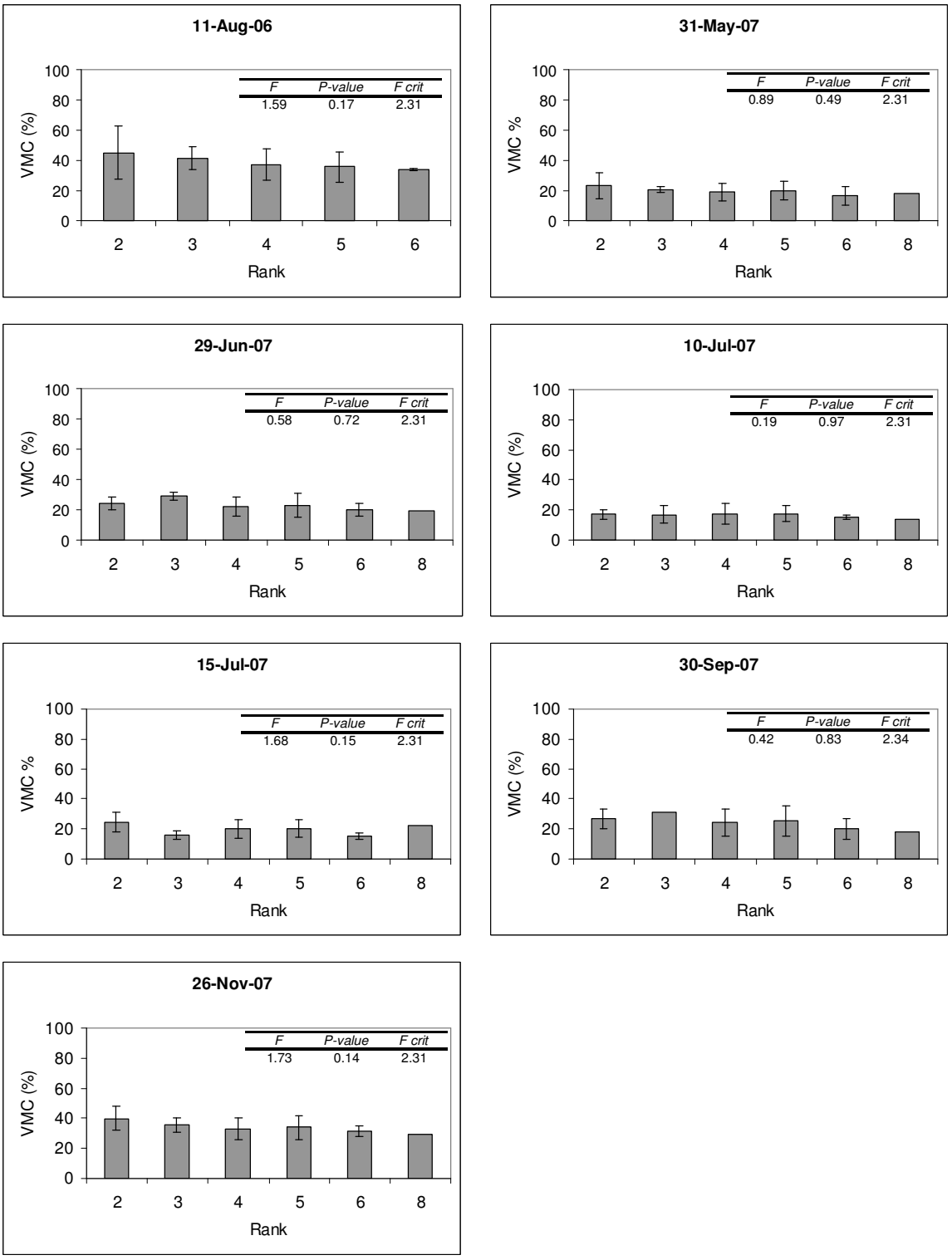

Figure 5.10 Bar charts for the Corn Field, 5 m DEM (50x200 Cell Neighbourhood)

For the 10 m SSLC modeled with the 50x200 cell neighbourhood and 10 m SSLC with the 200x500 cell neighbourhood 1 of the 7 dates of collection were consistent with the theory which revealed the trend of declining soil moisture relevant to increasing ranked SSLC for both datasets (Figure 5.11 and Figure 5.12). The ANOVA revealed that the means were significantly different in both instances. Therefore for the data collected on November 26, 2007 each of the SSLC models successfully represented the moisture distribution in the Corn Field.

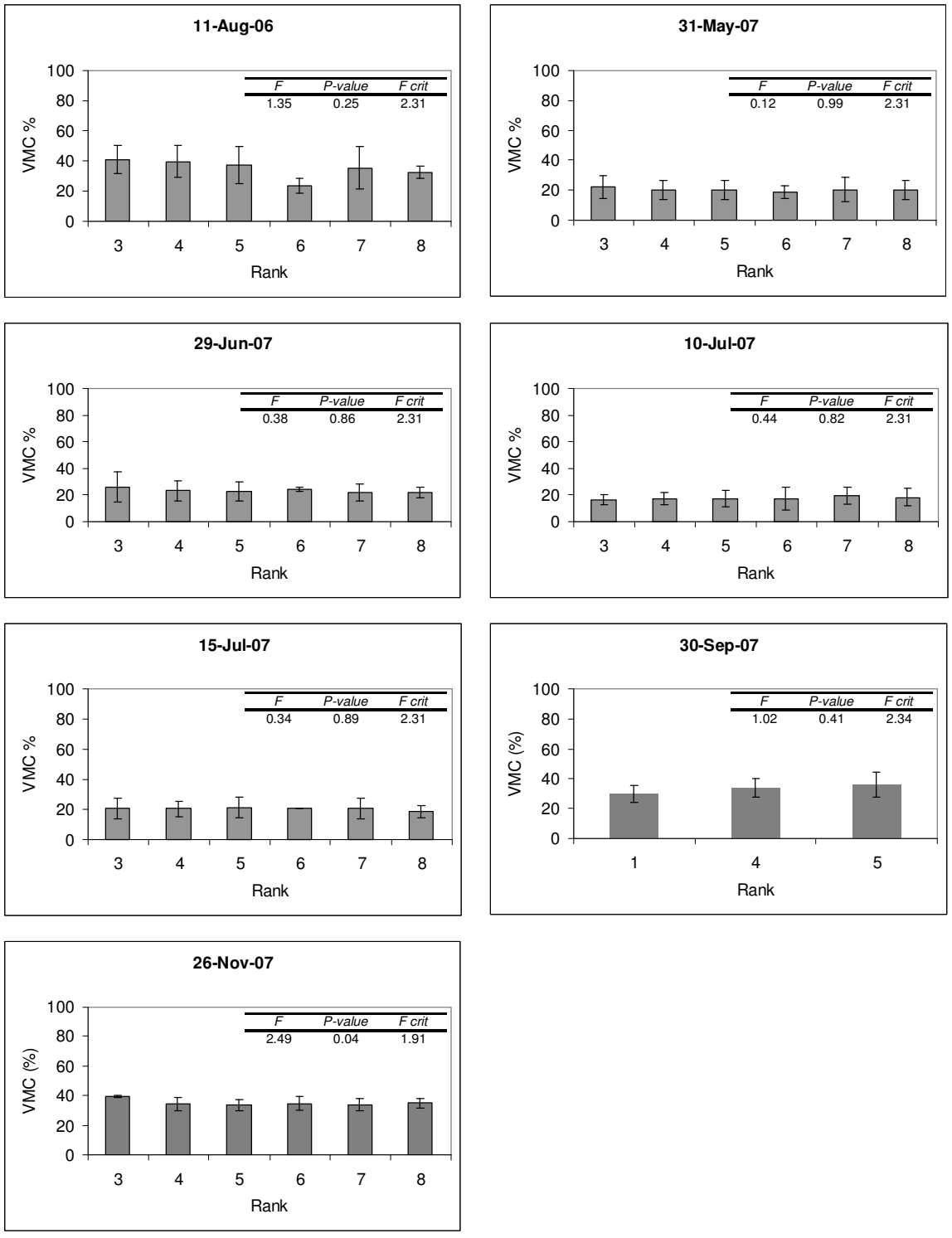

Figure 5.11 Bar charts for the Corn Field, 10 m DEM (50x200 Cell Neighbourhood)

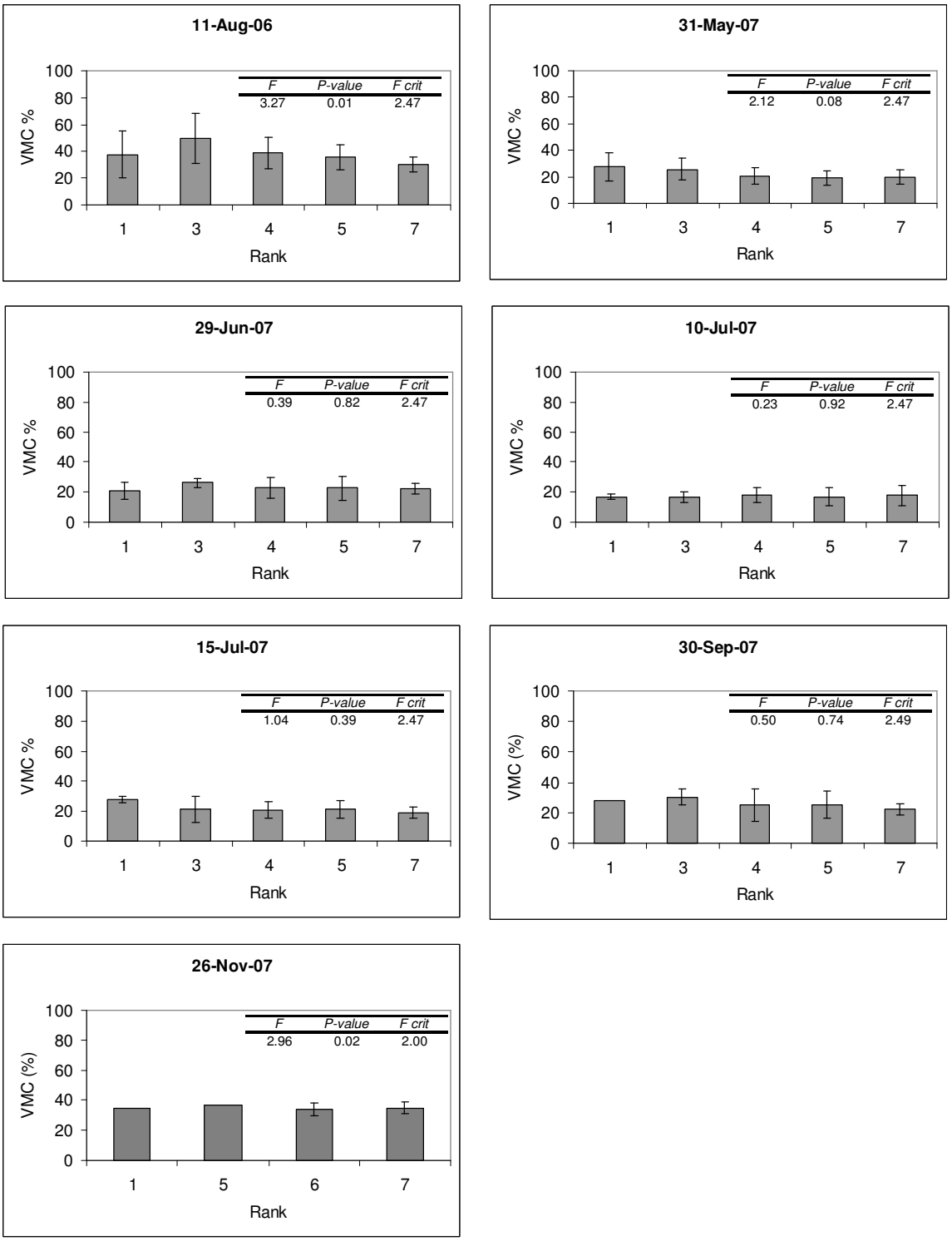

Figure 5.12 Bar charts for the Corn Field, 10 m DEM (200x500 Cell Neighbourhood)

The spatial pattern of soil moisture measurements was highly variable. When looking at the spatial distribution of soil moisture (See APPENDIX C: Corn Field Imagery) it was clear why the SSLC did not produce results in agreement with the theory for each day of ground data collection. The high values of wetness were inconsistent across the field and, at different times of data collection, were located in different areas of the field. These observations are common and consistent with other soil moisture survey studies (Burt and Butcher, 1985; Western *et al*, 1999). The modeled saturation values consistently followed the main flow pathways of the field. On the days where the ground sampled VMC data agreed with the modelled SSLC values there were some key observations as to why the data matched, first the soil moisture distribution within the field was more organised and followed the topographic drainage pathways, also the days of data collection were in periods of wetter surface conditions, which will lead to this better organization of soil moisture (Burt and Butcher, 1985; Western *et al,* 1999).

The Corn field was the only field that was known to be tile drained. It was also the field with the best results. The tile drainage would have helped in that during precipitation events the soil moisture would be draining in accordance to the tiled pattern of drainage piping. In this field the topography followed this pattern of tile drainage and the SSLC model therefore reflected the drainage pattern as well. The tile drainage would have allowed the soil moisture to be well organized and follow the subsurface lateral flow similar to the tile drainage pattern.

The dates of data collection where there was not agreement between the VMC data and the modelled SSLC data generally occurred during dry conditions and during the growing season. The vegetation would have played a role in causing the soil moisture distribution pattern to alter, as the vegetation would consume more of the water and cause faster infiltration after precipitation events (de Blij, 2005).

5.5.4 Hay Field Data Summary

There were 7 dates of soil moisture data collection in the Hay Field. The soil moisture data was compared to the 4 modelled SSLC layers. The result from each of the four scales of SSLC data revealed that there was little correlation between the ground sampled data and the modeled SSLC classes. For the 1 m and 5 m SSLC none of the measured data followed the hypothesized trend (Figure 5.13). All of the ANOVA tables revealed that the means were not significantly different. These observations about the data were also true for the three other SSLC scales (Figure 5.14, Figure 5.15, and Figure 5.16). None of the 4 SSLC scales successfully modeled the measured surface moisture for any of the days of data collection.

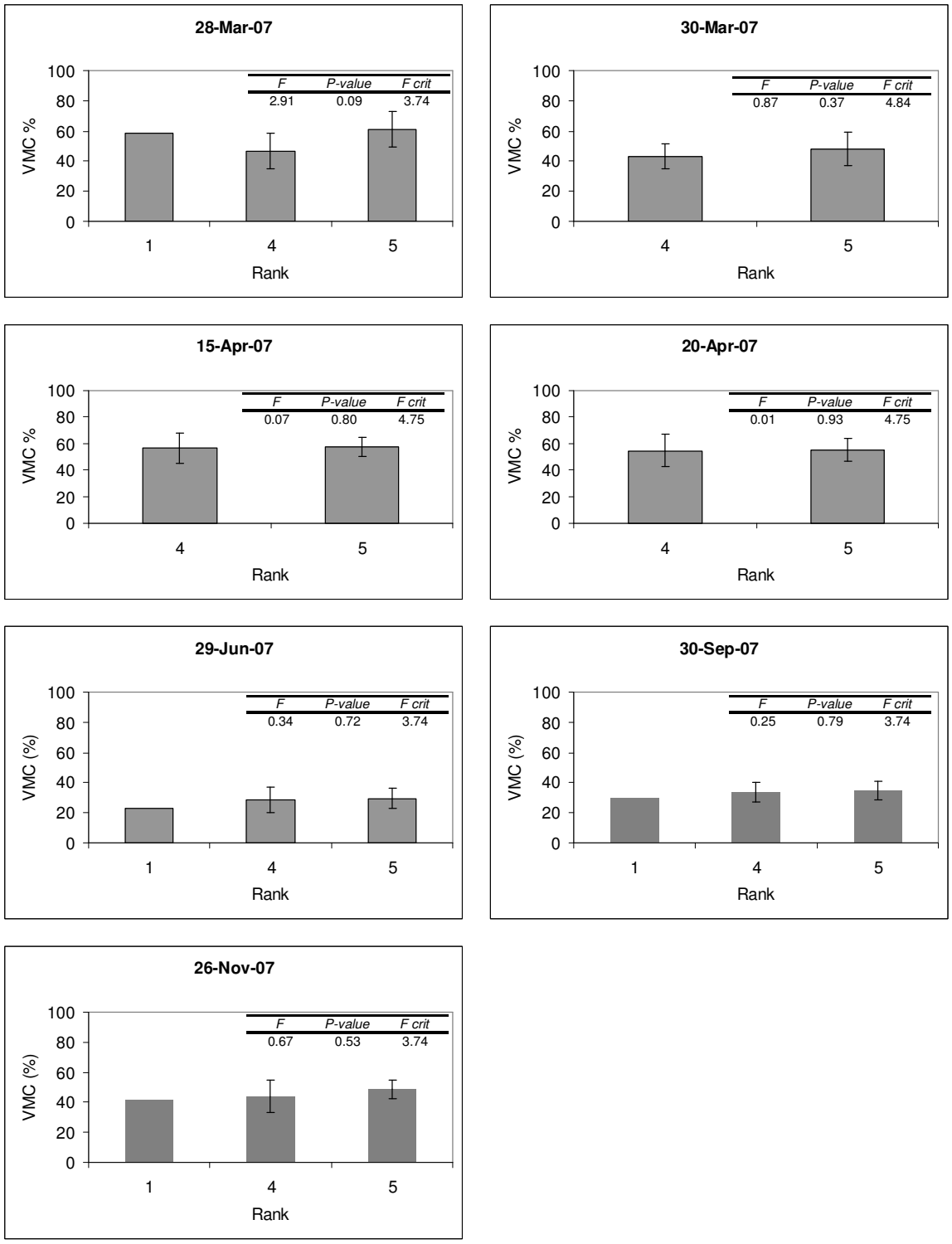

Figure 5.13 Bar charts for the Hay Field, 1 m and 5 m DEM (50x200 Cell Neighbourhood)

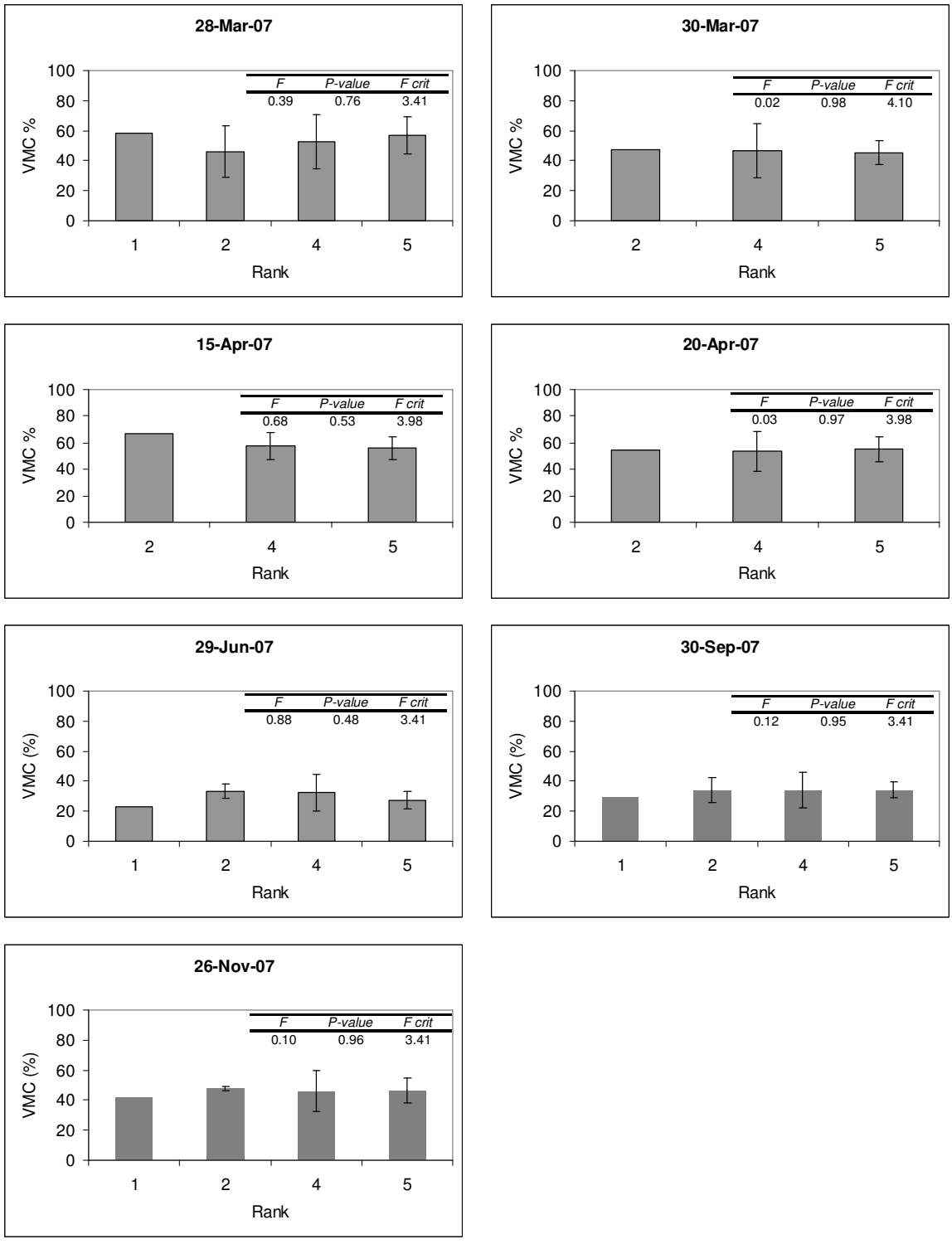

Figure 5.14 Bar Charts for the Hay Field, 5 m DEM (50x200 Cell Neighbourhood)

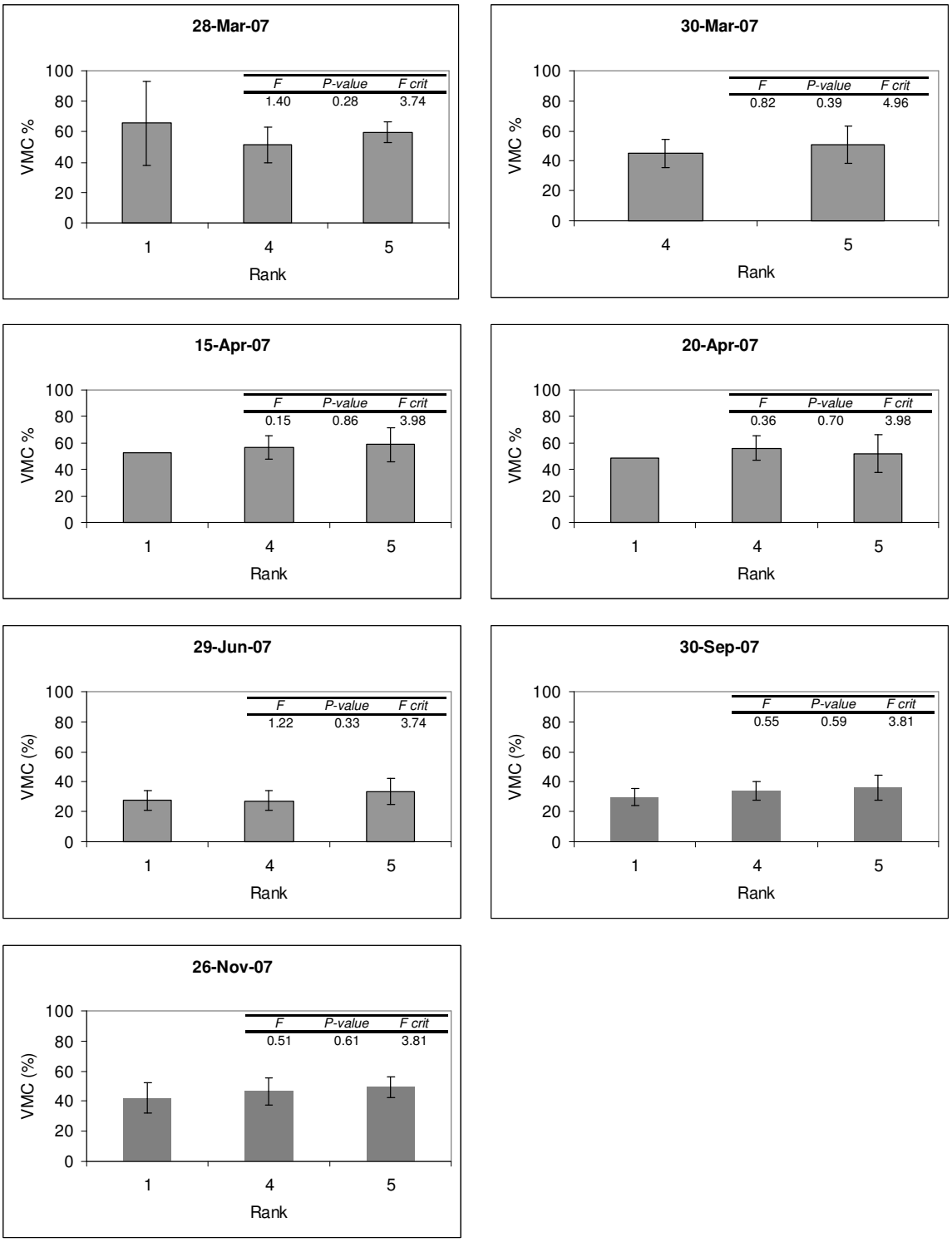

Figure 5.15 Bar charts for the Hay Field, 10 m DEM (50x200 Cell Neighbourhood)

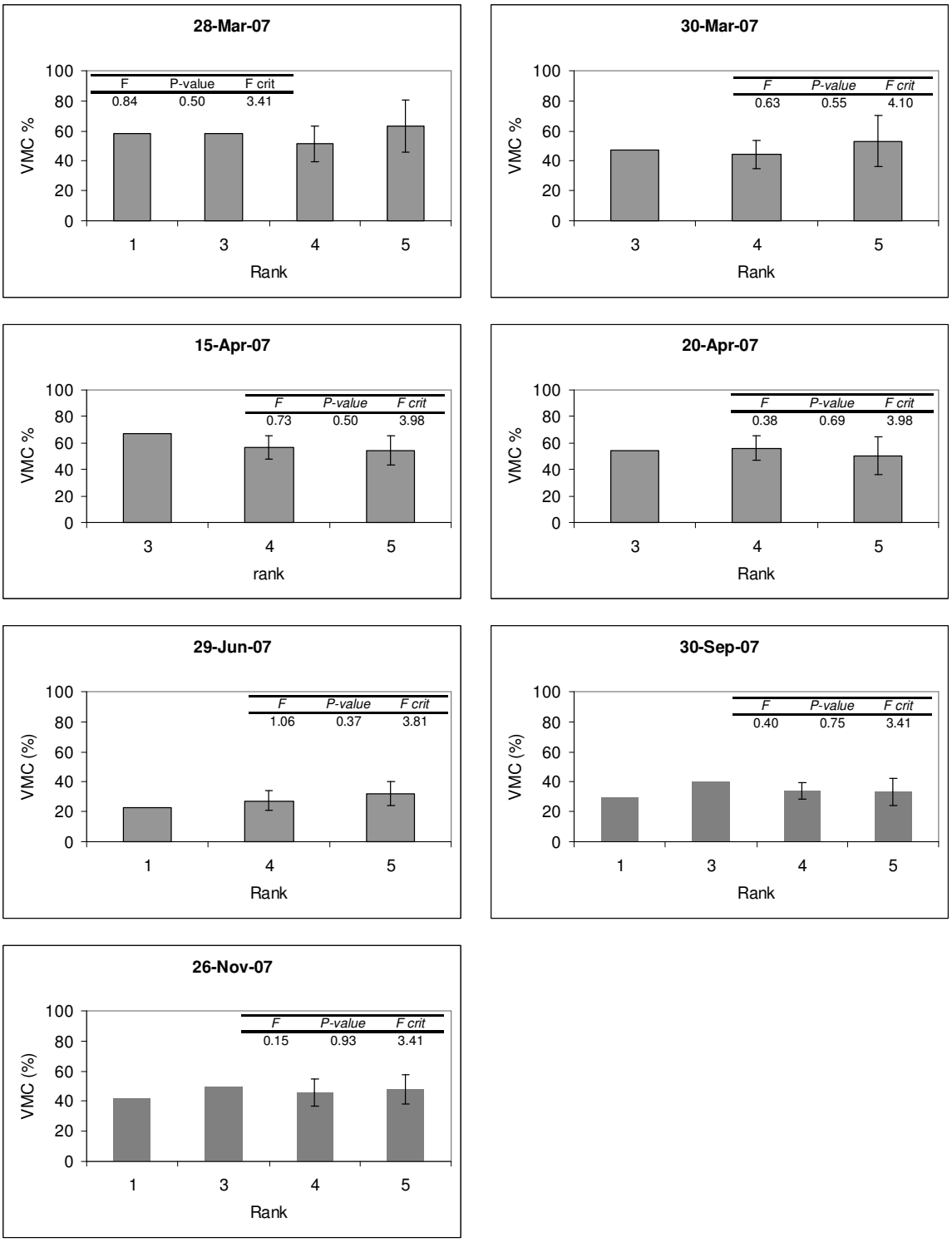

Figure 5.16 Bar charts for the Hay Field, 10 m DEM (200x500 Cell Neighbourhood)

The observations for the Hay Field revealed that the field was consistently saturated. The location of the field was near the outflow of the TBW and the water table at this point in the watershed was probably high. According to the Campbell Scientific Hydrosense Manual the typical saturation for a soil is 50% VMC. Many of the observations with the Hay field were >40% VMC (other than the June and September observations). That fact may have hindered the ability to accurately measure the subtle changes in the wetness due to topographic changes. It appeared that within this field the potential for runoff was low, the field had a low slope and there was often pooling water present in the field. This observation indicated that the water table at this location in the watershed was likely high and an in-depth study of the water table in this field would have been beneficial to understanding the moisture movement throughout the field. A regional scale modelled SSLC may be useful for identifying the difference between the local topographic influences on moisture and the regional influences. Such a study may reveal areas within the watershed which have a greater potential to be saturated due to the location within the greater watershed.

The imagery for the Hay Field revealed that the pattern of soil moisture was variable, however not as variable as the Corn Field observations (APPENDIX D: Hay Field Imagery). The measured soil moisture had higher values in the northern section of the field than the southern section of the field. The modelled SSLC did appear to pick up this area of increased moisture at the higher resolutions (5 m and higher). From ground truthing this field, it is known that in the northern part of this field there is an intermittent body of standing water. The ground sampled data appeared to capture the standing water body slightly better than the SSLC model.

5.5.5 Barley Field Data Summary

The Barley Field was located near the highest point in the watershed and had the most relief of the 3 subplots. The changing relief was captured by the SSLC modeling, at the higher resolutions there were 6 – 8 of the SSLC ranked units represented throughout this

field. In a small area, with high relief and multiple SSLC ranks, one would assume that the rate of change for moisture would be high and variable.

The soil moisture in the Barley field was measured 4 times. None of the soil moisture datasets corresponded to the hypothesized trend theory when compared to the various SSLC scales. The bar charts showed that none of the higher mean soil moisture values were modeled as being wetter than the other areas in the field (Figure 5.17, Figure 5.18, Figure 5.19 and Figure 5.20). The soil moisture throughout the Barley Field remained rather constant across the field on each collection date with little variation. There was some evidence throughout the field that suggested this field was artificially drained (e.g. tile drained), however after a visual inspection of the field it was inconclusive as to whether the field was in fact tile drained or not. Regardless, the field appeared to drain faster than the other fields, which was in part due to the higher slope angle, southern exposure, and vegetation coverage within the field. The observed moisture measurements were not well represented by the SSLC models, which predicted high degrees of moisture change throughout the Barley Field.

In many instances the soil moisture measurements in the Barley Field were the lowest recorded for the day of data collection. The field was drier than the other fields, and therefore better drained. The moisture within the field was moving rapidly from the surface to the water table.

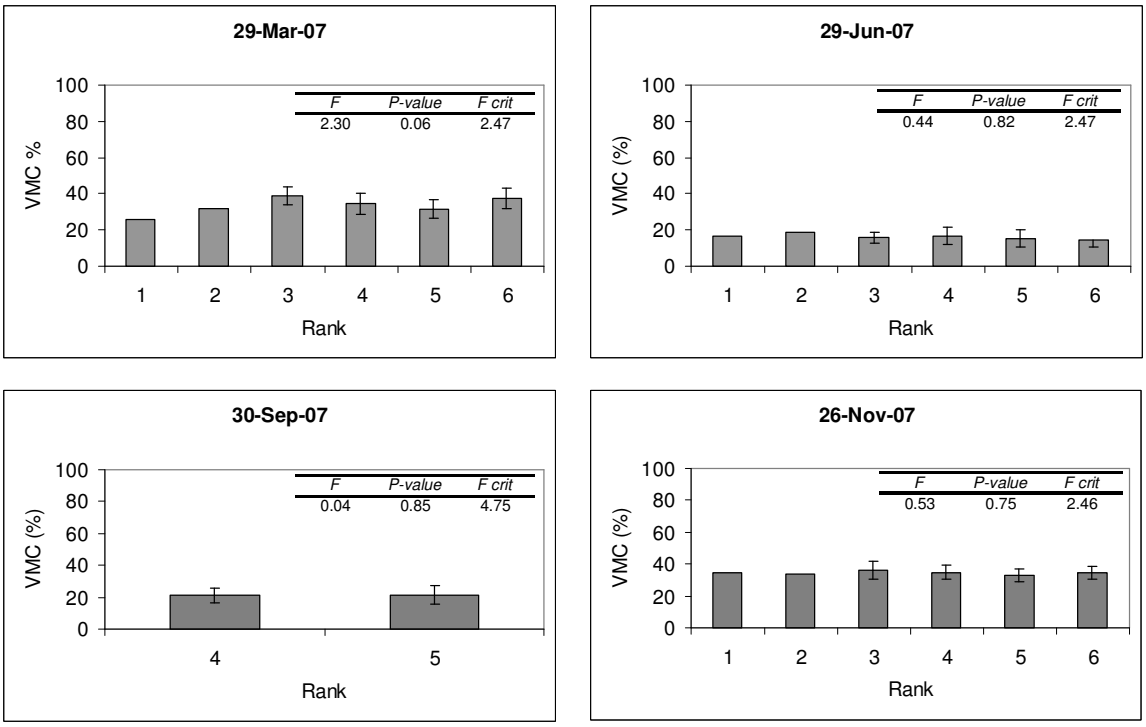

Figure 5.17 Bar Charts for the Barley Field, 1 m and 5 m DEM (50x200 Cell Neighbourhood)

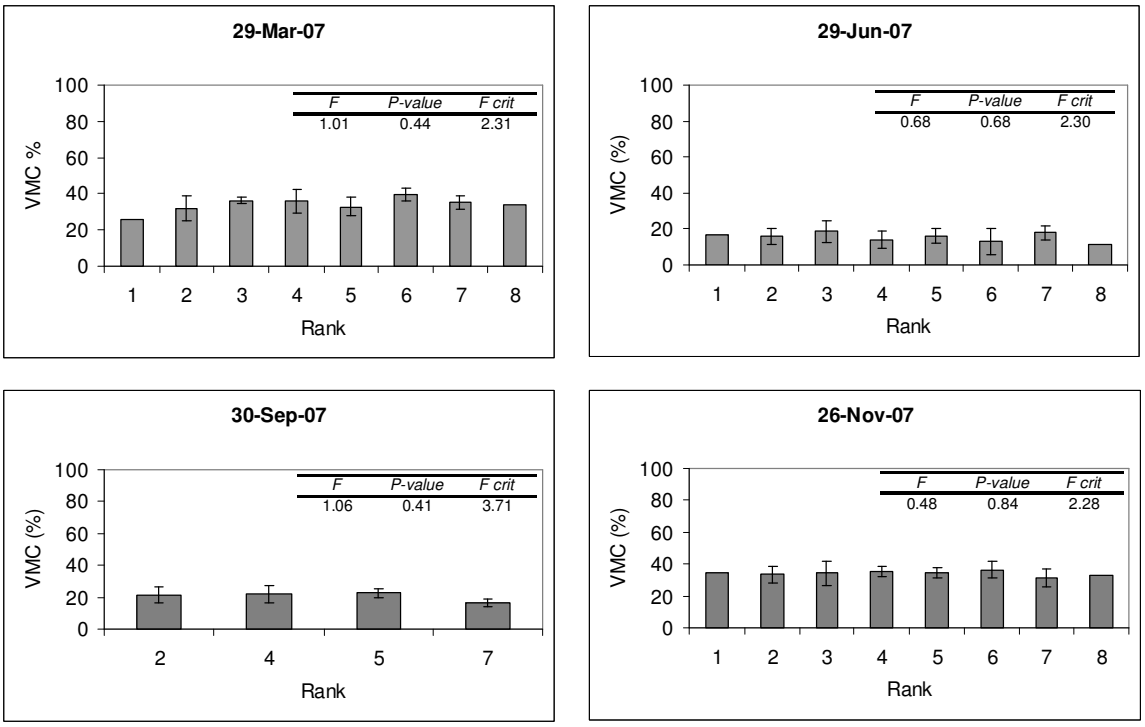

Figure 5.18 Bar charts for the Barley Field, 5m DEM (50x200 Cell Neighbourhood)

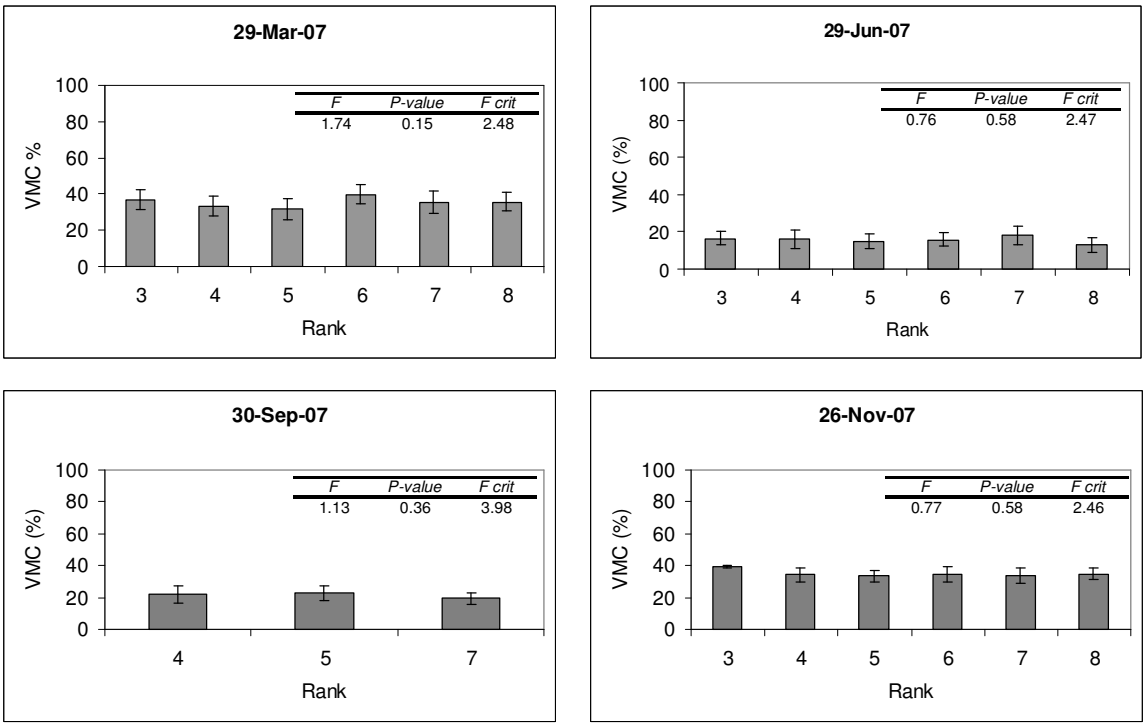

Figure 5.19 Bar Charts for the Barley Field, 10 m DEM (50x200 Cell Neighbourhood)

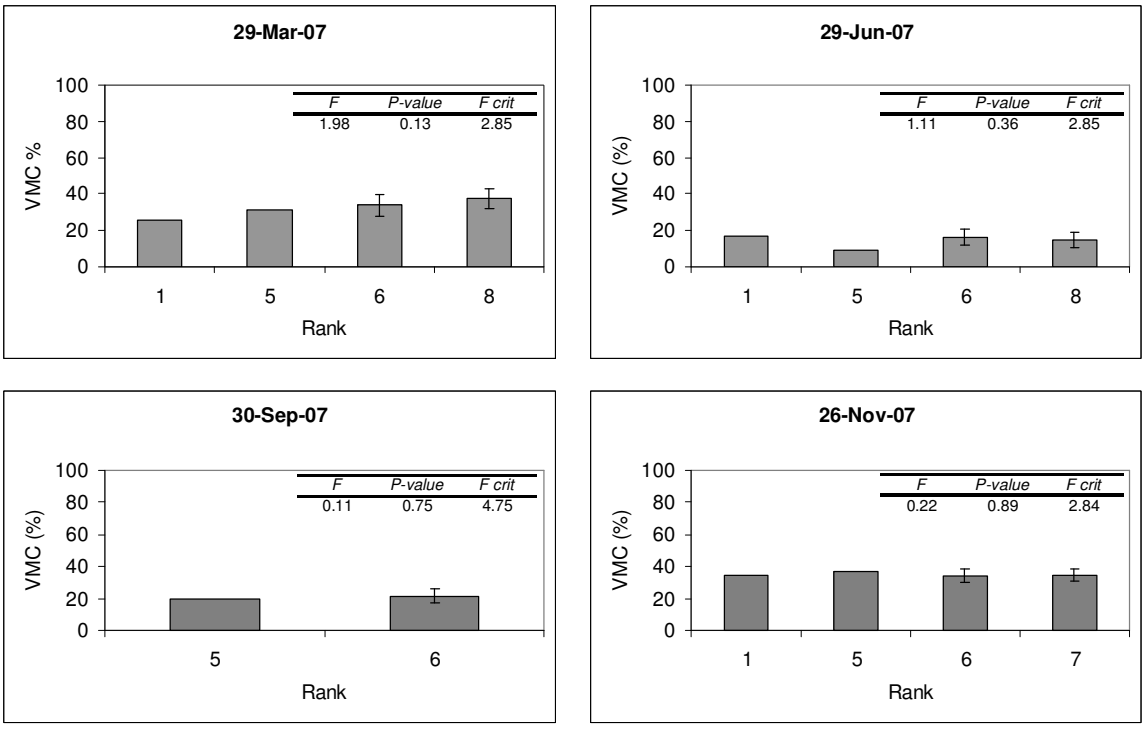

Figure 5.20 Bar charts for the Barley Field, 10 m DEM (200x500 Cell Neighbourhood)

The Barley Field imagery revealed spatial patterns of soil moisture (APPENDIX E: Barley Field Imagery). Of the 4 days of data collection the soil moisture did not appear to follow the modelled flow paths, but appeared to be fairly uniform across the field. The SSLC predicted a channel of flow directly through the middle of the field and, from ground truthing; this flow channel is a prominent surficial feature within the field. However, the pattern of soil moisture did not appear to follow the flow channel as expected. A potential rational for this observation would be that the majority of flow that occupies the channel during storm events comes from some other source than the moisture from within the field. This was substantiated by the fact that at the top of the field (i.e. the north) there was a culvert that funnelled water from the north side of the road into the Barley Field on the south side of the road. The channel would therefore be the result of over flow from this culvert and not the result of overland flow from the field. This observation is further substantiated when the moisture pattern is considered, as none of the measured moisture datasets would indicate lateral overland flow towards the channel.

5.6 CONCLUSION

In this chapter it was shown how to augment a landform classification algorithm to incorporate primary topographic derivatives and generate the Surface Saturation Landform Classification (SSLC). The SSLC was then calculated four times using three DEM resolutions (1 m, 5 m and 10 m). Each of the SSLC was compared to datasets of ground sampled VMC data in an effort to determine which SSLC scale was the most accurate at modelling surficial moisture conditions.

The performance of the classification was mixed. The 1 m and 5 m SSLC modelled with the 50 cell TPI and the 200 cell TPI showed the strongest results with 3 out of the 7 days of moisture data collection in the Corn Field successfully modeled. Of the 3 days of data that were in agreement with the theory 2 days (August 11, 2006 and November 26, 2007) had similar precipitation conditions which precluded the data collection (fresh precipitation prior to VMC data collection). The fresh precipitation may have played a role in the VMC data correlating with the modeled SSLC. During the May 31, 2007 dataset, while statistically the mean values were different, the trend in the data did not follow the theory of consistently lowering moisture values as SSLC ranks increased. This could also be related to the precipitation and highlights that recent precipitation may be a useful variable to consider when calibrating the SSLC in future studies. The 5 m SSLC, and both 10 m SSLC models, successfully modelled the moisture distribution collected on 1 of the 7 data collection days (November 26, 2007). In a bare earth field the moisture patterns could be successfully modeled using the SSLC when the surface conditions are wet.

The moisture patterns in the two other fields were not successfully modelled at any scale. In both fields none of the SSLC models successfully predicted the measured moisture distributions. In the Hay Field the moisture measurements were consistently at, or just below, the VMC% saturation level. The Hay Field was located near the outflow of the watershed and at the lowest relief of the watershed, which indicated that the moisture in the field was likely being influenced by the underlying water table more so than the local topography within the field. This observation suggests that modeling the SSLC at a much

larger scale may be useful to capture this type of moisture pattern. Conducting a study into water table profiling in this field may also be useful in this situation.

The Barley Field was located in the upper part of the watershed, it too revealed that none of the dates of data collection were successfully modelled. The field was located near the origin of the watershed and near the highest elevation of the watershed. The field was influenced by rapid relief changes and incoming sources of moisture from adjacent fields. This field was also densely vegetated. Under these conditions (vegetation, high slope) the infiltration capacity would be high and the runoff would be high. This meant that this field was consistently drier at the surface level. Western *et al* (1999) demonstrated that under dry conditions soil moisture is poorly organized and difficult to model. It was thought that the moisture movement potential within this field and the hay field was also being driven by the larger landform processes prevalent within the watershed more so than the local topography within the fields. This indicated that using a regional scale SSLC of the larger watershed (e.g. the Cornwallis River watershed) may reveal useful information about the overall moisture distribution within the TBW.

In an agricultural watershed the moisture movement potential was often artificially augmented. The Barley Field was directly impacted by culvert drainage which lead to the development of a channel in the middle of the field that was modelled as a "wet area", however the measured VMC data did not reflect this. The Corn Field, on the other hand, was artificially drained via a tile drainage system installed by the farmer and the measured VMC values under wet conditions closely followed the underlain drainage infrastructure. An interesting observation about this study was that the field with artificial drainage was also the only field with bare soil (during non-growing season) and the most representative of the SSLC model. It would seem that the SSLC model had much more success in bare earth fields than vegetated surfaces. Vegetation played a more dominant role in surface moisture distribution.

This modelling technique has value for future study in that it would be a valuable layer to add to a watershed analysis model, such as SWAT. By incorporating the SSLC into

SWAT modelling the technique may benefit from SWAT's usage of hydrologic response units, where a watershed is divided into land parcels based on soil type and distribution, land use and vegetation distribution. These land features were not accounted for in the SSLC but were identified as key components to surfical moisture distribution.

This technique would also have value in a larger scale watershed or agricultural study. The model may work well in areas of flat terrain, such as in the Prairies and Midwestern USA. In these areas where widespread agricultural operations are ongoing a modelling technique to account for the distribution of surfical moisture would be quite useful.

Another valuable application of this technique would be that of under canopy identification of wetlands. In Nova Scotia, for instance, the current provincial map of wetlands in known to be under representative of wetlands in forested areas, as the map was generated using photogrammetric methods. This technique could assist in updating the provincial wetlands map by being employed on DEMs that cover large areas of forest within the province.

CHAPTER 6 CONCLUSION

The DEM and airborne laser scanning (ALS) are powerful tools for landform analysis and geographic studies. In this project we demonstrated two approaches to modeling a watershed for the generation of a surface saturation map. The first method was to examine the influence of surficial moisture, and other land surface features, on ALS backscattered intensity values with the hypothesis that surficial saturation patterns would be identifiable in the intensity data (Chapter 3). The second approach was to utilize a DEM to generate topographic parameters and employ a landform classification algorithm to map surface saturation patterns throughout the watershed (explored in Chapter 4 and Chapter 5).

It was demonstrated, in Chapter 3, that the intensity signal of a LiDAR laser pulse was affected by the reflectance characteristics of different surficial features. Further, it was shown that over bare earth areas, such as the Corn Field, the signal was affected by surficial saturation. It was also shown that vegetation played a dominant role in signal attenuation over surficial saturation. An additional finding was that intensity data on a flightline by flightline basis gave a better representation of surficial reflectance than intensity data that has been mosaicked together to form a multiple flightline dataset.

In general, it was concluded that in this particular watershed study area LiDAR could not be used to map zones of surficial saturation directly. Vegetation played a dominant role in influencing the backscattered intensity of the pulse signal, which therefore affected the sensor's ability to record the direct influence of surficial saturation. In areas where there was no vegetation cover or tall vegetation cover that could be filtered, the intensity signal was shown to be affected by the surface reflectance influenced by surficial saturation and the potential was there to generate accurate moisture maps. At the watershed scale, however, monitoring surficial wetness zones within individual fields was not possible due to vegetation cover.

In Chapter 4 four primary topographic derivatives were identified as having an influence on surficial saturation levels. The four topographic layers were modelled and tested against ground sampled volumetric moisture content (VMC) data. The DEM resolution was set to 5 m because this was a more common DEM resolution and we wanted to learn if we could successfully model surface moisture at this resolution. It was shown that the Catchment Area topographic layer was able to model the moisture distribution of the ground sampled data in up to 65% of the tests. The Slope topographic model was shown to model the ground sampled VMC data in up to 95% of the tests. The Topographic Wetness Index (TWI) was shown to model moisture in 82% of the tests. The results also showed that the Curvature model was somewhat unreliable at the 5 m resolution. These results are consistent with the literature on the topic of surface saturation prediction using modeled topographic indices. Burt and Butcher (1985) had similar results using a different approach to measuring soil saturation (a grid pattern of tensiometers). In their research they suggested that a simple linear relationship was not sufficient to predict soil saturation using topographic indices and suggested that a general distribution of the soil saturation should be incorporated into the modeling.

The results also revealed that the D8 method of modelling topographic derivatives was very similar to the D-Infinity method and it was decided that the D8 method could be used for future modelling. It was believed that the high-resolution DEM was sufficient for modeling directional flow using the D8 method and that the D-infinity method did not add any substantial information to the model. This result is consistent with other studies on comparisons between the D-8 and D-infinity methods (Murphy *et al*, 2009). It was noted in Tarboton (1997) that differences between the D8 and D-infinity methods were more pronounced as data resolution increased and hillslopes increased. At the 5 m resolution the change in local slope gradient was minimal from cell to cell in many instances and this was the likely reason why the D-infinity did not reveal a significantly different directional flow model than the D8 method.

The tests revealed that the linear relationships between the topographic models and the ground sampled moisture data were not strong, this has been found in other studies on

topography and soil moisture distribution (Burt and Butcher, 1985; Grayson *et* al, 1997; Western *et al,* 1999). In many instances within the literature on the subject of topography prediction of soil saturation it is noted that DEM resolution is a critical component to successfully modeling surficial saturation (Quinn, 1991; Moore, 1993; Zhang and Montgomery, 1994; Wise, 2007; Weschler, 2007; and Murphy *et al,* 2009). The general consensus in the literature is that higher resolution models will yield better results. It was concluded that the 5 m DEM resolution was adequate for modeling surface moisture, however changing the scale of the DEM and the topographic models could potentially increase the strength of the relationship, which led to the methodology employed in Chapter 5.

In Chapter 5 the LiDAR data was resampled to 1 m, 5 m and 10 m and each of the topographic models were generated at each DEM resolution. The topographic models were then incorporated into a landform classification algorithm in accordance with their relationship to hydrologic processes. The new classification model was called the "Surface Saturation Landform Classification" (SSLC). The SSLC was modelled at four different scales and tested against the ground sampled VMC data. The multi-resolution modelling effort was conducted to identify the most appropriate scale for surface saturation prediction within this watershed. The results showed that the model performed well in the Corn Field, with 3 of the 7 days of data collection successfully modelled by the 1m and 5m SSLC layer. Of each of the DEM resolutions the finest resolution was the most successful at predicting surface saturation. As the resolution decreased (i.e. got coarser) the modeling was less accurate. The moisture patterns in the two other fields were not successfully modelled at any scale. The spatial distribution of soil moisture VMC values revealed that under dryer conditions the distribution pattern was disorganized. This was especially recognized under the vegetated fields as in all of the VMC datasets collected the values appeared disorganized.

The successful results found in the corn field were due to the vegetation conditions and organization of the soil moisture distribution. When the corn field was sampled during times when there was little or no vegetation, and after precipitation events, the VMC was

shown to be highly organized and closely matched the modelled drainage pattern throughout the field, therefore it was able to be predicted by the higher resolution SSLC model. Under drier conditions, and more densely vegetated conditions (e.g. during the growing season), the VMC values showed that the moisture distribution was scattered and disorganized. Western *et al*, (1999) and Grayson *et al,* (1997) demonstrated that during wetter seasons soil moisture patterns are more organized and more influenced by topography, but during dryer seasons the moisture distribution becomes disorganized. We saw these types of patterns in this study. Under wetter surface conditions we were able to show that the SSLC was successful at modeling surficial moisture in real world environmental conditions.

Throughout this thesis project two emergent themes were consistent in each of the three analysis chapters. The first was that of vegetation and its influence on surface moisture throughout the watershed. In our approach we purposely examined only topographic influences on surficial moisture, as was shown in the LiDAR intensity study and the topographic modelling studies. However, in both studies it was shown that vegetation likely had dominating influences on the surface moisture distribution than that of the topography. In the intensity study we saw that the backscattered data was directly affected by the vegetation in that it caused signal attenuation and was a source of separation from the soil surface which was measured via the TDR probe. In the topographic modelling studies we saw consistently that the successful models were only found in the bare earth, Corn Field, study area. The other two subplots were vegetated and both plots had poor results in the topographic models and SSLC models.

The second theme that emerged throughout the thesis was that of scale. In two ways scale was deemed to be important, the first being that the systematic approach to ground sampling VMC and whether the scale at which the measurements were acquired appropriately captured the moisture distribution within the subplots. The second was the GIS modeling approach and whether the appropriate modeling scale was achieved to capture the surface moisture variability within the subplots. Within the Cornfield subplot the spatial distribution of the surficial moisture was captured by the VMC data. In this

field the VMC data was collected on a regularly spaced grid and this technique proved to be a better representation of the soil moisture distribution than the more random sample pattern collected in the other subplots. Throughout the studies in this project it was shown that the Cornfield consistently preformed better than the other two subplots at modeling the surface moisture. We were also able to show that the finer resolution DEM's lead to better representation of the surface moisture distributions than coarser resolution DEMs.

The research conducted in this thesis project will contribute to the overall topographic study of the TBW and be useful for continuing the discussion on surface saturation distribution within the agriculturally rich environment. The SSLC model will be useful for incorporating the surface moisture distribution into the SWAT modeling algorithm. It is believed that the SWAT model may be able to further enhance the SSLC model by providing measures of vegetation variability, soil distribution, and landuse to the topographically centric SSLC that were not accounted for in this study. There may also be some benefit to the SSLC model by applying the HRU approach to watershed delineation that was adopted by the SWAT model. Future studies will be able to utilize the information from this research to enhance the spatial prediction of soil denitrification areas within agriculturally rich environments.

6.1 RECOMMENDATIONS

- Evaluation of the LiDAR intensity mapping technique would have benefited from a refined surface saturation measuring methodology. A suggested method would be to identify areas within the study are that are visibly moist (i.e. puddles, standing water, streams, drainage channels, dark soil, etc.) and map the extent of such areas via GPS. The comparison could then be made between known wet surfaces and known dry surfaces and the intensity values measured from the LiDAR data.
- The VMC measuring technique needs to be refined. Collecting one moisture reading at every GPS point did not give a confident reading of surface saturation. A suggested methodology that may increase the confidence in the data would be to

reduce the sampling error by observing a series of VMC readings within a 1 m radius of the GPS points, and then take the average of those readings.

- Another method to ensure confidence with the VMC data would be to conduct a second series of measurements using a different methodology. A gravimetric sampling test conducted monthly, or bi-annually depending on the monitoring time frame, would be a secondary source of surface saturation information to compare with the models and to reinforce the confidence of the TDR measurements.
- While collecting VMC data other physical measurements could be acquired to assist with mapping the surficial moisture distribution. Water table elevation measuring, soil compaction observations, the presence of hydric vegetation, soil profiling could prove to be useful information that would complement a suite of VMC data points.
- The surficial saturation monitoring should be regulated to bi-weekly, or monthly, data collections and should be focused around rainfall events. During the SSLC analysis it was identified that collecting VMC data after precipitation events leads to values correlating with the higher resolution SSLC models.
- The ground sampling program should be reformatted based on the modeled SSLC maps. The SSLC models should be created first and areas of high moisture and low moisture identified. The ground sampling should then be focused on the identified areas throughout the study area.
- A potentially better test of the accuracy of the SSLC would be to characterise zones of wetness based on seasonal measurements of soil moisture, and thus test the SSLC using the trends of moisture distribution rather than point source data. The point data was too variable to accurately predict.
- The SSLC output should be refined so that the data format is a contoured shapefile rather than a raster. The SSLC raster can be further processed, converted to a shapefile, and then contours of moisture can be constructed. This would broaden the spatial coverage of wetness zones. In its current format the SSLC is a rigid measurement of Wet vs. Dry areas of surface saturation. By generating a contoured map of SSLC values, zones of wetness could be identified and tested against the sampled moisture data.

- Additional data layers, such as soil type and vegetation, should be considered in the SSLC algorithm. It was recognized that soil type, and distribution, play an important role in surface moisture movement, although it was outside of the scope of this project to examine its influence. Incorporating soil drainage potential into the model could improve wetness prediction accuracy. During the project it was found that vegetation played an important role in affecting surficial saturation and therefore it should be a factor in the SSLC algorithm.
- The corn field study area performed better than the other two study areas in most of the tests. These techniques could be expanded to incorporate closer examinations of other bare earth fields to determine the utility of these techniques for modeling moisture in unvegetated landscapes.

REFERENCES CITED

Antonarakis, A.S., Richards, K.S., and Brasinton, J., 2008. Object-based land cover classification using airborne lidar. *Remote Sensing of Environment*, Vol. 112, No. 6, 2988 – 2998.

Axelsson, P., 1999. Processing of laser scanner data – algorithms and applications. *Journal of Photogrammetry and Remote Sensing.* 54, 138 – 147.

Baltsavias, E.P., 1999. Airborne laser scanning: basic relations and formulas. *Journal of Photogrammetry and Remote Sensing.* 54, 199 – 214.

Beaujouan, V., Durand, P., Ruiz, L., Aurousseau, P., and Cotteret, G., 2002. A hydrological model dedicated to topography-based simulation of nitrogen transfer and transformation: rationale and application to the geomorphology–denitrification relationship. *Hydrological Processes* 16, 493– 507.

Beven, K J and Kirkby, M J. 1979. A physically based variable contributing area model of basin hydrology. *Hydrology Science Bulletin*, 24(1), 43 – 69.

Beven, K. 1997. Topmodel: a critique. *Hydrological Processes* 11(9) 1069 – 1085.

Boyd, D.S., and Hill, R.A., 2007. Validation of airborne LiDAR intensity values from a forested landscape using HYMAP data: preliminary analysis. *IAPRS* 37(3) 71 – 76.

Brennan, R., and Webster, T.L., 2006. Object-oriented land cover classification of lidar-derived surfaces. *Canadian Journal of Remote Sensing,* Vol. 32, No. 2, 162 – 172.

Burt, T.P., Butcher, D.P., 1985. Topographic controls of soil moisture distribution. *Journal of Soil Science*, 36, 469–486.

Cann, D.B., MacDougall, J.L., and Hilchey, J.D., 1965. Soil Survey of Kings County, Nova Scotia. *Canada Department of Agriculture* and *Nova Scotia Department of Agriculture and Marketing.* Truro, Nova Scotia, Report No. 15.

Carroll, T.R., 1981. Airborne Soil Measurements using natural terrestrial gamma radiation. *Journal of Soil Science*, 148(6): 436 – 447.

Christopherson, R. W., 2003. Geosystems: an introduction to physical geography. *Prentice Hall*, Upper Saddle River, New Jersey, USA. 5th Edition. ISBN: 0-13-066824-9

Conrad, R., 1996. Soil microorganisms as controllers of atmospheric trace gasses (H_2, CO, CH_4, OCS, N_2O, and NO). *Microbiological Reviews*, 60, 609 – 640.

Coren, F., and Sterzai, P., 2006. Radiometric correction in laser scanning. *International Journal of Remote Sensing*, Technical Note and Cover 27(15) 3097 – 3104.

Curcio, J.A., and Perry, C.C., 1951. The near infrared absorption spectrum of liquid water. *Journal of the Optical Society of America*, Vol. 41, No. 5, 302 – 304.

de Blij, H.J., Muller, P.O., Milliams, R.S., Conrad, C.T., and Long, P., 2005. Physical geography: the global environment, Canadian Edition. *Oxford University Press.* Canada. ISBN: 0-19-542115-9.

Environment Canada, 2006. Environment Canada Climate Normal database. [http://www.climate.weatheroffice.ec.gc.ca/climate_normals/index_e.html] Accessed September 2006.

ESRI, 2007. ArcGIS 9.2 Desktop Help Document.

Florinsky, I.V., McMahon, S., and Burton, D.L., 2004. Topographic control of soil microbial activity: a case study of denitrifiers. *Geoderma*, 119, 33 – 53.

Franchini, M., Wendling, J., Obled, C., and Todini, E., 1996. Physical interpretation and sensitivity analysis of the TOPMODEL. *Journal of Hydrology,* 175, 293 – 338.

Garten, C.T., Huston, M.A., and Thoms, C.A., 1994. Topographic variation of soil nitrogen dynamics at Walker Brance Watershed, Tennessee. *Forest Science*, 40, 497–512.

Gassman, P.W., Reyes, M.R., Green, C.H., and Arnold, J.G., 2007. The soil and water assessment tool: historical development, applications,and future research directions. *American Society of Agriculturaland Biological Engineers,* Vol. 50(4), 1211 – 1250.

Grayson, R.B, Western, A.W., Chiew, F.H.S., 1997. Preferred states in spatial soil moisture patterns: local and nonlocal controls. *Water Resources Research*, Vol 33, No. 12, 2897 – 2908.

Groffman, P.M., and Hanson, G.C., 1997. Wetland denitrification: influence of site quality and relationships with wetland delineation protocols. *Soil Science Society of America Journal*, 61, 323 – 329.

Hellweger, F., 1997. AGREE – DEM surface reconditioning system. [www.ce.utexas.edu/prof/maidment/gishydro/ferdi/research/agree/agree.html] Accessed December 5, 2006.

Hewlett, J.D., and Troendle, C.A., 1975. Non-point and diffused water sources: a variable source area problem, in *Proceedings of symposium on watershed management. American Society of Civil Engineers*., New York. 21 – 46.

Hollaus, M., Wagner, W., and Kraus, K., 2005. Airborne laser scanning and usefulness fro hydrological models. *Advances in Geosciences*, 5, 57 – 63.

Hopkinson, C., 2007. The influence of flying altitude, beam divergence, and pulse repetition frequency on laser pulse return intensity and canopy frequency distribution. *Canadian Journal of Remote Sensing*, Vol. 33, No.4, 312 – 324.

Hopkinson, C., and Chasmer, L.E., 2007. Modelling canopy gap fraction from lidar intensity. *ISPRS,* Workshop on Laser Scanning 2007 and Silvilaser 2007, Espoo, September 12 – 14, 2007, Finland.

Hopkinson, C., Chasmer, L.E., Sass, G., Creed, I., Sitar, M., Kalbfleisch, W., and Treitz, P., 2005. Vegetation class dependent errors in LiDAR ground elevation and canopy height estimates in a boreal wetland environment. *Canadian Journal of Remote Sensing*, Vol. 31, No.2, 191 – 206.

Hopkinson, C., and Demuth, M.N., 2006. Using airborne lidar to assess the influence of glacier downwasting to water resources in the Canadian Rocky Mountains, *Canadian Journal of Remote Sensing*, 32 (2) pp. 212 – 222.

Jackson, T.J., Le Vine, D.M., Hsu, A.Y., Oldak, A., Starks, P.J., Swift, C.T., Isham, J.D., and Haken, M., 1999. Soil moisture mapping at regional scales using microwave radiometry: The Southern Great Plains hydrology experiment. IEEE Trans. *Geoscience And Remote Sensing*. 37(5): 2136 – 2151.

Jamieson, R.C., Gordon, R.J., Tattrie, S.C., and Stratton, G. W., 2003. Sources and persistence of fecal coliform bacteria in a rural watershed. *Water Quality Resources Journal of Canada*, vol. 38, no. 1, 33 – 47.

Kaleita, A. L., Tian, L.F., and Hirschi, M.C., 2005. Relationship between soil moisture content and soil surface reflectance. *American Society of Agricultural Engineers*. 48(5): 1979 – 1986.

Kaasalainen, S., Ahokas, E., Hyyppä, J. and Suomalainen, J., 2005. Study of surface brightness from backscattered LiDAR intensity: calibration of laser data. *IEEE Geoscience and Remote Sensing Letters* 2 255 – 259.

Kaasalainen, S., Hyyppa, J., Litkey, P., Hyyppa, H., Ahokas, E., Kuuko, A., and Kaartinen, H., 2007. Radiometric calibration of ALS intensity. *IAPRS*, Vol. XXXVI, Part 3/W52, 201 – 205.

Lobell, D.B., and Asner, G.P., 2002. Moisture Effects on Soil Reflectance. *Soil Science Society of America Journal*, Vol. 66, 722 – 727.

Lillesand, T. M., and Kiefer, R. W., 2000. Remote Sensing and Image Interpretation: Fourth Edition. *John Wiley & Sons*. ISBN 0-471-25515-7.

Manis, G., Lowry, J., and Ramsey, D., 2001. Preclassification: an ecologically predictive landform model. *USGS Gap Analysis Bulletin*. (10) 11 – 13

Mazzarini, F., Pareschi, M.T., Favalli, M., Isola, I., Tarquini, S., and Boschi, E., 2007. Lava flow identification and aging by means of LiDAR intensity: Mount Etna case. *Journal of Geophysical Research*, Vol. 112, DOI 10.1029/2005JB004166.

Moore, I.D., Grayson, R.B., and Ladson, A.R., 1991. Digital terrain modeling: a review of hydrological, geomorphological and biological applications. *Hydrological Processes*, 5, 3 –30.

Moore, I.D., Gessler, P.E., Nielsen, G.A., and Peterson, G.A., 1993. Soil attribute prediction using terrain analysis. *Soil Science Society of America Journal*, 57, 443– 452.

Murphy, P.N.C., Ogilvie, J., and Arp, P., 2009. Topographic modelling of soil moisture conditions: a comparison and verification of two models. *European Journal of Soil Science*, 60, 94 – 109.

O'loughlin, E.M., 1981. Saturation regions in catchments and their relations to soil and topographic properties. *Journal of Hydrology.* 53 (3-4) 229 – 246.

O'Loughlin, E.M., 1986. Prediction of surface saturation zones in natural catchments by topographic analysis. *Water Resources Research* 22(5) 794 – 804.

Parker, A. J., 1982. The topographic relative moisture index: an approach to soil-moisture assessment in mountain terrain. *Physical Geography*, 3(2) 160 – 168.

Price, J.C., 1982. On the use of satellite data to infer surface fluxes at meteorological scales. *Journal of Applied Meteorology,* 21(8): 1111 – 1122.

Quinn, P., Beven, K., Chevallier, P., and Planchon, O., 1991. The prediction of hillslope flow paths for distributed hydrological modeling using digital terrain models. *Hydrological Processes*, vol. 5: 59-79.

Quinn, P., Beven, K.J., and Lamb, R., 1995. The ln(a/tanB) index: how to calculate it and how to use it within the TOPMODEL framework. *Hydrological Processes*, vol. 9, 161 – 182.

Saunders W., 2000. Preparation of DEMs for use in environmental modeling analysis. In Maidment and Djokic, 2000, Hydrologic and Hydraulic modeling support with geographic information systems. *Environmental Systems Research Institute Press* – Redlands, California. ISBN 1-879102-80-3.

Schmidt, F., and Persson, A., 2003. Comparison of DEM data capture and topographic wetness indices. *Precision Agriculture*, 4, 179 – 192.

Tarboton, D. G., 1997. A New Method for the Determination of Flow Directions and Contributing Areas in Grid Digital Elevation Models. *Water Resources Research*, 33(2): 309-319.

Tarboton, D., 2005. Terrain Analysis Using Digital Elevation Models (TauDEM). Utah State University [http://www.engineering.usu.edu/dtarb/].

USDA, 2007. Spatial Analyst – Module 3: Curvature Model. United States Department of Agriculture, Natural Resources Conservation Service, Montana. Accessed online August 2008. [http://www.mt.nrcs.usda.gov/soils/mtsoils/ArcGIS/module3.html].

Webster, T.L., Forbes, D.L., MacKinnon, E., and Roberts, D., 2006a. Flood – risk mapping for storm-surge events and sea-level rise using lidar for southeast New Brunswick. *Canadian Journal of Remote Sensing*, 32, no.2: 146 – 211.

Wechsler, S.P., 2007. Uncertainties associated with digital elevation models for hydrologic applications: a review. *Hydrology and Earth System Sciences*, 11, 1482 – 1500.

Wehr, A., and Lohr, U., 1999. Airborne laser scanning – an introduction and overview. *Journal of Photogrammetry and Remote Sensing.* 54, 68 – 82.

Weidong, L, Baret, F., Xingfa, G., Qingxi, T., Lanfen, Z., and Bing, Z., 2002. Relating soil surface moisture to reflectance. *Remote Sensing of Environment,* Vol. 81, 238 – 246.

Weiss, A., 2001. Topographic position and landforms analysis. Poster Presentation, ESRI User Conference, San Diego, CA.

Western, A.W., Grayson, R.B., Bloschl, G., Willgoose, G.R., and McMahon, T.A., 1999. Obsered spatial organization of soil moisture and its relation to terrain indices. *Water Resources Research,* Vol. 35, No. 3, 797 – 810.

Wise, S.M., 1998. The effect of GIS interpolation errors on the use of digital elevation models in geomorphology. "Landform Monitoring, Modelling and Analysis." *John Wiley and Sons Ltd.* Edited by S.N. Lane, K.S. Richards, and J.H. Chandler, Chapter 7, 1998.

Wise, S.M., 2007. Effect of differing DEM creation methods on the results from a hydrological model. *Computers & Geosciences* 33, 1351 – 1365.

Whiting, M.L., Li, L., and Ustin, S.L., 2004. Predicting water content using Gaussian model on soil spectra. *Remote Sensing of Environment*. Vol. 89, 535 – 552.

Wu, S., Peng, B., Chung, Y., and Hsieh, Y., 2009 (Currently under review). Using lidar multiple-return and intensity data to approach the structure characterization and

classification of different forest types. *Canadian Journal of Remote Sensing*, CJRS-09-0050.

Zhang, W.H. and Montgomery, D.R., 1994. Digital elevation model grid size, landscape representation and hydrologic simulations. *Water Resources Research*, 30, 1019 – 1028.

Zhou, Q., and Liu, X., 2004. Analysis of errors of derived slope and aspect related to DEM data properties. *Computers and Geosciences*, 30, 369 – 378.

APPENDIX A Surfer Script used for automation of converting *.xyz files to Arc GIS raster files

```
Sub Main
'This script was created by Doug Stiff & Jon Kwong on June 16th and 19th, 2006 and is for
academic use only.
'This script: takes an xyz file, determines the max and min xs and ys and removes a
twenty metre buffer around
'it then uses these values to grid based on IDW (the parametres can be adjusted below)
'this program should open an xyz file and grid it
' the x and y max and min will be the value + or - twenty and rounded to the nearest
integer...


'step one open an xyz file

'Declare SurferApp as an object
 Dim Fnum As Integer                    ' > File number
 Dim xyzline As String
 Dim cur_X As String
 Dim cur_Y As String
 Dim cur_ymax As Double
 Dim cur_ymin As Double
 Dim cur_xmax As Double
 Dim cur_xmin As Double
 Dim i As Integer
 Dim SurferApp As Object
 Dim HmyFileNon As String
' Creates an instance of the Surfer Application Object And assigns
'it to the variable named "SurferApp"
 Set SurferApp = CreateObject("Surfer.Application")
'Makes Surfer visible - must be visible to view reports
 SurferApp.Visible = True
Debug.Clear
Begin Dialog UserDialog 480,238,"XYZ to GRD to ARC convertor" ' %GRID:10,7,1,1
               GroupBox 20,14,450,210,"XYZ to GRD (to ASC?) conversion",.GroupBox1
               GroupBox 40,98,240,112,"XYZ to GRD conversion",.GroupBox2
               CheckBox 70,161,200,14,"Add Northings And Eastings To grd File
Name",.addENcheckbox
               Text 40,35,330,28,"Please enter the directory containing XYZ or GRD files
you wish to process",.Text1
               TextBox 40,70,400,21,.Str
               CheckBox 70,140,200,14,"Convert final files to Arc grids",.contoarc
               OptionGroup .Group1
                       OptionButton 60,119,90,14,"Ground",.convertground
                       OptionButton 160,119,110,14,"Non Ground ",.convert1ground
                       OptionButton 310,119,130,14,"GRD to ASC",.convert2ground
               OKButton 310,140,110,28,.ok
               CancelButton 310,175,110,28,.cancel
               Text 90,175,140,14," to final file name",.Text3
       End Dialog


Dim dlg As UserDialog

dlg.Str = "D:\KevinGarroway\TBWS\SurferWORK\"

result = Dialog(dlg)
strpath = dlg.Str
adden = dlg.addENcheckbox
groundornot = dlg.group1
toarc = dlg.contoarc
starttime = Timer
```

```
'
If result = 0 Then End  'this happens if cancel is pressed.

If groundornot = 2 Then
        toarc = 1
        adden = 0
    HmyFile = Dir$(strPath & "*.grd")
Else
        HmyFile = Dir$(strPath & "*.xyz")
End If

Do While Len(HmyFile) > 0
               xyzfile = strPath & HmyFile
               Debug.Print "Finding corners of: " & xyzfile
If groundornot <> 2 Then
xystarttime = Timer
Const ForReading = 1
Set objFSO = CreateObject("Scripting.FileSystemObject")
Set objTextFile = objFSO.OpenTextFile(xyzfile, ForReading)
         xyzline = objTextFile.ReadLine
         cur_xmax=Val(Left$(xyzline,11))
         cur_xmin=Val(Left$(xyzline,11))
         cur_ymax=Val(Mid$(xyzline,12,11))
         cur_ymin=Val(Mid$(xyzline,12,11))
objTextFile.Close

Set objFSO = CreateObject("Scripting.FileSystemObject")
Set objTextFile = objFSO.OpenTextFile(xyzfile, ForReading)
Do While Not objTextFile.atendofstream
               xnow = Val(Left$(xyzline,11))
               ynow = Val(Mid$(xyzline,12,11))
               If xnow > cur_xmax Then       ' > extract x  and compare
                       cur_xmax = xnow
               ElseIf xnow < cur_xmin Then
                       cur_xmin = xnow
               End If

           If  ynow > cur_ymax Then
                       cur_ymax =     ynow
               ElseIf  ynow < cur_ymin Then
                       cur_ymin = ynow
               End If
         xyzline = objTextFile.ReadLine
Loop

objTextFile.Close

'  > Close the file'
'       'remove the 20 metre buffer
        Debug.Print "removing 100 metre buffer"
        maxxlessbuffer = Round((cur_xmax-100),0)
        minxlessbuffer = Round((cur_xmin+100),0)
        maxylessbuffer = Round((cur_ymax-100),0)
        minylessbuffer = Round((cur_ymin+100),0)

        Debug.Print "Using...."
        Debug.Print "MaxX " & maxxlessbuffer & "MinX " & minxlessbuffer & "MaxY " &
maxylessbuffer & "MinY " & minylessbuffer

xyendtime = Timer
Debug.Print Round(xyendtime-xystarttime,3)
        If adden = 1 Then
                lowerleftx = Round((minxlessbuffer / 100),0)
                lowerlefty = Round((minylessbuffer / 100),0)
                tempfilename = Left$(hmyfile, (Len(hmyfile)-4))
                temp2filename = tempfilename & "_" & lowerleftx & "_" & lowerlefty &
".grd"
                xyzfileout = strPath & temp2filename
        Else
                xyzfileout = Left$(xyzfile,(Len(xyzfile)-4)) & ".grd"
        End If
```

```
        Debug.Print "Gridding: " & xyzfileout

xcol = maxxlessbuffer - minxlessbuffer + 1
ycol = maxylessbuffer - minylessbuffer + 1


' this uses IDW to grid the ground data....

'       If groundornot = 0 Then
'       Debug.Print "Ground..."
'               SurferApp.GridData(DataFile:=xyzfile, xCol:=1, yCol:=2,
xmax:=maxxlessbuffer, xmin:=minxlessbuffer, ymax:=maxylessbuffer, ymin:=minylessbuffer, _
'               zCol:=3, Algorithm:=srfInverseDistance, ShowReport:=True,
SearchEnable:=True, SearchRad1:=10, SearchRad2:=10, SearchAngle:=0, _
'               numcols:=1001, numrows:=1001, SearchMinData:=2, SearchDataPerSect:=64,
SearchNumSectors:=2, SearchMaxEmpty:=2, outgrid:=xyzfileout, OutFmt:=srfGridFmtS7)
'       End If


        If groundornot = 0 Then
        Debug.Print "Ground..."
                SurferApp.GridData(DataFile:=xyzfile, xCol:=1, yCol:=2,
xmax:=maxxlessbuffer, xmin:=minxlessbuffer, ymax:=maxylessbuffer, ymin:=minylessbuffer, _
                zCol:=3, Algorithm:=srfInverseDistance, ShowReport:=True,
SearchEnable:=True, SearchRad1:=10, SearchRad2:=10, SearchAngle:=0, _
                numcols:=xcol, numrows:=ycol, SearchMinData:=2, SearchDataPerSect:=64,
SearchNumSectors:=2, SearchMaxEmpty:=2, outgrid:=xyzfileout, OutFmt:=srfGridFmtS7)
        End If

'       If groundornot = 1 Then
'       Debug.Print "Non Ground..."
'    ' this is IDW and filter on nonground data
'               SurferApp.GridData(Datafile:=xyzfile, xCol:=1, Ycol:=2, Zcol:=3,
ShowReport:=True, numcols:=1001, numrows:=1001, _
'               dupmethod := srfDupMaxZ, xduptol:=0.5, yduptol:=0.5,
xmax:=maxxlessbuffer, xmin:=minxlessbuffer, ymax:=maxylessbuffer, ymin:=minylessbuffer, _
'               algorithm:=srfInverseDistance, SearchEnable:=True,SearchMinData:=2,
SearchAngle:=0, SearchRad1:=3, SearchRad2:=3, SearchDataPerSect:=64, SearchNumSectors:=2,
SearchMaxEmpty:=2, outgrid:= xyzfileout, OutFmt:=srfGridFmtS7)
'       End If

        If groundornot = 1 Then
        'sleep 300
        Debug.Print "Non Ground..."
    ' this is IDW and filter on nonground data
                SurferApp.GridData(Datafile:=xyzfile, xCol:=1, Ycol:=2, Zcol:=3,
ShowReport:=True, numcols:=xcol, numrows:=ycol, _
                dupmethod := srfDupMaxZ, xduptol:=1.5, yduptol:=1.5,
xmax:=maxxlessbuffer, xmin:=minxlessbuffer, ymax:=maxylessbuffer, ymin:=minylessbuffer, _
                algorithm:=srfInverseDistance, searchenable:=True, SearchMinData:=5,
searchangle:=0, searchrad1:=3, searchrad2:=3, SearchDataPerSect:=64, SearchNumSectors:=4,
SearchMaxEmpty:=3, outgrid:= xyzfileout, OutFmt:=srfGridFmtS7)
        End If

End If  'ends my if groundornot <> 2

'dupmethod := srfDupMaxZ, xduptol:=1.5, yduptol:=1.5,

If toarc = 1 Then
        Debug.Print "Converting to arc...."
        'conversion to arc
        'Grd2arc converts a Surfer GRD file to ArcView, ArcINFO,
        ' Spatial Analyst ASC format.
        ' Converted from srf7_2aiGRD.frm from Johan.Kabout@MI.DHV.NL - TB Jan 00.
        ' TB - 19 Mar 00.---
        ' Integrated June 19th 2006

        If groundornot = 2 Then
                xyzfileout = strPath & HmyFile
        End If
```

```
        SurferGrid = xyzfileout   'xyzfileout is the grd file just created.

        'Mirror Y in Surfer GRD file, save to ASCII format.
      tempfile = "c:\temp\temp.dat"
      Set srf = CreateObject("Surfer.application")
        Set plot = srf.Documents.Add(srfDocPlot)
      ok = srf.GridTransform(SurferGrid, srfGridTransMirrorY, _
          OutGrid:=TempFile,OutFmt:=srfGridFmtAscii)

        lengthstr = Len(SurferGrid)
        ArcGrid = Mid(SurferGrid, 1, Len(SurferGrid)-3) + "ASC"
        Open TempFile For Input As #1
        Open ArcGrid For Output As #2

        'Skip the first line of the file.
        Line Input #1,a

        'Read number of columns and rows.
        Line Input #1,a
        nCol = Left(a,InStr(a," "))
        nRow = Right(a,Len(a)-InStr(a," "))

        'Read X min max.
        Line Input #1,a
        xMin = Left(a,InStr(a," "))
        xMax = Right(a,Len(a)-InStr(a," "))

        'Read Y min max.
        Line Input #1,a
        yMin = Left(a,InStr(a," "))
        yMax = Right(a,Len(a)-InStr(a," "))

        'Read Z min max (not used in Arc grid file).
        Line Input #1,a
        zMin = Left(a,InStr(a," "))
        zMax = Right(a,Len(a)-InStr(a," "))

        xCellSize = ((Val(xMax) - Val(xMin)) / (Val(nCol) - 1))
        yCellSize = ((Val(yMax) - Val(yMin)) / (Val(nRow) - 1))
        Diff = 100*(xCellSize - yCellSize) / xCellSize

     'Debug.Print "xCellSize, yCellSize, Diff =";xcellsize;" ";ycellsize;" ";diff
    '    If (xCellSize - yCellSize) / xCellSize > 1e-3 Then
     '     MsgBox("Cell dimensions are not square.  ("+Str(Diff)+ "%)." + _
      '      "Creating Arc grid with xCellSize: " + Str(xCellSize) )
       ' End If

        Print #2, "ncols         "; nCol
        Print #2, "nrows         "; nRow
        Print #2, "xllcorner     "; xMin
        Print #2, "yllcorner     "; yMin
        Print #2, "cellsize      "; xCellSize
        Print #2, "NODATA_value  1.70141e+038"
        Print #2, " "

        Do While Not EOF(1)
          Line Input #1, instring
          Print #2, instring
        Loop
        Close #1
        Close #2
     Kill(tempfile)


End If

HmyFile = Dir$()
keeptrack = keeptrack + 1
timenow = Timer
Debug.Clear
Debug.Print "Number of files processed: " & keeptrack
```

```
averagetime = Round(((timenow - starttime) / keeptrack),3)
Debug.Print "Running average time per file: " & averagetime & " s"
Loop
MsgBox("completed: average time per grid: " & averagetime & " seconds")
End Sub
```

APPENDIX B: ARCGIS MODELS

See attached electronic documents:

1) TPI_Model.emf
2) SSLC_50200_15
3) SSLC_50200_5
4) SSLC_50200_10
5) SSLC_200500_10

APPENDIX C: CORN FIELD IMAGERY

See attached electronic documents

APPENDIX D: HAY FIELD IMAGERY

See attached electronic documents

APPENDIX E: BARLEY FIELD IMAGERY

See attached electronic documents